ERDC/GSL TR-02-4

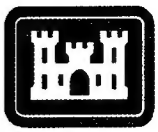

US Army Corps
of Engineers®
Engineer Research and
Development Center

Rapid Strengthening of Reinforced Concrete Beams with Mechanically Fastened, Fiber-Reinforced Polymeric Composite Materials

Lawrence C. Bank, Anthony J. Lamanna,
James C. Ray, and Gerardo I. Velázquez

March 2002

Geotechnical and Structures Laboratory

ERDC/GSL TR-02-4
March 2002

Rapid Strengthening of Reinforced Concrete Beams with Mechanically Fastened, Fiber-Reinforced Polymeric Composite Materials

by Lawrence C. Bank, Anthony J. Lamanna

Department of Civil and Environmental Engineering
University of Wisconsin-Madison
Madison, WI 53706

James C. Ray, Gerardo I. Velázquez

Geotechnical and Structures Laboratory
U.S. Engineer Research and Development Center
3909 Halls Ferry Road
Vicksburg, MS 39180-6199

Final report

Prepared for U.S. Army Corps of Engineers
Washington, DC 20314-1000

Contents

List of Figures

List of Tables

Preface

This study was conducted by personnel of the Department of Civil and Environmental Engineering, University of Wisconsin at Madison, under contract No. DACA42-00-P-044 and the U.S. Army Engineer Research and Development Center (ERDC), Geotechnical and Structures Laboratory (GSL), Vicksburg, MS. The study was part of the Department of the Army Project No. 4A162784AT40, Work Package No. 1259B, "Bridge Assessment and Repair," Work Unit No. BR002, "Rapid Bridge Repair and Retrofit," which is sponsored by Headquarters, U.S. Army Corps of Engineers.

The experimental work was accomplished January through October 2000 under the general supervision of Dr. Michael J. O'Connor, Director, GSL, Dr. Bryant Mather, Director Emeritus, GSL; Dr. Robert L. Hall, Chief, Geosciences and Structures Division (GSD), GSL; and Mr. James S. Shore, Chief, Structural Engineering Branch (StEB), GSL. Messrs. James C. Ray and Gerardo I. Velázquez were the project investigators for this effort. Professor Lawrence C. Bank and Graduate Student Mr. Anthony J. Lamanna were the Principal Investigators for the University of Wisconsin. The authors were also assisted in the preparation of this report by Ms. Christa M. Beasnett, Senior Technician, DynTel Corporation.

At the time of publication of this report, Dr. James R. Houston was Director of ERDC, and COL John W. Morris III, EN, was Commander and Executive Director.

Conversion Factors, Non-SI to SI Units of Measurement

Non-SI units of measurements used in this report can be converted to SI unit as follows:

Multiply	By	To Obtain
cubic feet	0.028317	cubic meters
fahrenheit degrees	(f-32)/1.8	celsius degrees
feet	0.304800	meters
grams	0.001	kilograms
gallons	0.00378	cubic meters
inches	0.025400	meters
inches	25.4	millimeters
miles	1.609	kilometers
ounces	0.00002957	cubic meters
pint	0.00004731	cubic meters
pounds (force) per square inch	0.006894757	megapascals
pounds per cubic foot	16.0	kilograms per cubic meter
square inches	0.000645	square meters

1 Introduction

Scenario: A U.S. Army task force deploys to an under-developed nation to complete a time-sensitive mission critical to U.S. security interests. Reconnaissance of the route from the port of debarkation to the mission area reveals the presence of a reinforced concrete bridge without a feasible bypass. The bridge does not have sufficient strength to safely support task force traffic. To support the mission, the task force engineer and assigned soldiers must expediently strengthen the bridge.

As the U.S. Army's role throughout the world has increased over recent years, the above scenario has become all too common. Current methods available to the military for bridge retrofit (i.e., upgrade) are time-consuming and difficult to accomplish with limited resources. Therefore, a research program is currently underway at the U.S. Army Engineer Research and Development Center (ERDC) to develop rapid bridge repair and retrofit techniques for the military.

The most promising rapid retrofit method involves the use of lightweight, nonmetallic, fiber-reinforced composite materials to repair and strengthen concrete structures (Emmons et al. 1998a,b). A common repair method currently in use is to adhesively bond strips or "plates" of thin composite material laminates to the surfaces of concrete beams or slabs to repair them or to increase their capacity. The key issues and background literature associated with retrofitting concrete beams with fiber-reinforced polymeric (FRP) strips can be found in the paper by Buyukozturk and Hearing (1998).

The method used to repair concrete beams with composite strips is similar to one that has been used to repair concrete beams with steel plates (Swamy, Jones, and Bloxham 1987). In one current method, the composite strip is adhesively bonded to the concrete surface with a room-temperature curing, two-part epoxy adhesive. This procedure is very time-consuming. It takes substantial time to clean and smooth the concrete surface, possibly sandblasting, to make it suitable for bonding. In addition, the two-part epoxy system must be mixed in a precisely controlled fashion and must be applied in a labor-intensive manner to produce a good bondline. Following the application of the adhesive, the strip must be clamped in place while the adhesive cures. Other systems that make use of preformed fiber fabrics and apply the epoxy resin system to the fabric and the concrete simultaneously encounter the same difficulties with concrete surface preparation and postcuring (Emmons et al. 1998a,b).

In addition to the difficulties associated with the bonding of the strips, there is a critical need to provide some form of mechanical anchorage to the composite strip at its ends to prevent catastrophic brittle failure of the strengthened beam by peeling or debonding (Spadea, Bencordino, and Swamy 1998, Buyukozturk and Hearing 1998, Arduini and Nanni 1997). Similar mechanical anchorages are also recommended for use with epoxy bonded steel plates (Hussain et al. 1995).

While these types of systems have been demonstrated as effective in a wide range of civilian applications, there are hindrances to the adoption of this technology for military use. Any adhesively bonded system will require time for the bondline to cure to ensure effective transfer of load from the existing member into the retrofit. In addition, proper surface preparation of the substrate must be completed for the bond to be effective. This often requires special tools and time-consuming labor. Environmental control during application is critical. Obviously, in many situations, Army personnel will not have the time nor equipment to effect a proper application of adhesively bonded FRP materials. Furthermore, Army operations are conducted under the broadest range of climatic conditions.

To overcome the hindrances described above for the military, this research study has investigated the use of powder-actuated fastening systems to attach the composite strips to the concrete. Such tools are readily available in military engineering and construction units and do not require trained personnel to operate. This repair method is extremely rapid and could meet the Army's need for rapid repair in the operational environment (Lamanna, Bank, and Scott 2001a).

During the first year of work, concluded in November 1999, several coupon tests were performed on fastened connections to examine the effects of driving the fastener though the composite strip and into the concrete. Small-scale beams, 152 x 152 x 1,219 mm (6 x 6 x 48 in.), were strengthened and tested to determine the feasibility of this method and compared to Whitney stress block models (Bank and Lamanna unpublished).

During coupon testing, it was discovered that several requirements must be met to develop strength in the connection. First, a neoprene-backed washer must be used to prevent damage to the composite strip when the fastener is attached. Second, a sufficient fastener embedment in the concrete substrate must be achieved. The third requirement is that the strip contain adequate bidirectional reinforcement to develop bearing capacity and prevent splitting failure during fastener penetration.

During beam testing, the edge distance played an important role in the amount of precracking that occurred when driving the fasteners into the concrete. The farther from the edge, the less precracking occurred. The attached composite strip also had a greater strengthening effect after yield if fewer cracks were caused when the strip was attached.

The second year has shown that this method is comparable to the current methods of strengthening reinforced concrete beams by bonding composite strips

(Lamanna, Bank, and Scott 2001b, Ray et al. 2000, and Mason 2000). The full-scale tests conducted during this study have proved that this method can be used on larger beams.

2 Technical Objective and Scope

The objective of the research was to continue the development of a unique method to rapidly strengthen concrete beams with FRP composite materials using powder-actuated fastening systems. The research was conducted during the second year of an ongoing study funded by ERDC.

The scope of the work during the second year study was to:

a. Develop an analytical model to predict the response of full-size strengthened beams.

b. Design a test plan for full-size beams.

c. Test full-size beams.

d. Analyze results of full-size beam tests.

e. Optimize pultruded strips.

3 Analytical Model

The analytical model employed in this work utilizes equilibrium, strain compatibility of the sections involved, and the constitutive relations of the materials. Several assumptions were made in developing this analytical model:

a. Plane sections remain plane after bending. That means there exists a linear variation in strain over the cracked concrete cross section.

b. The steel exhibits a bilinear stress-strain behavior. Coupon testing of steel rebars shows strain hardening properties after the yield stress is reached. A postyield modulus equal to 1.7 percent of the initial elastic modulus was used (Soroushian and Choi 1991).

c. No slip occurs between the steel bars and the surrounding concrete.

d. Concrete in compression follows the Hognestad stress-strain relationship (Wang and Salmon 1998).

e. The concrete in tension carries no load. This assumption was used because it was thought that the fasteners cause cracking in the tensile zone during the attachment of the strengthening strip.

f. There is uniform stress and strain throughout the depth of the composite strengthening strip. This model assumes the entire strip strains the same amount at each cross section. This assumption is valid, since the strip is very thin compared to the depth of the concrete beam.

g. There is uniform stress and strain across the width of the composite strengthening strip. This assumption ignores shear lag and assumes the stress is the same across the width of the strip.

h. The strengthening strip does not affect shear strength. This neglects any increase in the shear capacity through dowel action of the strip. Dowel action is usually neglected when determining the shear capacity of FRP reinforced concrete members (American Concrete Institute (ACI) 440H and ACI 440F (ACI 2000a,b)). Any reduction in shear capacity from cracks formed while attaching the strip is neglected. The cracks formed are small enough that shear can still be transferred through aggregate interlock.

i. The fasteners in the shear span transfer all of the load between the concrete and the FRP strip. This assumption is supported by the strain distributions obtained during the full-scale testing.

j. Strain compatibility along the entire strengthening strip and the concrete beam is maintained. Currently, this assumption neglects the effect of slip caused by rotation of the fasteners, crushing of the surrounding concrete, cracking of the concrete cover, and bearing damage in the composite strip.

The model will be modified during the third year of this project in an attempt to remove the need for the last assumption, *j*.

Moment-Curvature Relationship

The linear strain distribution through the cross section is shown in Figure 1. The notation is explained in the notation section of this report. Using similar triangles, the strain in the compression steel, tensile steel, and FRP strengthening strip can be found in terms of the strain in the concrete as follows:

$$\varepsilon_s = \frac{\varepsilon_c}{c}(d-c) = \varepsilon_c\left(\frac{d}{c}-1\right) \tag{1}$$

$$\varepsilon_s' = \frac{\varepsilon_c}{c}(c-d_{cs}) = \varepsilon_c\left(1-\frac{d_{cs}}{c}\right) \tag{2}$$

$$\varepsilon_{frp} = \frac{\varepsilon_c}{c}(d_{frp}-c) = \varepsilon_c\left(\frac{d_{frp}}{c}-1\right) \tag{3}$$

The corresponding stresses in the cross section under the given linear strain distribution and the corresponding forces are also shown in Figure 1.

The compression force in the concrete is expressed using a depth factor γ and a magnitude factor α, derived from the Hognestad model for concrete in compression (Wang and Salmon 1998). The Hognestad model for concrete in compression is shown in Figure 2 (Hognestad 1951). These depth and magnitude factors are:

For $\varepsilon_c \le 0.002$:

$$\alpha = -83{,}000\varepsilon_c^2 + 500\varepsilon_c$$
$$\gamma = \frac{\left(\frac{1}{3} - 41.7\varepsilon_c\right)}{\left(1-166.7\varepsilon_c\right)} \tag{4a}$$

For $0.002 < \varepsilon_c \le 0.0038$:

$$\alpha = 1.15 - 37.5\varepsilon_c - \frac{0.000817}{\varepsilon_c}$$
$$\gamma = 1 - \frac{\left(-25\varepsilon_c^3 + 0.575\varepsilon_c^2 - 0.0000004\right)}{\left(-37.5\varepsilon_c^3 + 1.15\varepsilon_c^2 - 0.000817\varepsilon_c\right)} \quad (4b)$$

Applying equilibrium to the cross section yields

$$C_c + C_s' - T_s - T_{frp} = \alpha c b f_c' + A_{cs}\sigma_s' - A_s\sigma_s - A_{frp}\sigma_{frp} = 0 \quad (5)$$

Using the stress-strain relationships for steel and FRP, this equation becomes

$$\alpha c b f_c' + A_{cs}E_s\varepsilon_s' - A_sE_s\varepsilon_s - A_{frp}E_{frp}\varepsilon_{frp} = 0 \quad (6)$$

When the tensile steel has not yielded, using Equations 1, 2, and 3, Equation 6 becomes

$$\alpha c b f_c' + A_{cs}E_s\varepsilon_c\left(1 - \frac{d_{cs}}{c}\right) - A_sE_s\varepsilon_c\left(\frac{d}{c} - 1\right) - A_{frp}E_{frp}\varepsilon_c\left(\frac{d_{frp}}{c} - 1\right) = 0 \quad (7)$$

After the tensile steel has yielded, Equation 6 becomes

$$\alpha c b f_c' + A_{cs}E_s\varepsilon_c\left(1 - \frac{d_{cs}}{c}\right) - A_s\left[f_y + E_{pys}\left(\varepsilon_c\left[\frac{d}{c} - 1\right] - \frac{f_y}{E_s}\right)\right] - A_{frp}E_{frp}\varepsilon_c\left(\frac{d_{frp}}{c} - 1\right) = 0 \quad (8)$$

Equations 7 and 8 are quadratic equations that can be solved in closed form in terms of the depth to the neutral axis, c. Thereafter, the depth to the neutral axis, c, can be used to solve for the moment on the cross section by taking the sum of moments about the concrete force resultant:

$$M = A_s\sigma_s\left(d - \gamma c\right) + A_{frp}\sigma_{frp}\left(d_{frp} - \gamma c\right) + A_{cs}\sigma_s'\left(\gamma c - d_{cs}\right) \quad (9)$$

The curvature is found from:

$$\phi = atan\left(\frac{\varepsilon_c}{c}\right) \quad (10)$$

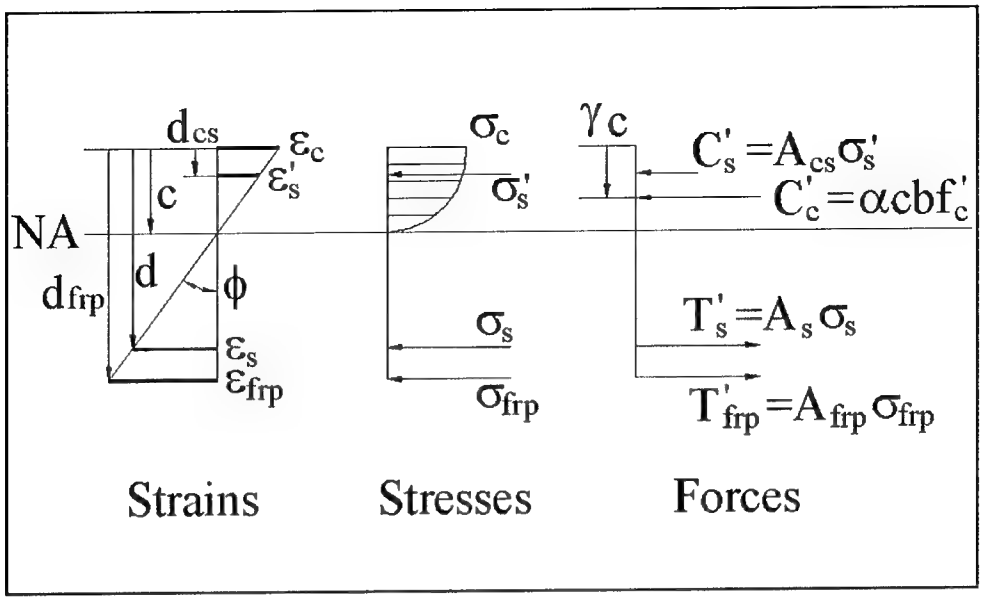

Figure 1. Reinforced concrete beam with attached composite strip

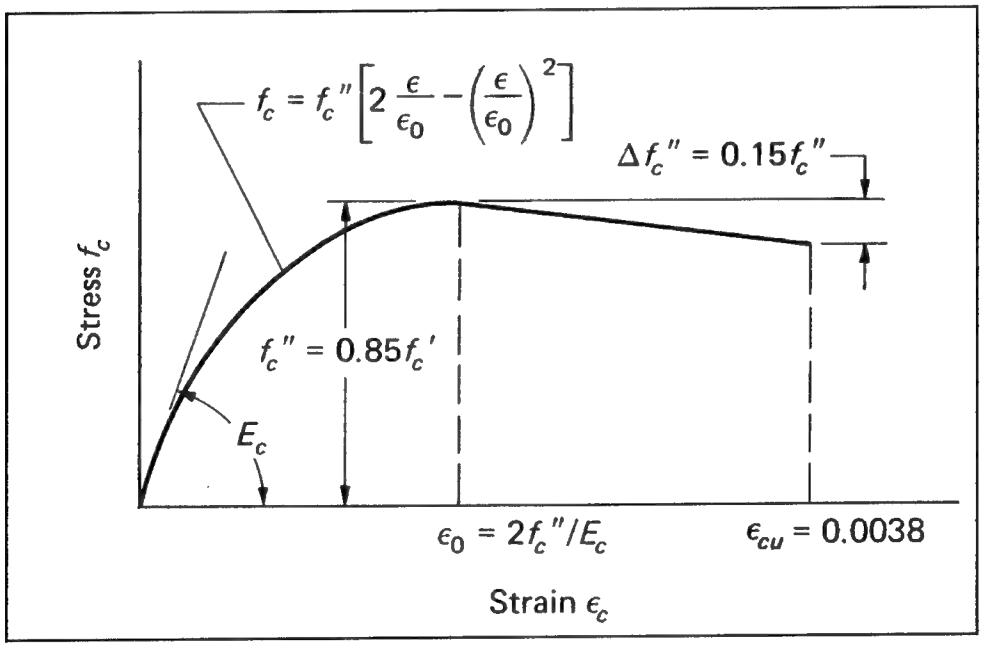

Figure 2. Hognestad's stress-strain diagram for concrete in compression

For any given strain in the extreme compression fiber of the concrete, the moment-curvature relationship can be found. The entire moment-curvature relationship can be found by incrementally increasing the strain in the top fiber until the stress in one of the material components exceeds the ultimate strength of that material, or until the concrete reaches the maximum compression strain of 0.0038. At each increment of strain in the top fiber, checks are made to ensure the composite strengthening strip has not failed and that the fasteners have not exceeded their maximum capacity. Each increment of strain results in a moment

and curvature pair. These pairs can be plotted to show the moment-curvature behavior of a beam with that cross section.

The maximum compression strain of 0.0038 comes from the Hognestad model that contains a linearly decreasing stress beyond the maximum strain that terminates at a strain of 0.0038. Since this model applies the stress over the entire compression region, the concrete at the top fiber may be in a state of less stress than the concrete lower in the section if the extreme concrete strain is in this linear region.

The typical method of determining the ultimate strength of reinforced concrete beams was modified for comparison purposes (Wang and Salmon 1998). The method was modified by adding the tensile force of the composite strengthening strip. This method utilizes the Whitney stress block to model the concrete stresses. This model was used both with and without compression steel for comparison purposes. It is important to note that in order to use the Whitney stress block models, the steel must be past its yield point when the concrete crushes. The Whitney stress block models assume the strip is still attached and does not fail before the concrete crushes.

Parametric Studies and Comparison of Models

Comparisons were made between the three available methods; the moment-curvature analytical model, the Whitney stress block with compression steel, and the Whitney stress block without compression steel. Parametric studies were conducted with all three models to study the effect of variations in material and geometric properties of the beams.

The configuration used for all three methods was the same as the beams tested at ERDC during July 2000: a 305 × 305 mm (12 × 12 in.) cross section, two #8 bars for tensile reinforcement, two #3 bars for compression reinforcement, and 35.3-MPa (5,113-psi) strength concrete with 25-mm (1-in.) clear cover. The large-scale beam dimensions and internal reinforcement layout are shown in Figure 3. A composite strip of area 323 mm^2 (0.5 $in.^2$) was used at the bottom of the beam for the baseline model. The analytical model was used with 46 fasteners per shear span, each with a strength of 4,448 N (1,000 lb) per fastener. The Whitney stress block methods assumed an infinitely strong and infinitely rigid connection between the composite strip and the concrete beam.

Variation of strip modulus

The ultimate strength of the strengthened beam was studied as a function of the strip modulus. All other parameters were unchanged from the baseline model. The modulus of this strip was varied from 0 to 96.6 GPa (14,000 ksi).

As expected, the ultimate moment of the strengthened beam increases with increasing modulus of the composite strip attached. Figure 4 shows the relationship between the ultimate moment and the strip modulus. The relationship is

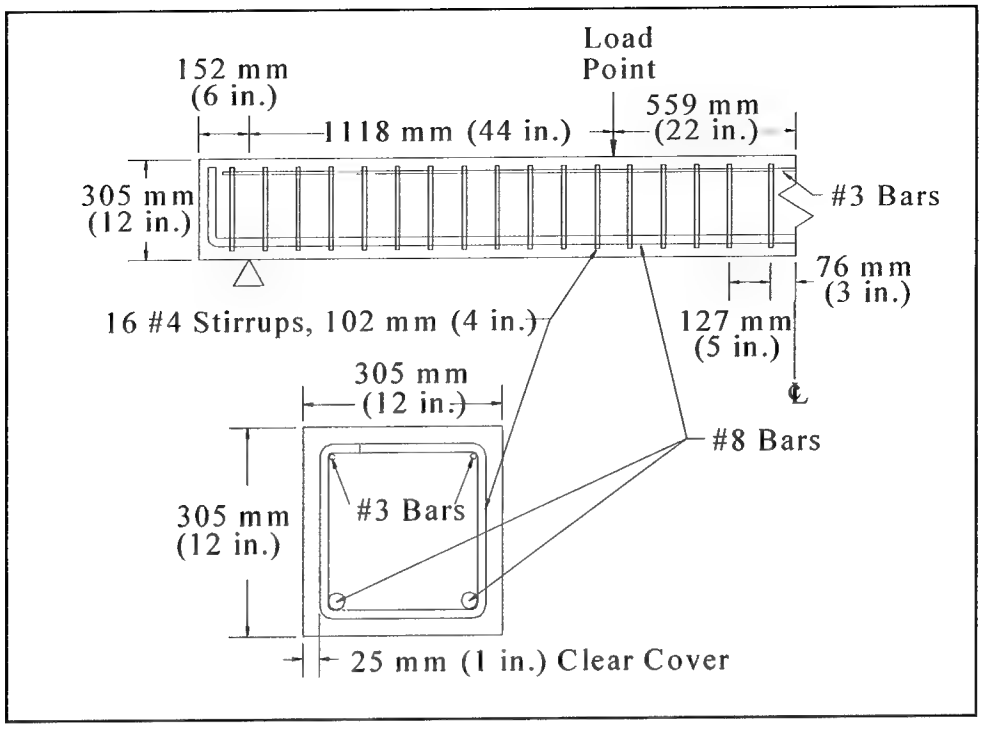

Figure 3. Large-scale beam dimensions and internal reinforcement layout

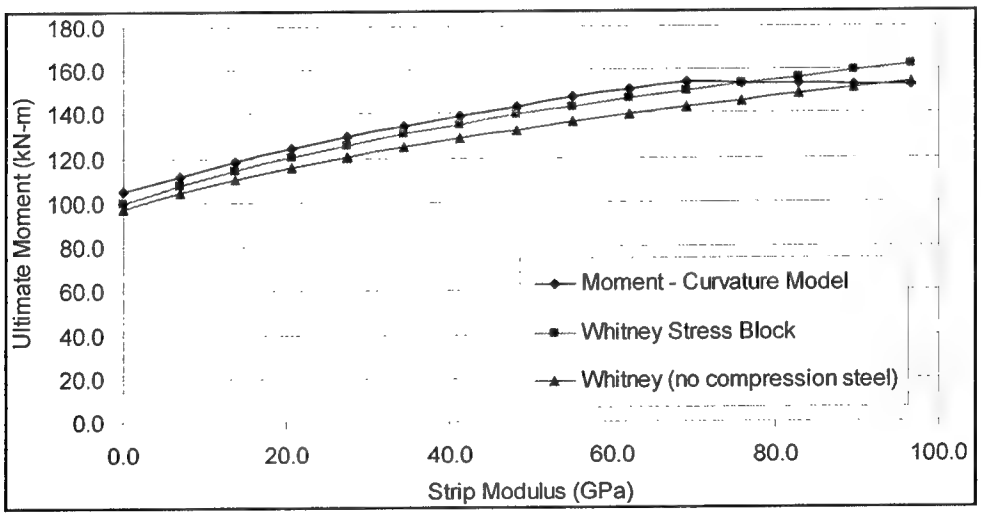

Figure 4. Ultimate moment versus strip modulus

fairly linear for all three methods up to a strip modulus of about 69.0 GPa (10,000 ksi). As the modulus of the strip is increased, the same amount of strain will induce more stress in the strip.

The forces in the strip must be transferred into the concrete through the fasteners. Increasing the modulus of the strip beyond 69.0 GPa (10,000 ksi) does not increase the ultimate moment of the strengthened beam, since failure of the beam results from the fasteners pulling out rather than failure of the concrete

compression. Increasing the modulus of the strip beyond the modulus that fails in the fasteners causes the ultimate moment to slowly decrease.

It is also useful to note the differences between the three methods. Until failure occurs in the fasteners, all three methods are fairly linear. In general, the Whitney stress block method predicts lower strengths than the analytical model. Neglecting the compression steel results in even lower strength predictions than the analytical model. However, the Whitney stress block methods do not include checks for fastener strength or strip strength. Once the analytical model becomes limited by these strength checks, the Whitney stress block method incorrectly predicts a higher strength than the analytical model.

It should also be noted that a strip of half the modulus but double the area resulted in the same strengthening effect. This shows that it is the total axial stiffness, EA, that increases the amount of strengthening.

Variation in concrete compressive strength

Another useful comparison is to examine the change in ultimate moment while changing the concrete compressive strength. Again, the beam dimensions used were the same that were tested at ERDC in July 2000. The strengthened beams for this comparison were strengthened with a Hybrid 1.5 strip of modulus 57.2 ± 4.5 GPa (8,291 ± 653 ksi) and area of 323 mm^2 (0.5 $in.^2$). The concrete strength was varied from 13.8 MPa (2,000 psi) to 69.0 MPa (10,000 psi), and the results are shown in Figure 5.

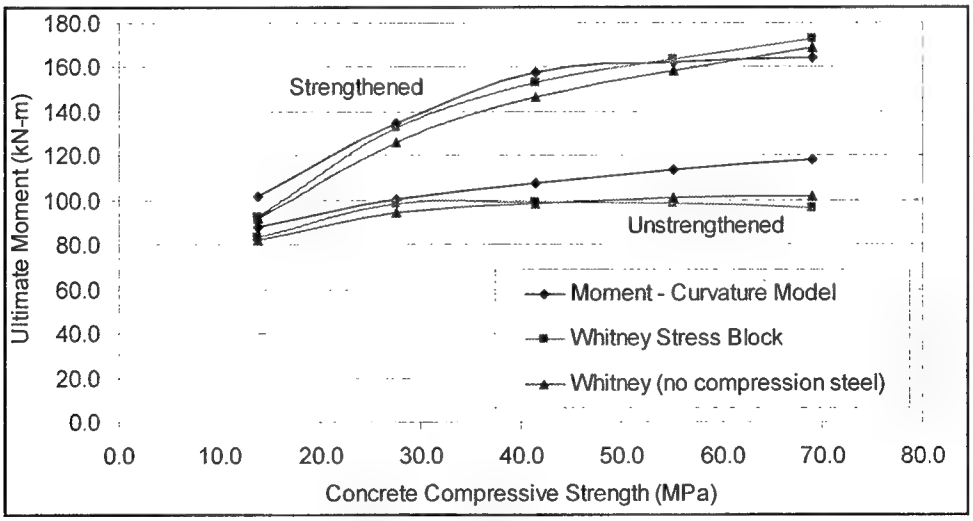

Figure 5. Ultimate moment versus concrete compressive strength

Predictions of the various methods are quite different for the unstrengthened beams. The analytical model shows a continuously increasing ultimate moment for increasing concrete compressive strength. The ultimate moment predicted by the Whitney stress block method that includes the compression steel increases when increasing the concrete compressive strength from 13.8 MPa (2,000 psi) to 41.4 MPa (6,000 psi). This begins to decrease upon further increase in the

concrete compressive strength. As the concrete compressive strength is increased, the neutral axis moves up through the compression steel. This change in the strength, resulting from the compression steel switch from compression to tension, is magnified by the use of the Whitney stress block. The ultimate strength predicted from the Whitney stress block method without compression steel continuously increases as the concrete compressive strength is increased. The rate of increase in the ultimate strength is less for higher concrete strengths because the beta factor, β_1, given by 10.2.7.3 of ACI 318-99 (ACI 1999) decreases for increasing concrete strengths up to 55.2 MPa (8,000 psi).

All three methods show that the amount of strengthening in the beams increases with increasing concrete strength. As with the case of increasing the strip modulus, increasing the concrete compressive strength beyond a certain point reduces the effect of the strengthening because the fasteners begin to fail. The Whitney stress block methods do not include the effect of the fasteners, which explains the higher concrete strength region of the graph where the Whitney methods predict higher strength than the analytical model.

Variation in reinforcement ratio

Reinforcement ratios are typically limited to 25 to 75 percent of ρ_{bal}, the balanced reinforcement ratio, to prevent sudden and catastrophic failure of the concrete member. The balanced reinforcement ratio is the reinforcement ratio at which the concrete would fail in compression at the same load level that the tensile steel would yield. Figure 6 shows the ultimate moment for an increasing reinforcement ratio of an unstrengthened beam and a beam strengthened using a strip of modulus 57.2 GPa (8,291 ksi) and area of 323 mm^2 (0.5 in.^{2}). This strip corresponds to the modulus of the Hybrid 1.5 strip described later. The area of the tension steel was varied to vary the reinforcement ratio. The reinforcement ratio is the tensile steel reinforcement ratio and neglects the addition of the FRP strip as tensile reinforcement.

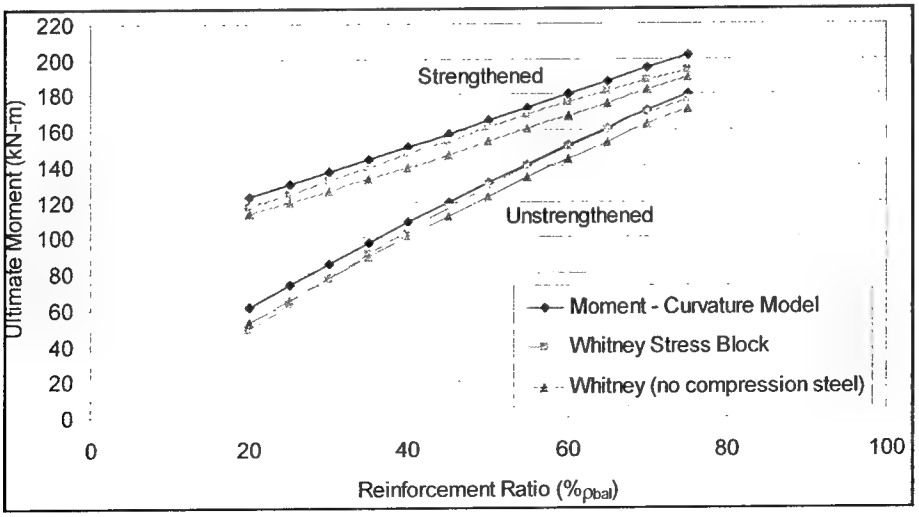

Figure 6. Ultimate moment versus reinforcement ratio as percent of ρ_{bal}

The most significant trend shown in Figure 6 is that as the reinforcement ratio increases, the amount the beam can be strengthened decreases. The ultimate moment of the strengthened beam and that of the unstrengthened beam converges as the reinforcement ratio approaches the balanced reinforcement ratio. This shows that more heavily reinforced beams cannot be strengthened as much as lightly or moderately reinforced concrete beams. The graph also shows that at a reinforcement ratio of about 60 percent that of ρ_{bal}, the ultimate moment predicted using the Whitney stress block method with compression steel is very close to the ultimate moment predicted by the analytical model for an unstrengthened beam. However, changing the reinforcement ratio in either direction causes the ultimate moment predicted by the Whitney stress block model with compression steel to be less than that predicted by the analytical model.

Variation in depth to tensile steel

Increasing the depth from the top compression fiber of the concrete to the layer of tensile steel typically increases the ultimate moment of a reinforced concrete beam. The three models were used to predict the ultimate moment of the concrete beam, while varying the depth to the tensile steel. The concrete cover was left the same, so the depth to the composite strengthening strip was always 52.39 mm (2.0625 in.) greater than the depth to the tensile steel. Figure 7 shows the variation in the ultimate moment with increasing depth to the tensile steel. Since the area of tensile steel is unchanged, the reinforcement ratio as a percent of ρ_{bal} is also plotted along the right hand axis. The ρ_{bal} of the beams examined in this parametric study and the beams tested at ERDC was 3.43 percent.

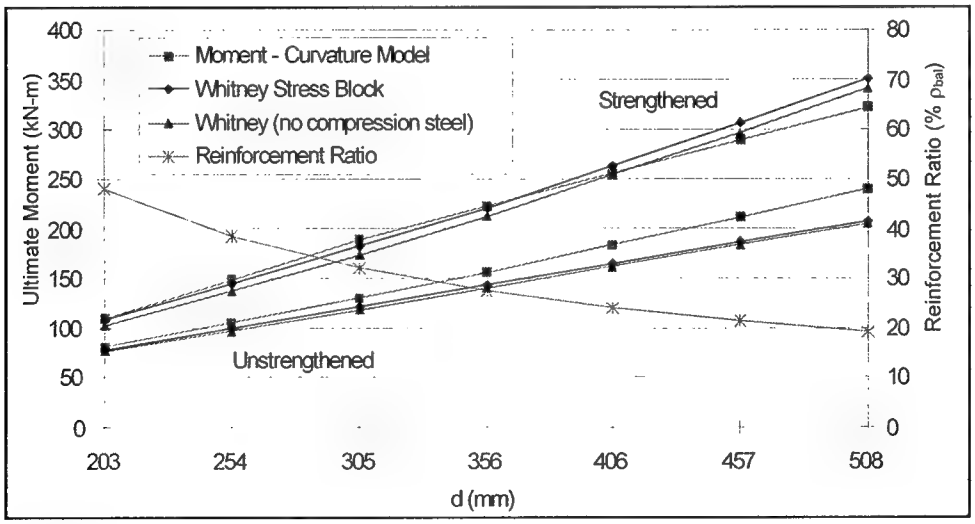

Figure 7. Moment versus depth to tensile steel holding A_s constant

As the depth to the tension steel, d, increases, the ultimate moment of the unstrengthened beams increases, because when calculating the moment, the lever arm is increased. This trend can be seen in all three models. The models also predict an increase in the ultimate moment of the strengthened beams. At values

of d over 356 mm (14 in.), the moment-curvature model predicts failure in the fasteners. This can be seen in the moment-curvature model predicting lower ultimate moments than the Whitney stress block models. This trend is similar to the trend seen in the variation of the reinforcing ratio. The higher the d value, the lower the reinforcement ratio.

To see the effect of increasing the depth to the tensile steel uncoupled from the effect of changing the reinforcement ratio, the three models were used to predict the ultimate moment of the beams while increasing the depth to the tensile steel. This time the area of tensile reinforcement was changed to maintain a reinforcement ratio of 1.3167 percent. This was the reinforcement ratio of the beams tested at ERDC. Figure 8 shows the variation in ultimate moment with increasing depth to the tensile steel, while holding the reinforcement ratio constant.

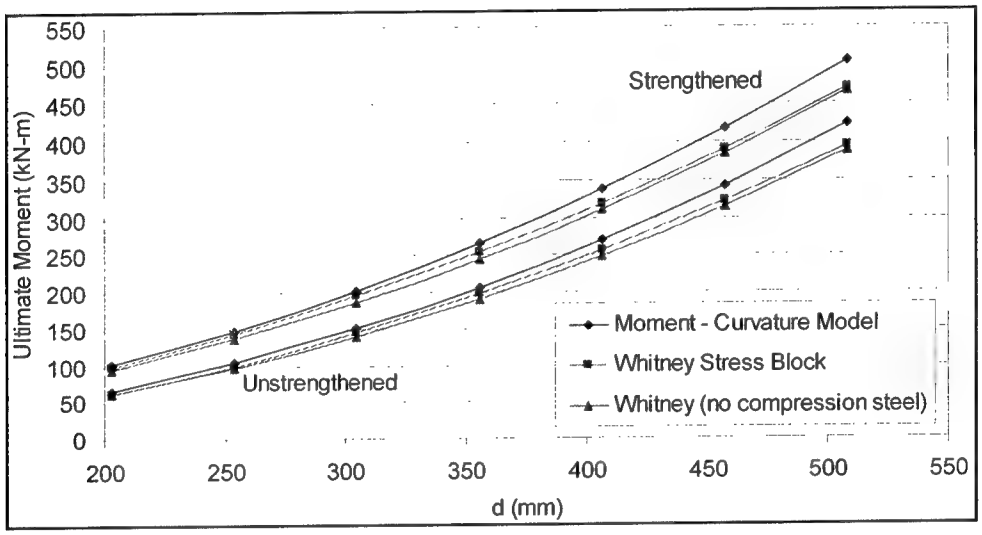

Figure 8. Moment versus depth to tension steel while holding the reinforcement ratio constant

Since the area of tensile steel was increased with the increasing depth, Figure 8 shows a greater rate of increase in the ultimate moment than Figure 7, which kept the area of tensile steel constant. The amount of the strengthening effect increases in amount slowly as the depth is increased, but the increase in ultimate moment decreases as a percent of the original unstrengthened moment. The strengthening effect is less for higher values of d because the area of steel is greater, but the area of the strengthening strip remains the same. This means the area of the strengthening strip is smaller in relation to the area of the steel reinforcement. Further studies will be conducted during the third year of research.

4 Optimization of FRP Strengthening Strips

FRP strips having three different target moduli were designed so that the effect of strip modulus could be studied in the full-scale beam experiments. Target moduli of 13.8, 27.6, and 55.2 GPa (2,000, 4,000, and 8,000 ksi) were chosen and termed standard, intermediate, and hybrid. Two hybrid strips were made, one with 1,484-g/m^2 (1.0-oz/ft^2) mats and one with 2,225-g/m^2 (1.5-oz/ft^2) mats. All strips were designed to have the same dimensions of 102 by 3.2 mm (4.0 × 0.125 in.) for reasons of economics.

All of the FRP strengthening strips were designed at the University of Wisconsin and specially pultruded for research purposes by Strongwell in Chatfield, MI. All strips were made using an identical vinylester resin with no pigments or fillers. Longitudinal tests according to American Society for Testing and Materials (ASTM) D 3039 (ASTM 1999) were conducted on the strips to determine their longitudinal elastic modulus and longitudinal tensile strength. A summary of the results of these tests is given in Table 1. Load-deflection curves and testing data for the FRP strengthening strips is presented in Appendix A.

Table 1
Longitudinal Properties of Manufactured FRP Strips

Strip Type	Elastic Modulus GPa	Standard Deviation GPa	COV %	Tensile Strength MPa	Standard Deviation MPa	COV %
Standard	15.2	2.9	19.0	325	81.7	25.1
Intermediate	26.3	1.0	3.7	695	35.5	5.1
Hybrid 1.0	56.9	2.1	3.6	916	29.0	3.1
Hybrid 1.5	57.2	4.5	7.9	828	63.0	7.7

Standard Strip

The standard strip was designed to contain only continuous strand mat and have a target modulus of 13.8 GPa (2,000 ksi). The continuous strand mats provide the bearing strength to the strengthening strip, which is needed in the area around the fasteners. This strip was designed to have two layers of 102-mm (4.0-in.)-wide, 1,484-g/m^2 (1.0-oz./ft^2) continuous strand mat, two layers of 108-mm (4.25-in.)-wide, 2,225-g/m^2 (1.5-oz./ft^2) continuous strand mat, and twenty 113-yield E-glass rovings. A 113-yield roving denotes there are

113 yd per pound or 227.5 m per kilogram. This is the "standard" reinforcement for a typical commercial grade FRP pultruded plate.

The standard strip had a modulus of 15.2 ± 2.9 GPa (2,205 ± 420 ksi) based on 11 tests and a strength of 325 ± 81.7 MPa (47.1 ± 11.8 ksi) based on 14 tests. The standard deviation of the tests was very high because the strips consisted of mostly continuous strand mat, which caused the failure to occur at random points of weakness within the specimen. The specimens cut from the standard strip failed by sudden fracturing across the width. An example of this failure mechanism is shown in Figure 9.

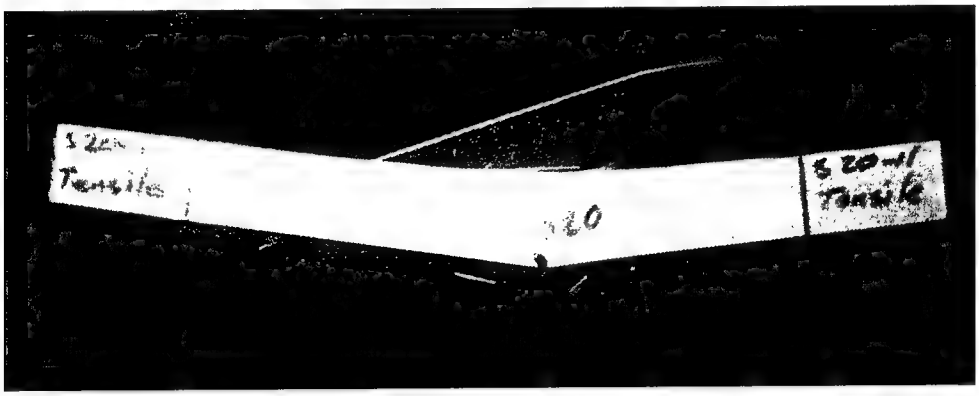

Figure 9. Failure across the standard strip

Intermediate Strip

The intermediate strip was designed to contain two layers of continuous strand mat and as many glass rovings as possible. This placed the target modulus at 27.6 GPa (4,000 ksi). The rovings provide the longitudinal stiffness and strength while the continuous strand mats provide the bearing strength around the fasteners and help keep the strip from splitting apart when the fasteners are driven through the strip and into the concrete. The strip was designed to have two layers of 108-mm (4.25-in.)-wide, 2,225-g/m^2 (1.5-oz/ft^2) continuous strand mat, and fifty-six 113-yield E-glass rovings.

The intermediate strip had a modulus of 26.3 ± 1.0 GPa (3,816 ± 140 ksi) based on 11 tests and a strength of 695 ± 35.5 MPa (100.8 ± 5.1 ksi) based on 13 tests. The standard deviation is much less than that of the standard strips because there were only two layers of mat in the intermediate strip instead of four layers as in the standard strip. The intermediate specimens failed first by failure in the glass rovings, which then immediately caused the mats to rupture. The high roving content caused the specimen to splinter. This failure mechanism is shown in Figure 10.

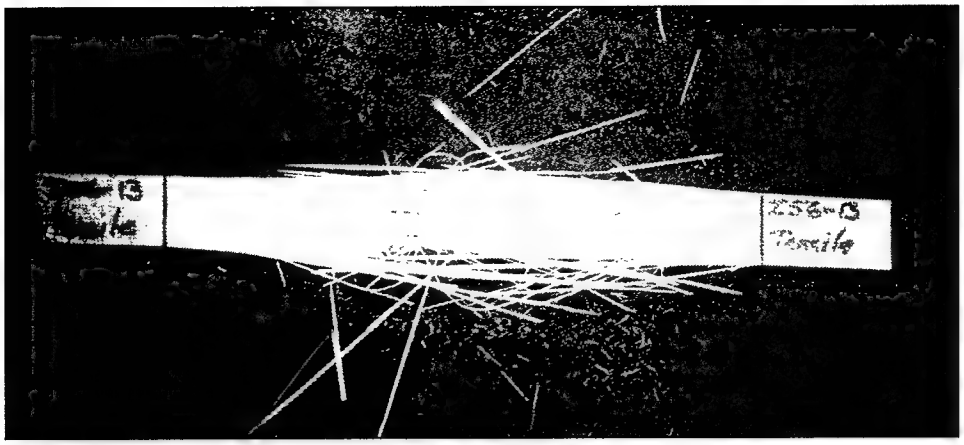

Figure 10. Splintering of the intermediate strip

Hybrid Strips

Hybrid strips were designed to utilize two layers of continuous strand mat and a combination of E-glass rovings and carbon tows to obtain a target design modulus of 55.2 GPa (8,000 ksi). To help understand the effect of the continuous strand mats on the bearing strength of the composite strengthening strips, two types of hybrid strips were designed, using different weight mats. The hybrid 1.5 strip was designed with two layers of 108-mm (4.25-in.)-wide, 2,225-g/m^2 (1.5-oz/ft^2) continuous strand mat, twenty-one 113-yield E-glass rovings, and 138 Graphil 12k standard modulus carbon tows. The Hybrid 1.0 mat was designed with two layers of 108-mm (4.25-in.)-wide, 1,484 g/m^2 (1.0-oz/ft^2) continuous strand mat, forty-five 113-yield E-glass rovings, and 109 Graphil 12k standard modulus carbon tows.

The Hybrid 1.5 strip had a modulus of 57.2 ± 4.5 GPa (8,291 ± 653 ksi) based on 16 tests and a strength of 828 ± 63 MPa (120.1 ± 9.2 ksi) based on 20 tests. The hybrid 1.0 strip was found to have a modulus of 56.9 ± 2.1 GPa (8,254 ± 301 ksi) based on 11 tests and a strength of 916 ± 29 MPa (132.9 ± 4.2 ksi). The hybrid specimens failed first in the carbon tows, which reduced the amount of load carried by the specimens by about one-half. The specimens then continued to carry this reduced amount of load until the glass rovings failed, which immediately caused the mats to rupture. A typical hybrid strip failure is shown in Figure 11.

Figure 11. Splintering failure of hybrid strip

5 FRP/Concrete Connection Tests

In order to understand the overall behavior of a beam strengthened by attaching a composite strengthening strip with powder-actuated fasteners, it is necessary to examine the behavior of individual connections. An individual connection consists of three components: the concrete substrate, the steel fastener and fastener accessories, and the FRP strip.

The majority of these tests were conducted on 305- x 203- x 102-mm (12- x 8- x 4-in.)-rectangular concrete blocks cast out of 41.4 MPa (6,000 psi) concrete with a maximum size aggregate of 25 mm (1 in.). The remaining tests were on blocks cut from the 1,219- x 152- x 152-mm (48- x 6- x 6-in.) beams untested from the first year of this project. Different types of fasteners and fastener configurations were tested, as well as all four types of composite strips designed for this project. FRP/Concrete testing data are presented in Appendix B.

Fastening System Description

A powder-actuated fastening system drives a fastener into a concrete substrate. As the fastener penetrates, the concrete is compressed as material is displaced. When the fastener is driven into the concrete, the surface of the fastener becomes deformed and generates friction with the surrounding material. The heat generated in this process causes sintering and creates a bond between the concrete and fastener (Comite Euro-International da Beton (CEB) 1994). These two factors give the fastener its holding capacity.

A Hilti DX A41 Powder-Actuated Fastening system was used for this research. The DX A41 uses a 6.8-mm (0.27-in.) caliber short gunpowder booster. The different varieties of fasteners are shown in Table 2. Fasteners of the same type are differentiated by listing the length in millimeters following the designation.

Table 2 Hilti Fasteners Used in Research			
Fastener #	**Type**	**Intended Use**	**Shank Diam, mm**
1	X-ALH	High-Strength Concrete and High-Grade Steel	4.0 (22-mm length), 4.5 (27-mm length)
2	X-DNI	Concrete and Steel	3.7
3	X-ZF	Concrete and Steel	3.5

Testing Procedure

A connection was prepared by resting the concrete block on the floor and holding the composite strip in place on the top of the concrete block. If the connection was predrilled, the predrilling was done with a DX-Kwik bit, which had a diameter of 4.76 mm (0.188 in.) and a drill bit length of 15.88 mm (0.625 in.). A standard hammer drill was used with this special bit. Figure 12 shows this special drill bit in a hammer drill. This special DX-Kwik bit was used to drill though the composite strip into the concrete. Then the gunpowder booster and the fastener were loaded into the Hilti gun, and the fastener was driven through the composite strip and into the concrete through the predrilled hole. If the connection was not predrilled, the fastener was then driven though the composite strip and into the concrete. All tests used an 18-mm (0.7-in.)-diameter neoprene-backed washer to provide clamping pressure and prevent the fastener head from digging into the composite strip causing premature failure.

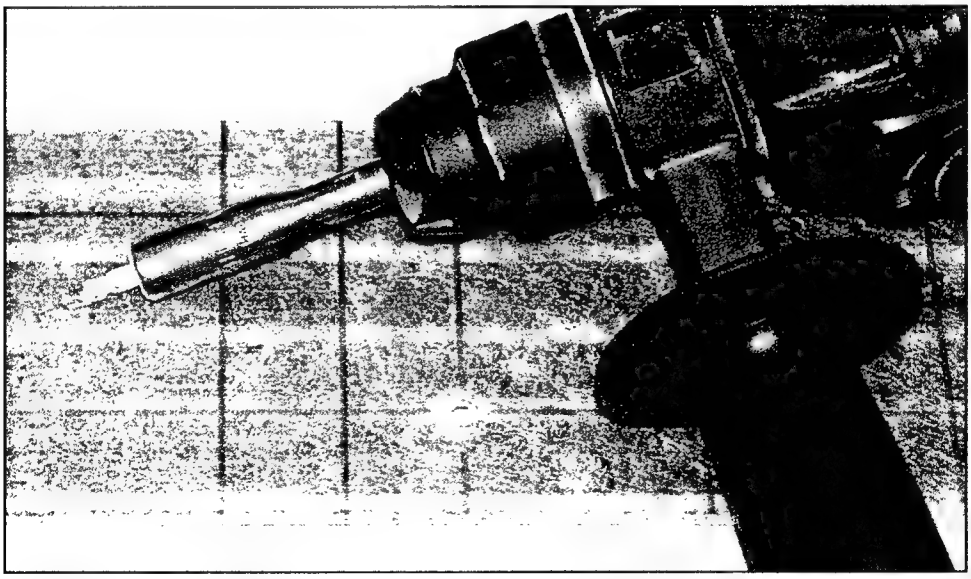

Figure 12. Hilti DX-Kwik bit in a hammer drill next to a hole drilled through the composite strip and into the concrete

The test specimen was then inserted into a 5-kip MTS test frame designed and used during the first year of research. The block was then held down by a steel plate and tightened with two 25-mm (1-in.) nuts. The composite strip was then held between two toothed clamps. The test fixture is shown in Figure 13.

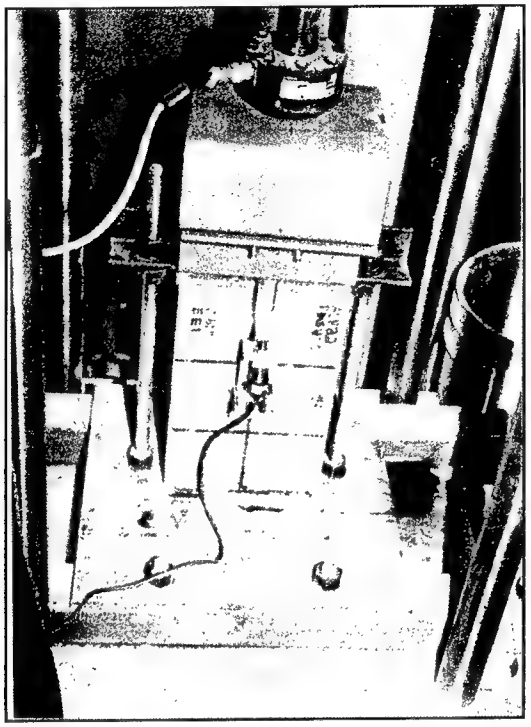

Figure 13. FRP/concrete connection test fixture

Standard Strip Connection Tests

Two sets of connection tests were performed on the standard strip. Both sets used a 25-mm (1-in.)-wide piece of the standard strip. The first set of tests was called Standard A and used a single 27-mm-long DNI fastener (Table 2). Standard B used a single 32-mm ZF fastener (Table 2). In both series of tests, there were a few specimens that failed at relatively low loads in the concrete substrate. These failures are initiated by spalling damage caused while driving the fastener into the concrete to make the connection. The remaining specimens failed by bearing in the composite strip, which resulted in a slot-shaped hole where the fastener ripped through the material. An example of this failure mechanism is shown in Figure 14. During the first year, tests conducted using only steel washers with no neoprene backing showed only cleavage failures. This shows that the bearing failure mode occurred instead of a cleavage-type failure mode, because the neoprene-backed washer confined the composite strip.

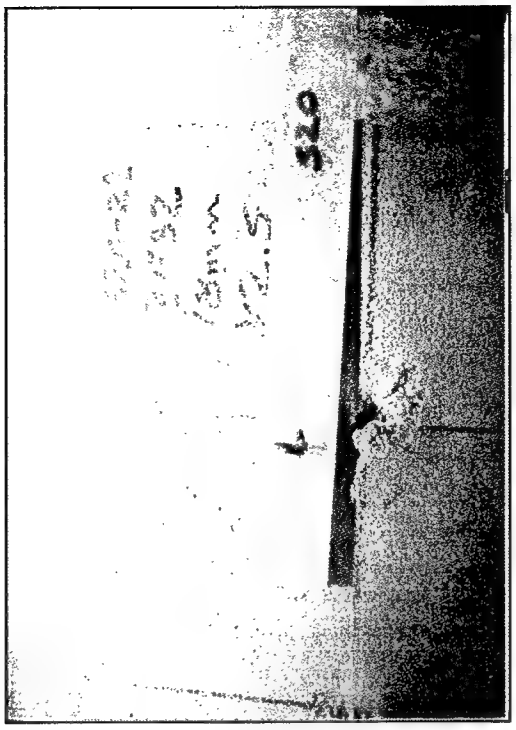

Figure 14. Slot-shaped hole signifying bearing failure

Standard A tests averaged a maximum load of 5.4 ± 2.4 kN (1,212 ± 530 lb) based on 10 tests. Three of the connections failed by bearing in the composite strip, while the other seven tests failed in the concrete substrate. Two specimens failed at low loads of 2.4 and 3.4 kN (530 and 757 lb); much lower than the remaining specimens. The coefficient of variation was 43.7 percent for this series of tests.

Standard B tests averaged a maximum load of 7.6 ± 2.5 kN (1,698 ± 566 lb) based on 10 tests. Six of the connections failed by bearing in the composite strip, while three failed in the concrete substrate, and one failed by fracture of the fastener. Similar to the standard A tests, this series had two concrete failures at low loads of 1.6 and 4.8 kN (352 and 1,070 lb).

Intermediate Strip Connection Tests

One set of connection tests were performed on the intermediate strip. This set used a single 32-mm ZF fastener through a 25-mm (1-in.)-wide piece of intermediate strip. These tests averaged a maximum load of 7.2 ± 2.4 kN (1,619 ± 547 lb) based on 10 tests. Five tests failed by bearing in the composite strip, one failed by cleavage in the composite strip, and four failed in the concrete substrate. A number of specimens failed at relatively low loads, 2.8 and 3.0 kN (630 and 679 lb), in the concrete substrate. These failures were initiated by spalling damage caused while driving fastener into the concrete to make the connection.

Hybrid 1.0 Strip Connection Tests

One set of connection tests were performed on the Hybrid 1.0 strip. This set used a single 32-mm ZF fastener through a 25-mm (1-in.)-wide piece of Hybrid 1.0 strip. These tests averaged a maximum load of 6.0 ± 2.6 kN (1,354 ± 587 lb) based on 10 tests. Four tests failed by bearing in the composite strip and six failed in the concrete substrate. There was one specimen that failed at a low load of 1.4 kN (937 lb) in the concrete substrate. This failure was initiated by spalling damage caused while driving the fastener into the concrete to make the connection.

Hybrid 1.5 Strip Connection Tests

Four sets of tests were performed with the Hybrid 1.5 strips, two with single fasteners, and two with multiple fasteners. Less spalling was observed upon the driving of the fastener through the Hybrid 1.5 strip than was observed driving the fastener though the other strips.

In Hybrid 1.5 A series tests, a single 32-mm ZF fastener was driven though a 25-mm (1-in.)-wide Hybrid 1.5 strip. These tests averaged a maximum load of 6.9 ± 1.5 kN (1,555 ± 348 lb) based on 10 tests. Two tests failed in the concrete substrate, while the rest failed by bearing in the composite strip. The two concrete failures occurred at higher loads than the concrete failures in the tests with other strips. The coefficient of variation was also reduced to 22.4 percent; much lower than the coefficients of 33.3, 33.8, and 43.3 percent for the standard B, intermediate A, and Hybrid 1.0 A tests.

In Hybrid 1.5 B series tests, a single 47-mm ALH fastener was driven into a predrilled hole through a 25-mm (1-in.)-wide Hybrid 1.5 strip. The hole was predrilled through the composite strip. There was concern with using the small concrete blocks with a long fastener because of edge effects. These tests averaged a maximum load of 5.6 ± 1.0 kN (1,251 ± 219 lb) based on 10 tests. Three tests failed by the concrete block's splitting apart, one by failure in the concrete substrate, one by fracture of the fastener, and five by bearing failure in the composite strip. The coefficient of variation was reduced even further, to 17.5 percent, than the Hybrid 1.5 A series.

In Hybrid 1.5 C series tests, two 47-mm ALH (Table 2) fasteners were driven into predrilled holes through a 25-mm (1-in.)-wide Hybrid 1.5 strip. These fasteners were aligned in series along the direction of the applied load. These tests were performed on 305- × 152- × 152-mm (12- × 6- × 6-in.) blocks cut from unused beams from the first year of the study. Some blocks were cut from beams containing rebar cages, while others were cut from beams without rebar cages. These tests averaged a maximum load of 14.7 ± 1.8 kN (3,308 ± 410 lb) based on 10 tests. The coefficient of variation of all 10 tests was 12.4 percent. For the six tests which were conducted on blocks with rebar cages, the COV was 8.7 percent, compared with a COV of 17.9 from the four tests without rebar cages. This shows that the short edge distance did play a role in the results of these tests, as the rebar cages helped hold the concrete block together.

In Hybrid 1.5 D series tests, two 47-mm ALH fasteners were driven into predrilled holes through a 102-mm (4-in.)-wide Hybrid 1.5 strip. These fasteners were aligned perpendicular to the direction of the applied load. These tests were performed on 305- x 152- x 152-mm (12- x 6- x 6-in.) blocks cut from unused beams with rebar cages from the first year. These tests averaged a maximum load of 12.4 ± 1.8 kN (2,798 ± 409 lb) based on five tests, and had a coefficient of variation of 14.6 percent.

Discussion of Connection Tests

It can be concluded from these tests that predrilling reduces the amount of spalling caused when driving the fastener into the concrete. The drilling reduces the amount of spalling by creating a larger area of material that can resist the forces induced by the penetrating fastener. As less spalling was observed in the predrilled tests, fewer low-load concrete failures occurred. The series of tests that were predrilled exhibited less variation in the results than the tests that were shot directly into the concrete. The results of the FRP/concrete connection tests are given in Table 3.

From these tests, it is apparent that the standard deviation decreases when longer fasteners are used in conjunction with predrilling. Hybrid 1.5 C and D series tests resulted in 7,358 and 6,223 N (1,654 and 1,399 lb), with both series having a standard deviation of 912 N (205 lb). ACI 440H (ACI 2000b) recommends using a design strength of the average minus three times the standard deviation when dealing with FRP materials; in this case the design

Table 3
Results of FRP/Concrete Connection Tests

Test Series	Fastener Type	Connection Strength N	Standard Deviation N	COV %	Load per Fastener N	St. Dev. Per Fastener
Standard A	DNI 27	5,391	2,356	43.7	5,391	2,356
Standard B	ZF 32	7,554	2,517	33.3	7,554	2,517
Intermediate A	ZF 32	7,200	2,432	33.8	7,200	2,432
Hybrid 1.0 A	ZF 32	6,021	2,610	43.3	6,021	2,610
Hybrid 1.5 A	ZF 32	6,916	1,548	22.4	6,916	1,548
Hybrid 1.5 B	ALH 47	5,563	974	17.5	5,563	974
Hybrid 1.5 C	ALH 47	14,715	1,823	12.4	7,358	912
Hybrid 1.5 D	ALH 47	12,446	1,822	14.6	6,223	912

strength for these two series of tests would be 4,622 and 3,487 N (1039 and 783 lb) per fastener. For the application of strengthening a reinforced concrete beam by using multiple fasteners along the length of the composite strengthening strip, there is a built-in redundancy with the large number of fasteners. Using a design strength of the average minus two times the standard deviation would make the design strength for these two series of tests 5,534 and 4,399 N (1,244 and 989 lb) per fastener. From these two design strengths, a design load of 4,448 N (1,000 lb) was chosen for use in the strengthening of reinforced concrete beams using AL47 fasteners with a hybrid strip.

Tests shot directly through the strip and into the concrete had much larger coefficients of variation. Hybrid 1.5 A series had an average of 6,916 N (1,555 lb) per fastener. Mean minus three standard deviations lower gives 2,272 N (510 lb), and mean minus two standard deviations gives 3,820 N (859 lb). Since the coefficient of variation and the spalling for the tests without predrilling is much greater than with predrilling, a design value of 2,224 N (500 lb) was chosen in the strengthening of beams using AL32 fasteners. Even though Hybrid 1.5 A series was performed using ZF32 fasteners, these tests gave the closest approximation to the AL32 fasteners later used in full-scale beam testing.

6 Preliminary Full-Scale Beam Test Plan

Based on the preliminary results from the modified Whitney stress block method, a preliminary test plan for the summer testing at the ERDC site, Vicksburg, MS, was developed in April 2000. The preliminary test plan is shown in Table 4. Beam designations begin with the type of composite strip used for strengthening. "S" for the standard strip of modulus 15.2 GPa (2,205 ksi), "I" for the intermediate strip of modulus 26.3 GPa (3,816 ksi), "H1.5" for hybrid of modulus 57.2 GPa (8,291 ksi) with 1.5-oz mats, and "H1.0" for hybrid of modulus 56.9 GPa (8,254 ksi) with 1.0-oz mats. The second part of the beam designation is the nominal width of the composite strengthening strip in inches. The third part is Y if the beam has fasteners in the moment span and N if there are no fasteners in the moment span. The fourth designation is the type and length in millimeters of fastener used; for example, AL42 designates AL fasteners with a shank length of 42 mm (1.65 in.) were used to attach the composite strip. The letter D was added to the fourth designation to indicate the fasteners were driven into predrilled pilot holes. The fastener spacing between rows for all beams was 51 mm (2 in.), and the fastener spacing along the length of the beam was 51 mm (2 in.) unless noted by a fifth designation, which is the fastener spacing along the length of the beam, in inches. The letter R was added to beams which were a repeat of a prior configuration. For example, beam H1.5-4-Y-AL47D-3-R was strengthened using a Hybrid 1.5 strip that was 102-mm (4-in.)-wide, attached by predrilling AL47 fasteners which were spaced 76 mm (3 in.) apart along the length of the beam. The fasteners were continuous through the moment span, and this beam was a repeat of a beam with the same configuration tested previously.

The first two beams tested were to be control beams, with no attached strengthening strip. The majority of the initial tests were to be preformed using the intermediate strip and small diameter ZF fasteners. Tests 3 and 4 were to examine the effect of fasteners in the moment span. If test 4 was similar to test 3, then fasteners could be left out of the remaining tests, saving a good deal of fasteners. Test 5 was the same as test 3, except that test 5 uses larger diameter DNI fasteners. Test 6 increases the strip width from 203 mm (8 in.) to 305 mm (12 in.), while test 7 reduces the strip width to 102 mm (4 in.). Tests 9 and 10 were to be repeats of the most successful tests up to this point.

Table 4
Preliminary Test Plan for ERDC Beams

SI Units

#	f'_c=5400 Test Name	Strip W (mm)	Strip Layup	Strip E (GPa)	Strip Str (MPa)	Open Hole Str (MPa)	Calculated Yield M (kN-m)	Calculated Yield Incr (%)	Calculated Yield FRP σ (MPa)	Calculated Yield FRP T (kN)	Calculated Ultimate M (kN-m)	Calculated Ultimate Incr (%)	Calculated Ultimate FRP σ (MPa)	Calculated Ultimate FRP T (kN)	Fastener Type	# Rows	Fastener Capacity (N)	Fasteners Required Per Shear Span	Fasteners per Shear Span per Row	In M Span	Failure Mechanism	Notes
1	Control 1						94 4				98 8											Without Plate
2	Control 2						94 4				98.8											Either bonded intermediate plate or a second control without plate
3	I-8-Y-ZF32	203	m/56/m	27 3	632	443	106.9	13.3	74 3	47.9	155.5	57 4	342.0	220.6	ZF 32	4	2224	100	25	Yes	Concrete crushing	
4	I-8-N-ZF32	203	m/56/m	27.3	632	443	106 9	13 3	74.3	47.9	155 5	57.4	342.0	220.6	ZF 32	4	2224	100	25	No	Concrete crushing	No fasteners in moment span. If the results of this test are comparable to I-8-Y-ZF32, then the remaining tests will be done without fasteners in the moment span
5	I-8-Y-DNI32	203	m/56/m	27 3	632	443	106 9	13.3	74 3	47.9	155 5	57 4	342.0	220.6	DNI 32	4	2224	100	25	Yes	Concrete crushing	Uses larger diameter DNI Fasteners
6	I-12-Y-ZF32	305	m/56/m	27 3	632	443	113 2	20.0	74.6	72 2	172.9	74 9	300 6	290.8	ZF 32	6	2224	131	22	Yes	Concrete crushing	
7	I-4-Y-ZF32	102	m/56/m	27 3	632	443	100 6	6.6	74.1	23.9	132 9	34 5	407.1	131.3	ZF 32	2	2224	60	30	Yes	Concrete crushing	
8	I-4-Y-ZF37	102	m/56/m	27 3	632	443	100 6	6 6	74.1	23 9	132 9	34 5	407.1	131 3	ZF 37	2	2669	50	25	Yes	Concrete crushing	Uses 5mm longer fasteners
9	REPEAT		m/56/m	27.3	632	443									ZF 32							Repeats with intermediate plate in a configuration decided during testing
10	REPEAT		m/56/m	27 3	632	443									ZF 32							Repeats with intermediate plate in a configuration decided during testing
11	S-4-Y-ZF32	102	m/0/m_d/0/m	13.8	232	162	97.6	3.4	37.6	12.1	112.6	13.9	161 6	52.1	ZF 32	2	2224	24	12	Yes	Plate Rupture	Standard plate ruptures before concrete crushing
12	S-8-Y-ZF32	203	m/0/m_d/0/m	13.8	232	162	100 7	6 7	37.7	24.3	126.2	27.7	161.6	104 3	ZF 32	4	2224	47	12	Yes	Plate Rupture	Standard plate ruptures before concrete crushing
13	H-4-Y-ZF32	102	m/carbon/m	55 2	506	354	107 1	13.5	151.4	48.8	127 5	29 0	352.1	113 5	ZF 32	2	2224	52	26	Yes	Plate Rupture	Hybrid plate ruptures before concrete crushing
14	H-8-Y-ZF32	203	m/carbon/m	55.2	506	354	119 9	27.0	152 2	98.2	157.5	59 3	353 7	228 1	ZF 32	4	2224	103	26	Yes	Plate Rupture	Hybrid plate ruptures before concrete crushing
15	H-12-Y-ZF32	305	m/carbon/m	55 2	506	354	132.5	40.4	152.9	147 9	185.7	87 9	354 3	342.7	ZF 32	6	2224	155	26	Yes	Plate Rupture	Hybrid plate ruptures before concrete crushing
16	REPEAT		m/carbon/m	55.2	506	354									ZF 32							Repeat of high modulus plate in a configuration decided during testing

(Continued)

Table 4 (Concluded)

U.S. Customary Units

#	f'_c=5400 Test Name	Strip W (in)	Strip Layup	Strip E (ksi)	Strip Str. (ksi)	Open Hole Str. (ksi)	Calculated Yield				Calculated Ultimate				Fastener Type	# Rows	Fastener Capacity (lbs)	Fasteners Required Per Shear Span	Fasteners per Shear Span per Row	In M Span	Failure Mechanism	Notes
							M (k-in)	Incr. (%)	FRP σ (ksi)	FRP T (k)	M (k-in)	Incr. (%)	FRP σ (ksi)	FRP T (k)								
1	Control 1						835				875											Without Plate
2	Control 2						835				875											Either bonded intermediate plate or a second control without plate
3	I-8-Y-ZF32	8	m/56/m	3,956	91.7	64.2	946	13.3	10.8	10.8	1,376	57.4	49.6	49.6	ZF 32	4	500	100	25	Yes	Concrete crushing	
4	I-8-N-ZF32	8	m/56/m	3,956	91.7	64.2	946	13.3	10.8	10.8	1,376	57.4	49.6	49.6	ZF 32	4	500	100	25	No	Concrete crushing	No fasteners in moment span; If the results of this test are comparable to I-8-Y-ZF32, then the remaining tests will be done without fasteners in the moment span.
5	I-8-Y-DNI32	8	m/56/m	3,956	91.7	64.2	946	13.3	10.8	10.8	1,376	57.4	49.6	49.6	DNI 32	4	500	100	25	Yes	Concrete crushing	Uses larger diameter DNI Fasteners
6	I-12-Y-ZF32	12	m/56/m	3,956	91.7	64.2	1,002	20.0	10.8	16.2	1,530	74.9	43.6	65.4	ZF 32	6	500	131	22	Yes	Concrete crushing	
7	I-4-Y-ZF32	4	m/56/m	3,956	91.7	64.2	891	6.6	10.8	5.4	1,177	34.5	59.0	29.5	ZF 32	2	500	60	30	Yes	Concrete crushing	
8	I-4-Y-ZF37	4	m/56/m	3,956	91.7	64.2	891	6.6	10.8	5.4	1,177	34.5	59.0	29.5	ZF 37	2	600	50	25	Yes	Concrete crushing	Uses 5mm longer fasteners
9	REPEAT		m/56/m	3,956	91.7	64.2									ZF 32							Repeats with intermediate plate in a configuration decided during testing
10	REPEAT		m/56/m	3,956	91.7	64.2									ZF 32							Repeats with intermediate plate in a configuration decided during testing
11	S-4-Y-ZF32	4	m/0/m_4/0/m	1,996	33.6	23.5	863	3.4	5.5	2.7	997	13.9	23.4	11.7	ZF 32	2	500	24	12	Yes	Plate Rupture	Standard plate ruptures before concrete crushing
12	S-8-Y-ZF32	8	m/0/m_4/0/m	1,996	33.6	23.5	892	6.7	5.5	5.5	1,117	27.7	23.4	23.4	ZF 32	4	500	47	12	Yes	Plate Rupture	Standard plate ruptures before concrete crushing
13	H-4-Y-ZF32	4	m/carbon/m	8,000	73.4	51.4	948	13.5	22.0	11.0	1,129	29.0	51.1	25.5	ZF 32	2	500	52	26	Yes	Plate Rupture	Hybrid plate ruptures before concrete crushing
14	H-8-Y-ZF32	8	m/carbon/m	8,000	73.4	51.4	1,061	27.0	22.1	22.1	1,394	59.3	51.3	51.3	ZF 32	4	500	103	26	Yes	Plate Rupture	Hybrid plate ruptures before concrete crushing
15	H-12-Y-ZF32	12	m/carbon/m	8,000	73.4	51.4	1,173	40.4	22.2	33.3	1,644	87.9	51.4	77.1	ZF 32	6	500	155	26	Yes	Plate Rupture	Hybrid plate ruptures before concrete crushing
16	REPEAT		m/carbon/m	8,000	73.4	51.4									ZF 32							Repeat of high modulus plate in a configuration decided during testing

Tests 11 and 12 were to be with standard strips of 102 mm (4 in.) and 203 mm (8 in.) in width. The next three tests, 13, 14, and 15 were then to be performed on 102-, 203-, and 305-mm (4-, 8-, and 12-in.)-width strips of the hybrid type. When this preliminary test plan was developed, it was thought that the beams strengthened with the standard and hybrid strips would fail by rupturing the composite strip before the concrete crushed.

This preliminary test plan was used as the basic outline for planning and scheduling the tests performed at ERDC. This test plan was modified to examine problems and phenomena that were discovered as testing progressed.

7 Results of Full-Scale Tests

Full-scale reinforced concrete beams were tested at the ERDC, Vicksburg, MS. The actual configurations tested are listed in Table 5 in the order that they were tested. The preliminary test plan was modified as testing progressed to attempt to understand the different variables that affect the overall strength. A short explanation of why each test was performed is included in the discussion of that individual test. Upon completion of testing, one beam less than originally planned was tested. Control 1 and Control 2 were tested with no attached strip for comparison purposes. Beam H1.5-4-B was strengthened by bonding the composite strengthening strip to the bottom surface.

Table 5
Beams Actually Tested at ERDC

Test Name	Date Performed
Control 1	7/6/00
I-4-Y-AL32	7/7/00
I-4-N-AL32	7/7/00
H1.5-4-Y-AL32	7/8/00
Control 2	7/10/00
S-4-Y-AL32	7/10/00
I-8-Y-AL32	7/11/00
H1.5-8-Y-AL32	7/11/00
I-4-Y-AL32-R	7/13/00
H1.5-4-Y-AL47D	7/14/00
H1.5-4-Y-AL42D	7/15/00
H1.5-4-Y-AL47D-3	7/17/00
H1.5-4-Y-AL47D-5	7/19/00
H1.5-4-Y-AL47D-3-R	7/21/00
H1.5-4-B	7/26/00

Test Specimens

Large-scale reinforced concrete beams were 3,658 mm (144 in.) long and had a cross section of 305 mm x 305 mm (12 in. x 12 in.). They were cast at ERDC, Vicksburg, MS, with concrete supplied by a local vendor. A pea gravel mix was used to facilitate casting. The pea gravel consisted of local chert, a very common but very hard aggregate. The measured concrete strength at 28 days was 32.7 MPa (4,740 psi). Most of the experiments were conducted after 32 days. The measured concrete strength at 35 and 42 days was 35.3 MPa (5,113 psi).

The beams were designed in accordance with ACI 318-99 (ACI 1999). Primary tension steel was provided by two #8 Grade 60 deformed bars for a reinforcement ratio of 1.32 percent. Two #3 Grade 60 deformed top bars were used to provide stability to the rebar cage during casting. A strain gage was mounted to each primary tension bar at midspan and to a 610-mm (24-in.)-long #3 bar attached at midspan between the top bars. These gages were Micro Measurement WK-06-20CBW-350 gages. Shear reinforcement was provided in the form of closed stirrups of #4 Grade 60 deformed bars. Stirrups were placed at 102 mm (4 in.) on center throughout the shear span of the beam and into one-third of the moment span. Spacing of stirrup was increased to 127 mm (5 in.) and then 152 mm (6 in.) in the center of the moment span. This stirrup spacing ensured that a shear failure in the strengthened beams would be avoided. Figure 3, shown previously, shows the beam dimensions and the location of the internal steel. The beams were tested on a 3,353-mm (132-in.) total span, with each shear span and the moment span being 1,118 mm (44 in.), so that the strengthening strip terminated 76.2 mm (3 in.) from the supports.

The Hilti DX A41 Powder-Actuated Fastening system was used to attach the composite strips to the concrete beams. The DX A41 uses a 6.8-mm (0.27-in.) caliber short gunpowder booster. Purple boosters, signifying extra heavy charge, were used in conjunction with X-ALH fasteners for attaching the strip. The X-ALH fasteners are made of specially heat-treated high-strength steel that is zinc plated to resist corrosion. These fasteners were chosen because of the hardness of the chert aggregates used in the concrete beams. It was found in preliminary tests that ZF and DNI fasteners did not have adequate strength to penetrate into the concrete. The fasteners would strike a piece of chert aggregate and bend, a failure mode called "J-ing." The fasteners used were of varying lengths. Tests with a "D" following the fastener type were predrilled. Predrilling was done with a DX-Kwik bit, which had a diameter of 4.76 mm (0.188 in.) and a drill bit length of 15.88 mm (0.625 in.). A standard hammer drill was used with this special bit. Figure 12 shows this special drill bit in a hammer drill.

FRP Strip Attachment Procedure

The reinforced concrete beam was turned over, so that the tensile steel was facing upward. The fastener locations were marked on the strengthening strip. The strengthening strip was centered with the concrete beam from side-to-side and end-to-end and held in place at each end. The strengthening strip was terminated 76.2 mm (3 in.) from the supports in all tests.

In the tests that were not predrilled, the fasteners were inserted into the Hilti DX A41 tool, lined up with the marked fastener locations, and driven directly through the composite strip and into the concrete. A large amount of spalling was observed in these beams.

In the tests that were predrilled, two shallow pilot holes were drilled in a line perpendicular to the length of the beam at the center of the beam. These holes were drilled through the 3.175-mm (0.125-in.) thick strengthening strip so that they extended approximately 12.7 mm (0.5 in.) into the concrete. The two holes

were drilled in approximately 10 sec. Then the fasteners were inserted into the Hilti DX A41 tool, lined up with the holes, and driven into the concrete. The fasteners were drilled and driven by twos continuing to one end of the beam, and from the center to the other end of the beam. Very little spalling was observed, and the complete attachment of the strengthening strip took about approximately 30 min.

The beam was then turned back over, so that the tensile steel was on the bottom, taking care not to damage the attached strip or fasteners, and placed on the supports. Micro Measurements strain gages (CAE-06-250UW-350) were attached to the composite strip at midspan, with one in the middle and another at one fastener spacing to either side of the middle gage. A single gage (WK-06-20CBW-350) was mounted on the top of the beam at midspan.

Testing

A lightweight aluminum frame was attached to the beam at half of the depth at the supports. Small plexiglas blocks were attached to the sides of the beam at half of the depth at the midspan with a two-part epoxy. Two LVDTs were attached to the aluminum frame to read the deflection of the beam on both sides. The beams were tested on a span of 3,353 mm (132 in.), with the load applied at 1,118 mm (44 in.) from the supports using a spreader bar. The frame and LVDTs are shown in Figure 15.

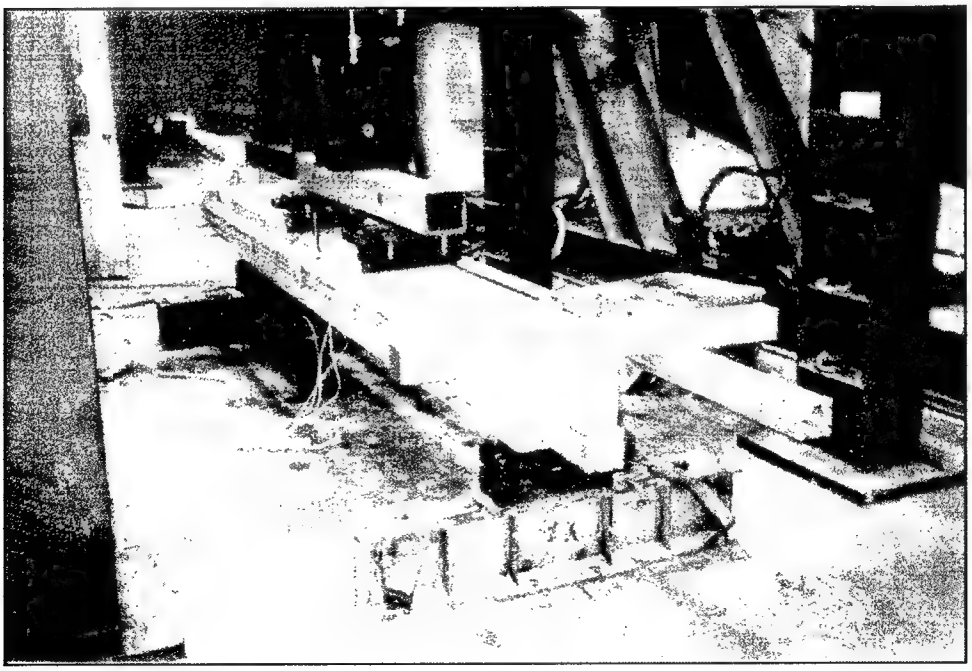

Figure 15. Test fixture and aluminum LVDT frame

An MTS Testar system was used to control the 490-kN (110-kip) hydraulic actuator. An Optim Megadac was used for data collection. The beams were placed directly on the supports, and thin wood strips, similar to those used in split tensile tests, were placed under the load points. The beams were loaded at the rate of 1.3 mm/min (0.05 in./min.) to an actuator displacement of 25 mm (1 in.), and then at a rate of 2.5 mm/min (0.1 in./min.) to failure.

Discussion of Individual Tests

All of the concrete beams showed signs of shrinkage cracking on the top surfaces. These cracks spanned the entire width of the beam and were present on the top surface along the entire length of the beam. They were not deep and were more pronounced toward the ends of the beams. Poor finishing techniques were the apparent cause of these cracks. These cracks were not thought to adversely impact the test results.

Increases in yield and ultimate of up to 21.6 and 20.1 percent were achieved with strengthening by attachment with powder-actuated fasteners. In cases where longer fasteners were used and holes were predrilled, the strengthened beams showed ductility similar to the unstrengthened control beams. A summary of test data is presented in Table 6. Appendix C contains the moment-deflection curves, as well as a photograph of the crack pattern and a close-up of the crack pattern in the moment span for each beam configuration.

Control 1

Control 1 was tested without wood strips under the loading points. During testing, flexural cracks first appeared in the midspan between the loading points as expected. These cracks became visible before the yield load was reached. As the ultimate load was approached, cracking noises could be heard from the concrete. The concrete failed suddenly in compression in the midspan near the north load point.

The beam yielded approximately 122.3 kN-m (1,082 k-in.), and the ultimate moment was 136.4 kN-m (1,207 k-in.). Only flexural cracks were observed throughout the testing.

Control 2

Control 2 was tested using wood strips under the loading points. During testing, flexural cracks first appeared in the midspan between the loading points as expected. These cracks became visible before the yield strength was reached. As the ultimate strength was approached, cracking noises could be heard from the concrete. The concrete failed suddenly in compression in the midspan near the north load point. The beam yielded at 122.3 kN-m (1,082 k-in.), and the ultimate moment was 136.5 kN-m (1,208 k-in.). Only flexural cracks were observed throughout the testing.

Table 6
Summary of Tests Conducted at ERDC

SI Units

Beam	Test Date	Strip Modulus (MPa)	Number of Fasteners	Approx. Yield Moment (kN-m)	% Inc	Ultimate Moment (kN-m)	% Inc	Midspan FRP Strain at Ultimate (με)	FRP Stress at Ultimate (MPa)	Max Ext Concrete Strain (με)	Failure Mechanism
Control 1	7/6/00			122.3		136.4				-2,604	Concrete
Control 2	7/10/00			122.3		136.4				-3,067	Concrete
S-4-Y-AL32	7/10/00	323	124	126.0	3.0	142.6	4.5	10,368	3.35	-2,466	Concrete
I-4-N-AL32	7/7/00	550	90	130.1	6.4	141.3	3.6	6,175	3.39	-1,811	Concrete
I-4-Y-AL32	7/7/00	550	124	133.6	9.2	150.4	10.3	7,646	4.20	-2,374	Concrete
I-4-Y-AL32-R	7/13/00	550	124	130.9	7.0	156.1	14.4	9,285	5.10	-3,281	Concrete
I-8-Y-AL32	7/11/00	550	248	138.5	13.3	152.8	12.0	3,906	2.15	-2,817	Strip Debonding
H1.5-4-Y-AL32	7/8/00	1,202	124	139.1	13.8	146.2	7.2	3,355	4.03	-2,710	Strip Debonding
H1.5-4-Y-AL42D	7/15/00	1,202	124	136.2	11.4	152.4	11.7	5,971	7.18	-2,288	Concrete
H1.5-4-Y-AL47D	7/14/00	1,202	124	139.1	13.8	163.9	20.1	7,740	9.31	-2,727	Concrete
H1.5-4-Y-AL47D-3	7/17/00	1,202	84	139.1	13.8	159.4	16.9	7,129	8.57	-2,671	Concrete
H1.5-4-Y-AL47D-3 -R	7/21/00	1,202	84	139.1	13.8	158.3	16.1	5,435	6.53	-3,020	Concrete
H1.5-4-B	7/26/00	1,202	NA	148.0	21.1	163.2	19.7	5,891	7.08	-3,293	Strip Debonding
H1.0-4-Y-AL47D-5	7/19/00	1,197	50	122.3	0.0	136.0	-0.3	3,834	4.59	-2,283	Concrete
H1.5-8-Y-AL32	7/11/00	1,249	248	148.7	21.6	148.7	9.0	2,762	3.45	-2,264	Strip Debonding

(Continued)

Table 6 (Concluded)

U.S. Customary Units

Beam	Test Date	Strip Modulus (ksi)	Number of Fasteners	Approx. Yield Moment (k-in)	% Inc	Ultimate Moment (k-in)	% Inc	Midspan FRP Strain at Ultimate (με)	FRP Stress at Ultimate (ksi)	Max Ext Concrete Strain (με)	Failure Mechanism
Control 1	7/6/00			1,082		1,207				-2,604	Concrete
Control 2	7/10/00			1,082		1,208				-3,067	Concrete
S-4-Y-AL32	7/10/00	2,226	124	1,115	3.0	1,262	4.5	10,368	23.1	-2,466	Concrete
I-4-N-AL32	7/7/00	3,790	90	1,151	6.4	1,250	3.6	6,175	23.4	-1,811	Concrete
I-4-Y-AL32	7/7/00	3,790	124	1,182	9.2	1,331	10.3	7,646	29.0	-2,374	Concrete
I-4-Y-AL32-R	7/13/00	3,790	124	1,158	7.0	1,381	14.4	9,285	35.2	-3,281	Concrete
I-8-Y-AL32	7/11/00	3,790	248	1,226	13.3	1,352	12.0	3,906	14.8	-2,817	Strip Debonding
H1.5-4-Y-AL32	7/8/00	8,291	124	1,231	13.8	1,294	7.2	3,355	27.8	-2,710	Strip Debonding
H1.5-4-Y-AL42D	7/15/00	8,291	124	1,205	11.4	1,348	11.7	5,971	49.5	-2,288	Concrete
H1.5-4-Y-AL47D	7/14/00	8,291	124	1,231	13.8	1,450	20.1	7,740	64.2	-2,727	Concrete
H1.5-4-Y-AL47D-3	7/17/00	8,291	84	1,231	13.8	1,411	16.9	7,129	59.1	-2,671	Concrete
H1.5-4-Y-AL47D-3 -R	7/21/00	8,291	84	1,231	13.8	1,401	16.1	5,435	45.1	-3,020	Concrete
H1.5-4-B	7/26/00	8,291	NA	1,310	21.1	1,444	19.7	5,891	48.8	-3,293	Strip Debonding
H1.0-4-Y-AL47D-5	7/19/00	8,254	50	1,082	0.0	1,204	-0.3	3,834	31.6	-2,283	Concrete
H1.5-8-Y-AL32	7/11/00	8,615	248	1,316	21.6	1,316	9.0	2,762	23.8	-2,264	Strip Debonding

S-4-Y-AL32

This beam was strengthened with using a single 102-mm (4-in.)-wide standard strip. The beam was tested in this configuration to see the strengthening effect of a single low-modulus strip. In the beginning stages of testing, occasional cracking sounds could be heard coming from the bottom of the beam. The source of these sounds was thought to be the fasteners as they adjusted to begin carrying load, causing microcracking in the concrete substrate and a minor amount of local damage in the composite strip immediately around the fastener.

The beam failed by concrete compression failure, similar to the control beams, in the midspan, near the north load point. The test was allowed to continue, and shortly after compression failure, the strip fractured, directly underneath the concrete compression failure, as shown in Figure 16. This failure caused a second drop in moment from approximately 120 kN-m (1,061.9 k-in.) to 110 kN-m (973.5 k-in.). The test continued until there was more concrete compression failure at the location of the first concrete compression failure.

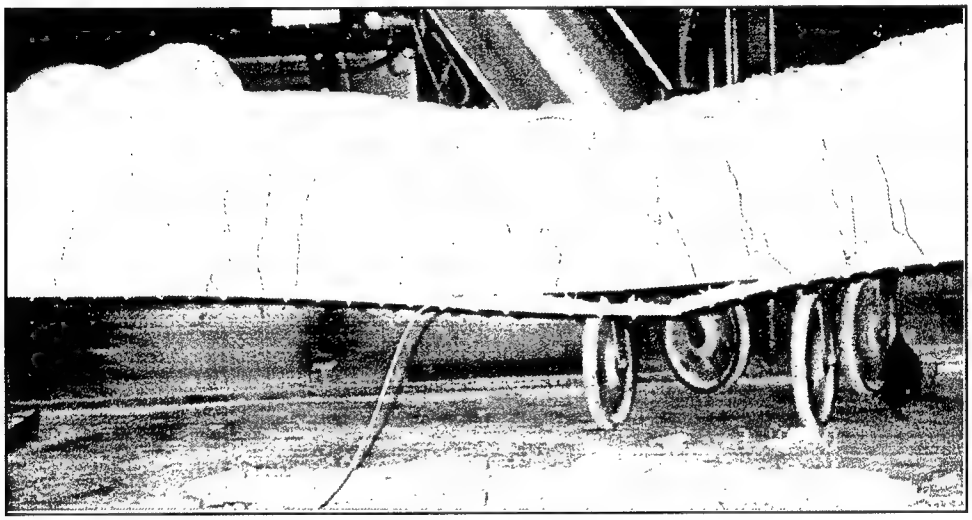

Figure 16. Fractured strip on beam S-4-Y-AL32 after test was concluded

The beam yielded at 126.0 kN-m (1,115 k-in.), and the beam failed by concrete compression at an ultimate strength of 142.6 kN-m (1,262 k-in.). The strengthening in this beam increased the ultimate moment by 4.5 percent and increased the yield strength by 3 percent. The ductility of the beam did not appear to be impacted by the strengthening, as seen in the moment-deflection curve.

I-4-N-AL32

This beam was strengthened by using a single 102-mm (4-in.)-wide intermediate strip. This configuration was used to observe the effect of omitting fasteners in the moment span. It was intended to have no fasteners in the moment span, but fasteners were needed to keep the strip aligned. A fastener spacing of 203 mm (8 in.) was used in the moment span, and the standard 51-mm

(2-in.) spacing was used outside the moment span. The fastener spacing in the moment span is shown in Figure 17.

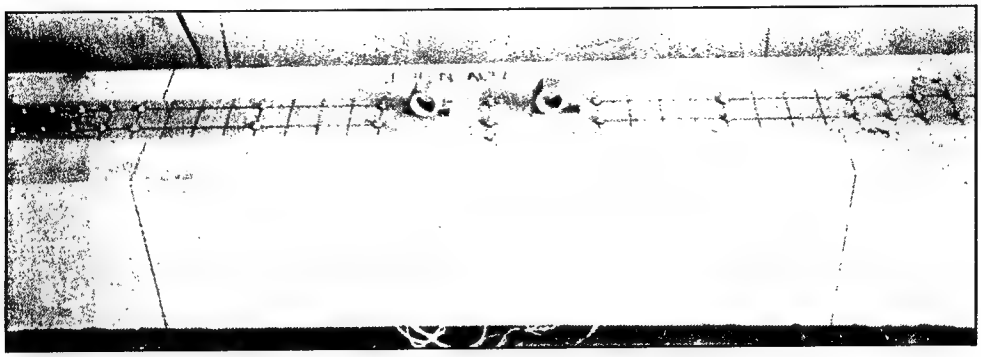

Figure 17. Fastener spacing in the moment span of beam I-4-N-AL32

The beam failed by concrete compression failure, similar to the control beams, in the midspan, near the north load point. The concrete started to crush gradually before a large chunk of concrete suddenly crushed. The gradual crushing caused a slight decline in the moment-deflection curve before the sharp drop that indicated the sudden crushing of the large concrete chunk. This gradual crushing is attributed to local crushing under the load point. The beam continued to hold the lower load until a much larger chunk of concrete crushed. The test was ended at this point. The composite strengthening strip remained attached to the concrete beam during the entire test.

The beam yielded at 130.1 kN-m (1,151 k-in.), and the ultimate strength of 141.3 kN-m (1,250 k-in.) was reached when the crushing was initiated in the concrete. The strengthening in the beam increased the ultimate strength by 3.6 percent, and increased the yield strength by 6.4 percent. The preyield stiffness was increased over that of the control beams, but the overall ductility of the beam was less than the control beams. The maximum measured external concrete strain in this beam was 1,811 με, which is much lower than the next lowest failure strain of 2,288 με.

I-4-Y-AL32 and I-4-Y-AL32-R

A single 102-mm (4-in.)-wide intermediate strip was used to strengthen each of these beams. The first test was used to compare with beam I-4-N-AL32, which had no fasteners in the moment span. The second test was conducted to obtain verification of the first test, which achieved a good level of strengthening, and to obtain a stress distribution along the length of the composite strengthening strip. Fasteners were spaced 51 mm (2 in.) apart. The spacing was the same over the entire length. The crack pattern for these two beams was similar. Flexural cracks became visible in the midspan at about half of the yield strength. As the tests approached the yield strength of the beams, flexural cracks began to appear

outside of the load points. After the beams had yielded, the flexural cracks outside the moment span began to "bend over" and become flexural-shear cracks. As the beams failed in compression, shear cracks formed about 380 mm (15 in.) from the supports.

These beams failed in concrete compression, near the north load point. Both beams failed by concrete compression. The tests were continued beyond the initial concrete crushing. At the conclusion of the tests, the strips were firmly attached to the beams.

Beam I-4-Y-AL32 yielded at 133.6 kN-m (1,182 k-in.) and reached an ultimate strength of 150.4 kN-m (1,331 k-in.). The strengthening increased the yield and ultimate strengths over those of the control beams by 9.2 and 10.3 percent. Beam I-4-Y-AL32-R yielded at 130.9 kN-m (1,158 k-in.) and reached an ultimate strength of 156.1 kN-m (1,381 k-in.). The strengthening increased the yield and ultimate strengths over those of the control beams by 7.0 and 14.4 percent. The preyield stiffness and postyield stiffness of these beams was greater than those of the control beams. The postyield ductility of these beams was about the same as that of the control beams.

I-8-Y-AL32

This configuration was chosen to examine the effect of a larger area of composite strip and to determine the effect of edge distance. This beam was strengthened using two 102-mm (4-in.)-wide intermediate strips. The strips were placed next to each other and held in place by weights and two laboratory technicians. As with beams strengthened using a single composite strip, two rows of fasteners were used per strip, for a total of four rows of fasteners. This resulted in an edge distance of 76 mm (3 in.) rather than an edge distance of 127 mm (5 in.) as in the beams where only one strip was used. This decreased edge distance caused a large amount of initial cracking when the fasteners were driven into the beam. Figure 18 shows the initial cracking that occurred. The V shaped cracks along the edge of the beam are the same types of cracks seen in the small-scale beams tested during the feasibility study.

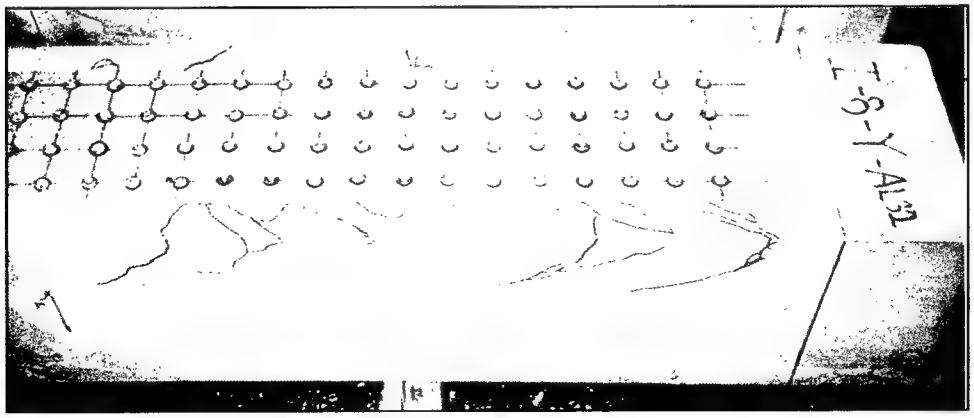

Figure 18. Initial cracking in I-8-Y-AL32 caused by the attachment of the strip

The beam first failed by the sudden detachment of one of the two strips. A few seconds later, the second strip detached. One strip remained attached in each shear span, each having begun detachment from a different end of the beam. The beam with detached strips is shown in Figure 19. The beam then acted as an unstrengthened beam, similar to a control beam, until the concrete crushed in the moment span near the south load point. The first drop in load corresponds to the detachment of the first strip and is followed by the drop caused by the detachment of the second strip. The beam then behaves in a manner similar to the control beams until the concrete crushes.

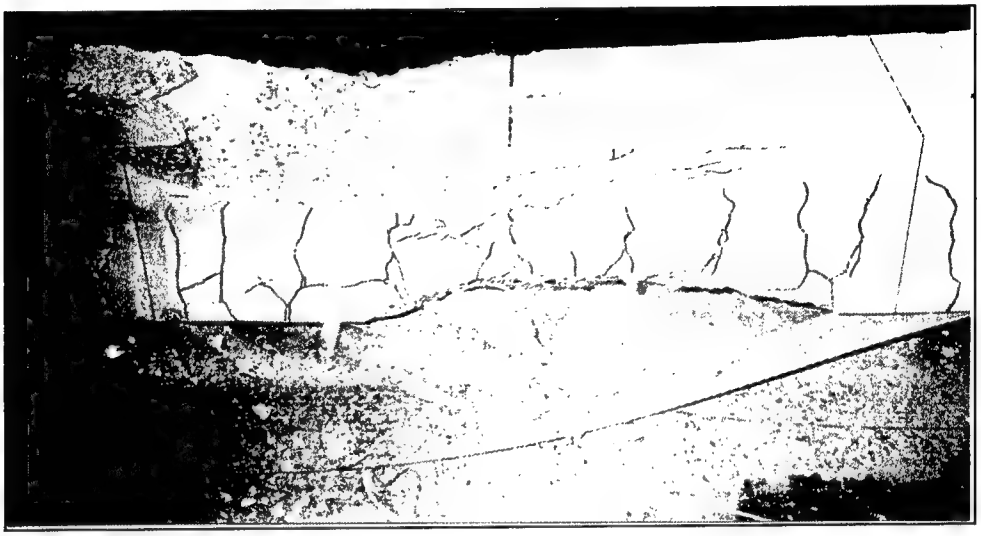

Figure 19. The strips detached, seen here after testing, one from each shear span in beam I-8-Y-AL32

Since the fasteners pulled out of the concrete and caused the strip to detach, it is instructive to examine the force per fastener. The strain in the composite strengthening strips immediately prior to detachment was measured at the mid-span with strain gages centered between the rows of fasteners. The average of three gages was taken and along with the modulus determined from previous tests, the stress in the strips at detachment was calculated to be 2.1 MPa (14.8 ksi). For a cross-sectional strip area of 645 mm^2 (1 $in.^2$), the force that must be transferred by the fasteners is 65.8 kN (14.8 kips). Assuming the 80 fasteners in each shear span transferred this force equally, this results in a load of 823 N (185 lb), well under the 2,272-N (510-lb) design limit for 32-mm (1.26-in.)-long fasteners.

This beam yielded at 138.5 kN-m (1,226 k-in.) and reached ultimate at 152.8 kN-m (1,352 k-in.), increases of 13.3 and 12.0 percent over the control beams. The yield was increased more than the ultimate, because the strips detached from the beam; had they remained attached until concrete failure, the ultimate strength would have been increased by more than 12 percent. The preyield stiffness was greater in this beam than the control beams, as was the postyield strength before the strips detached.

H1.5-4-Y-AL32

This configuration was tested to benchmark the behavior of the hybrid strip. Beam H1.5-4-Y-AL32 was strengthened with a 102-mm (4-in.)-wide hybrid strip that contained two 1.5-oz continuous strand mats. After attaching the strengthening strip, a large amount of spalling was visible, projecting up to 38 mm (1.5 in.) from the edges of the strip. The beam failed by the sudden detachment of the composite strip from one end of the beam.

The beam yielded at 139.1 kN-m (1,231 k-in.) and reached ultimate at 146.2 kN-m (1,249 k-in.), increases of 13.8 and 7.2 percent over the control beams. The yield was increased more than the ultimate because the strip detached from the beam; had it remained attached until concrete failure, the ultimate strength would have been increased by more than 7.2 percent. The preyield stiffness was greater in this beam than the control beams, as was the postyield strength before the strips detached. It should also be noted that the stress in the composite strips was about double that of beam I-8-Y-AL32, the load per fastener was 1,600 N (360 lb), still well below the design limit of 2,272 N (510 lb) for 32-mm (1.26-in.)-long fasteners.

H1.5-4-Y-AL42D

This configuration was chosen to determine the effect of using a predrilled pilot hole. The length of fastener was chosen so that the same embedment below the pilot hole would be achieved as with beam H1.5-4-Y-AL32. This beam was strengthened using a single 102-mm (4-in.)-wide hybrid strip. The strip was aligned and held in place by two technicians. Two holes were drilled side by side at the center of the strip, one from each of the two rows. The holes were drilled through the composite strip into the concrete. Fasteners were then driven through these holes into the concrete substrate. This drilling visibly reduced the amount of spalling that occurred from the initial attachment of the strip. Holes were drilled and then fasteners were driven in sets of two proceeding outward toward one end of the strip. Then the holes were drilled and the fasteners driven in sets of two from the center toward the other end of the strip. The free ends of the strip were held in place by technicians throughout the entire process.

Small flexural cracks formed in the moment span shortly after loading began. As the beam approached its yield strength, flexural cracks started to appear in the shear span, near the loading points. As the beam yielded and continued to gain strength, these cracks began to "bend over" into flexural-shear cracks. The beam reached ultimate strength as the concrete failed in compression in the moment span near the north load point. At this time, the composite strip was still firmly attached to the concrete beam. Immediately following the concrete compression, shear cracks formed in the shear spans near the supports. A short time after the compression failure, loud cracking noises could be heard from the tensile side of the beam. Gradually, under the north load point, the composite strip detached as large chunks of concrete began to fall out of the concrete beam (Figure 20).

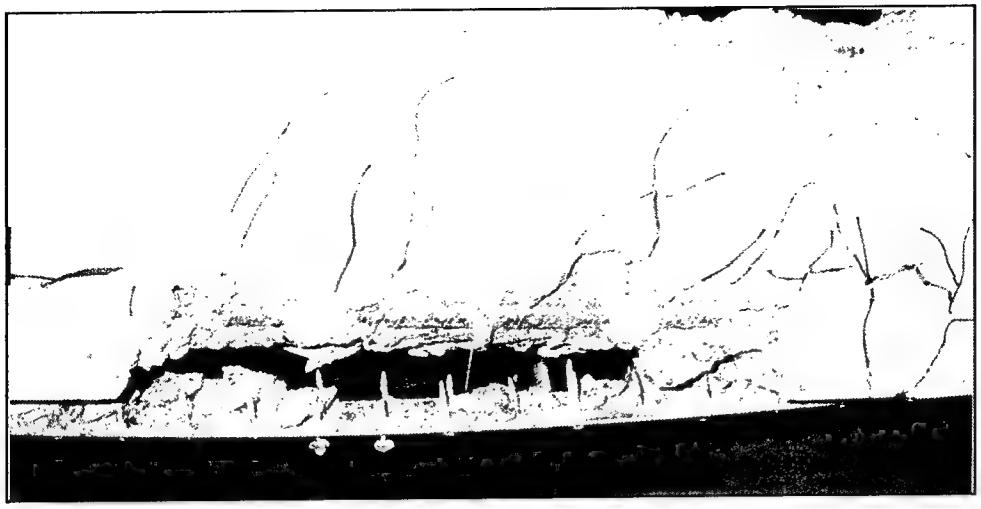

Figure 20. After testing, large chunks of concrete had fallen out of beam H1.5-4-Y-AL42D

The beam yielded at 136.2 kN-m (1,205 k-in.) and reached ultimate at 152.4 kN-m (1,348 k-in.), increases of 11.4 and 11.7 percent over the control beams. The preyield and postyield stiffnesses of the strengthened beam were greater than those of the control beams. The ductility of the strengthened beam was less than the ductility of the control beams. The first drop in moment corresponds to the concrete compression failure, and the following downward slope shows the gradual detachment of the composite strip.

H1.5-4-Y-AL47D

This configuration was chosen to use the longest fastener that could be fully embedded into the predrilled hole. Beam H1.5-4-Y-AL47D was strengthened using a single 102-mm (4-in.)-wide hybrid strip. The strip was aligned and held in place by two technicians. Two holes were drilled side by side at the center of the strip, one from each of the two rows. The holes were drilled through the composite strip into the concrete. Fasteners were then driven through these holes into the concrete substrate. Holes were drilled and then fasteners were driven in sets of two proceeding outward toward one end of the strip. Then the holes were drilled and the fasteners driven in sets of two from the center toward the other end of the strip. The free ends of the strip were held in place by technicians throughout the whole process.

Small flexural cracks formed in the moment span shortly after loading began. As the beam approached its yield strength, flexural cracks began to appear in the shear span, near the loading points. As the beam yielded and continued to gain strength, these cracks began to "bend over" into flexural-shear cracks. The beam reached ultimate strength as the concrete failed in compression in the moment span near the north load point. At this time, the composite strip was still firmly attached to the concrete beam. Immediately following the concrete compression, shear cracks formed in the shear spans near the supports. Some time after the compression failure, loud cracking noises could be heard from the tensile side of

the beam, and suddenly, under the north load point, the composite strip detached, and large chunks of concrete fell out of the concrete beam (Figure 21). These chunks were roughly the same size and shape as those that fell out of beam H1.5-4-Y-AL42D.

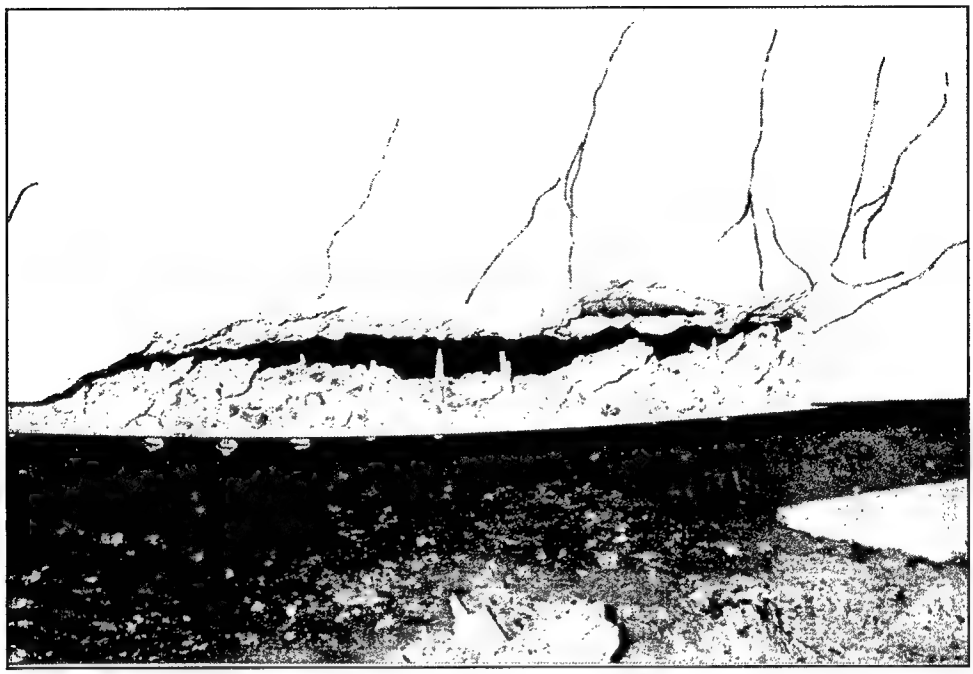

Figure 21. After testing, large chunks of concrete had fallen out of beam H1.5-4-Y-AL47D

The beam yielded at 139.1 kN-m (1,231 k-in.) and reached ultimate at 152.4 kN-m (1,450 k-in.), increases of 13.8 and 20.1 percent over the control beams. The preyield and postyield stiffnesses of the strengthened beam were greater than those of the control beams. The first drop in moment corresponds to the concrete compression failure, and the second drop in moment corresponds to the composite strip detaching from the concrete beam. This beam had the same ductility as the unstrengthened control beams. The highest amount of strengthening was exhibited in this test.

H1.5-4-Y-AL47D-3 and H1.5-4-Y-AL47D-3-R

The first beam was tested to see the effect of using a larger fastener spacing, ultimately using less fasteners than in beam H1.5-4-Y-AL47D. The results of the first test with 76-mm (3-in.) spacing were close enough to the results of the test with 51-mm (2-in.) spacing that a repeat of the 76-mm (3-in.) spacing was done to conserve fasteners. A single 102-mm (4-in.)-wide hybrid strip was used to strengthen each of these beams. Fasteners were spaced 76-mm (3-in.) apart. The spacing was the same over the entire length. The crack pattern for these two beams was similar. Flexural cracks became visible in the midspan at about half of the yield strength. As the tests approached the yield strength of the beams, flexural cracks started to appear under the load points. As the beams failed in compression, shear cracks formed in the shear span. At this time, the composite

strip was still firmly attached to the concrete beam. After compression failure, the strip on beam H1.5-4-Y-AL47D-3 remained firmly attached throughout the rest of the test, while the strip on beam H1.5-4-Y-AL47D-3-R detached soon after the beam failed in concrete compression.

Both beams yielded at 139.1 kN-m (1,231 k-in.), a 13.8 increase over the control beams. Beams H1.5-4-Y-AL47D-3 and H1.5-4-Y-AL47D-3-R reached ultimate strengths of 159.4 kN-m (1,411 k-in.) and 158.3 kN-m (1,401 k-in.), respectively, increases of 16.9 and 16.1 percent over the ultimate strength of the control beams. The preyield and postyield stiffnesses of these beams were greater than those of the control beams. The ductility of these beams was about the same as that of the control beams.

H1.5-4-B

This beam did not utilize the fastening technique of attachment. The strengthening strip was bonded by using a technique commonly used in practice for comparison purposes. The bottom of the concrete beam was sandblasted until smooth. An outline of the strip was traced on the prepared surface of the beam. A trace was created 13 mm (0.5 in.) larger than this outline on the prepared surface of the concrete using duct tape. The surface was then cleaned with acetone and allowed to dry. A single 102-mm (4-in.)-wide hybrid strip was sanded on one side with 400-grit sandpaper until the resin rich surface was removed. Sikadur Hex 300, a product of the Sika Corporation, was thickened by using fumed silica and applied to the prepared concrete surface and to the prepared strip surface. The strip was aligned at one end with the outline, adhesive side down, and pushed down from the aligned end to the other end. This squeezed out excess adhesive, and then 730 N/m (50 lb/ft) of weights were applied to the strip. The beam was covered in black plastic and left to cure in the sun for 5 days before testing. No special anchorage was provided at the ends of the composite strip.

As beam neared the yield point, hairline flexural cracks were visible in the constant moment region. One flexural crack appeared on the outside of the loading points shortly after the yield strength was passed. As soon as shear cracks appeared in the shear spans near the loading points, the beam failed in a sudden manner, with the composite strip suddenly delaminating from the concrete and striking the floor. After the strip delaminated, the beam behaved as an unstrengthened control beam until the concrete crushed. The delaminated strip had pieces of concrete, a few millimeters thick, attached to it in several places, as seen in Figure 22, which makes it difficult to ascertain whether the failure was initiated by a failure of the bond between the concrete and adhesive or by a failure a few millimeters into the surface of the concrete.

The beam yielded at 148.0 kN-m (1,310 k-in.) and reached ultimate at 163.2 kN-m (1,444 k-in.), increases of 21.1 and 19.7 percent over the control beams. The preyield and postyield stiffnesses of the strengthened beam were greater than those of the control beams, and the stiffer than all the other beams tested.

Figure 22. The delaminated strip from beam H1.5-4-B had pieces of concrete, a few millimeters thick, attached to it in several places

The first drop in moment corresponds to the delamination of the composite strip from the concrete beam, and the second drop in moment corresponds to crushing of the concrete. This beam had a much lower ductility than the control beams.

H1.0-4-Y-AL47D-5

This beam was strengthened with a single 102-mm (4-in.)-wide hybrid strip with two 1-oz. continuous strand mats. This strip, with a lower bearing strength and the spacing of 127 mm (5 in.), was chosen in an attempt to create bearing failure in the composite strengthening strip. The beam had the same yield and ultimate strengths as the controls, 122.3 kN-m (1,082 k-in.) and 136.4 kN-m (1,207 k-in.), and appeared to fail in concrete compression. Upon completion of the test, the strengthening strip was not firmly attached to the concrete. A pry bar was used to remove the strip, and it was seen that bearing failure was indeed initiated around the fasteners. The typical keyhole slot bearing failures around the fasteners in the strip from beam H1.0-4-Y-AL47D-5 is shown in Figure 23.

H1.5-8-Y-AL32

This beam was strengthened using two 102-mm (4-in.)-wide hybrid strips. This configuration was chosen to utilize a smaller edge distance and a larger strip area. The strips were placed next to each other and held in place by weights and two laboratory technicians. As with beams strengthened using a single composite strip, two rows of fasteners were used per strip, for a total of four rows of fasteners. This resulted in an edge distance of 3 in. rather than an edge distance of 127 mm (5 in.) as in the beams where only one strip was used. This decreased edge distance caused a large amount of initial cracking when the fasteners were driven into the beam, similar to beam I-8-Y-AL32.

The beam failed by the sudden detachment of both of the strips. The beam then acted as an unstrengthened beam, similar to a control beam, until the concrete crushed in the moment span near the north load point. After testing,

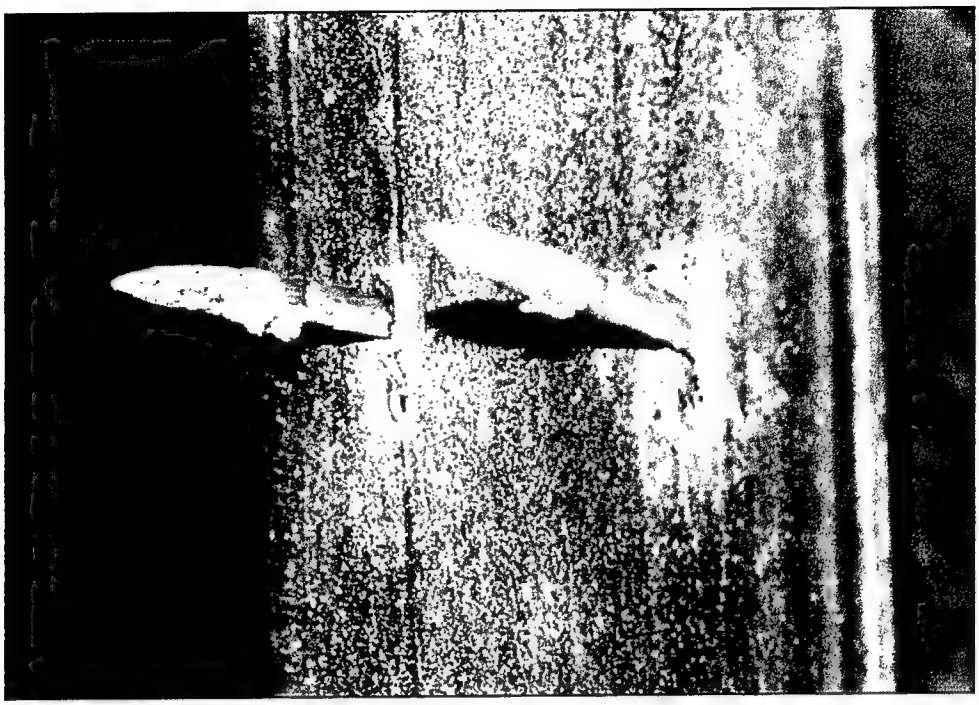

Figure 23. The typical keyhole slot bearing failures around the fasteners in the strip from beam H1.0-4-Y-AL47D-5

severe cracking was visible along the lower edges of the beam. The beam just began to yield as the strips detached, so the ultimate strength is the same as the yield strength, 148.7 kN-m (1,316 k-in.), a 21.6-percent increase over the yield of the control beams. However, this beam failed suddenly at this point, possessing no postyield ductility.

Discussion of Strain Distribution Along FRP Strip

Strain gages were attached to the strengthening strip at short intervals from the midspan to one end of the strip on beams I-4-Y-AL32-R, H1.5-4-Y-AL47D-3-R, H1.0-4-Y-AL47D-5, and H1.5-4-B. The distribution for beam I-4-Y-AL32-R is shown in Figure 24 as an example. All of the strain distributions are shown in Appendix D. All of the plots show the strain at given moments along the center span. The strain lines start getting further apart when the beam begins to yield because the beam deflects much more for a given increment in moment. The average strain at ultimate is shown with a thick black line on each plot. The average strain within the moment span is found by averaging the strain gages in this span. The average strain in the shear span is found by taking a linear regression of the strain gages in the shear span. It should also be noted that in beams I-4-Y-AL32-R and H1.5-4-Y-AL47D-3-R and possibly H1.0-4-Y-AL47D-5, the close proximity of the fasteners to the strain gages might have caused local stress concentrations, affecting the strain contours.

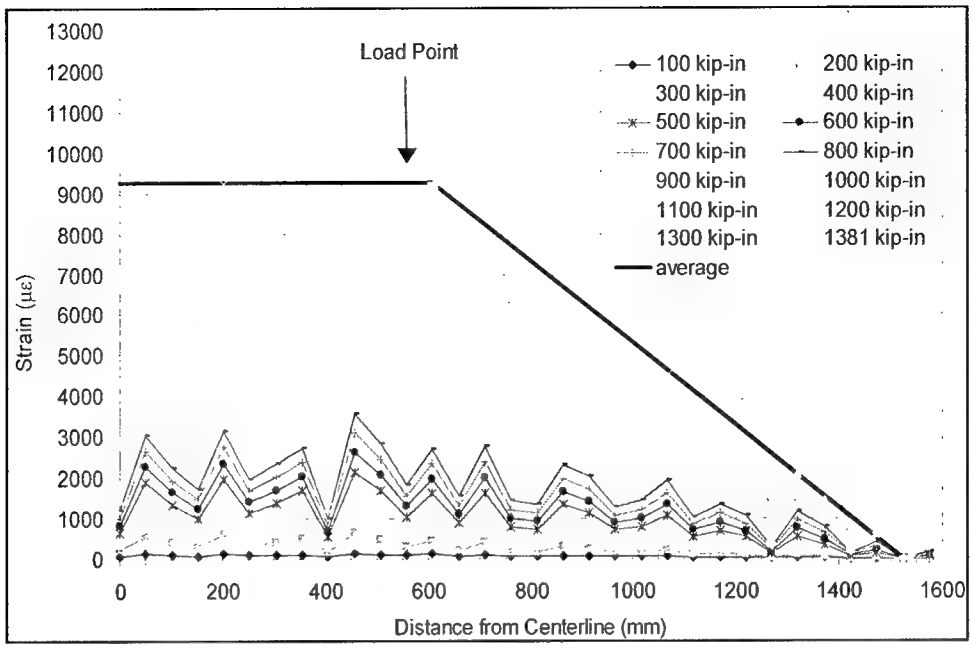

Figure 24. The strain distribution in the strip attached to beam I-4-Y-AL32-R

All four strain contour plots show a constant strain region within the constant moment span. For the beams with fastened strips, this constant strain region extends past the loading points into the shear span. Within the shear spans, there is a linear decrease in strain. This linear decrease in strain is seen almost perfectly in beam H1.5-4-B, the beam with a bonded strengthening strip. The other three beams show a jagged decrease in strain, the peaks and valleys most likely caused by stress concentrations and the variability of fastener strength. If the peaks and valleys are smoothed, a linear decrease in strain can be seen, which confirms the prior assumption that the load is transferred equally among all the fasteners in the shear span.

Strain Gage Data

Strain data from the gages mounted on the top concrete surface, the internal compression steel, the internal tension steel, and the FRP strip at midspan is given in Appendix E. The maximum external concrete strain data are bilinear for all beams up until ultimate moment. The compression steel strain is jumpy for most of the beams. The tensile steel strains are fairly bilinear for some of the beams. It is thought that the beams for which the strain readings from the internal gages were sporadic or very low lacked sufficient bond to the rebar or were damaged during the casting of the concrete beams.

The FRP center strain was bilinear for all of the tests. The strains were recorded at the midspan on the bottom surface of the composite strengthening strip. If two or more gages were used in the moment span of the beam, the average was taken as the stress in the strip. The FRP end strain was taken from a strain gage on the end of the strengthening strip, outside the last set of fasteners. If there was peeling at the end of the strip, the gage mounted on the surface of the

strip would go into compression. Most of the beams only exhibited about 300 με in this gage, but beam I-4-Y-AL32 showed about 490 με at ultimate and beam I-4-N-AL32 showed about 730 με at ultimate. These strain data will be utilized in the third year of the study to help refine the analytical model.

Discussion of Fastener Loads

In each test, a minimum of two strain gages was placed on the composite strengthening strip in the moment span. The strain in the strip at failure is listed in Table 6. The stress in the strip was calculated by using these strain data and the modulus determined by coupon testing. The force in the strip was calculated by using the area of the strip, and then the load per fastener was calculated. The load per fastener data at ultimate strength is given for the full-scale beams in Table 7.

Table 7
Load per Fastener Information at Ultimate Strength

Test Name	# of Fasteners	# of Fasteners In Shear Span	Average Midspan FRP Stress (MPa)	Force In FRP (kN)	Force per Fastener (N)	% of Design Load[1]
S-4-Y-AL32	124	40	3.35	51.4	1,284	57.1
I-4-N-AL32	90	40	3.39	52.0	1,301	57.8
I-4-Y-AL32	124	40	4.20	64.5	1,612	71.6
I-4-Y-AL32-R	124	40	5.10	78.3	1,957	87.0
I-8-Y-AL32	248	80	2.15	65.8	823[2]	36.6[2]
H1.5-4-Y-AL32	124	40	4.03	61.8	1,546[2]	68.7[2]
H1.5-4-Y-AL42D	124	40	7.18	110.1	2,752	61.2
H1.5-4-Y-AL47D	124	40	9.31	142.8	3,570	79.3
H1.5-4-Y-AL47D-3	84	28	8.57	131.4	4,694	104.3
H1.5-4-Y-AL47D-3-R	84	28	6.53	101.0	3,606	80.1
H1.5-4-B	-	-	7.08	108.5	-[2]	-[2]
H1.5-4-Y-AL47D-5	50	16	4.59	70.3	4,392	97.6
H1.5-8-Y-AL32	248	80	3.45	105.9	1,323[2]	58.8[2]

[1] Design load of 2,224 N for AL32 fasteners; 4,448 N otherwise.
[2] Beam failed by strip detaching.

All of the beams strengthened by using fasteners to attach the composite strengthening strip failed by concrete compression with the exception of three. The three beams that failed by the strip detaching used AL32 fasteners without predrilling. These detachments occurred at lower fastener loads than the 2,224-N (500-lb) design limit calculated for the 32-mm (1.26-in.) fasteners.

The loads per fastener for the three beams that failed by strip detachment occurred at a much lower load than other beams using the same type of fastened connection. Two of the tests that failed by strip detachment used two 102-mm (4-in.)-wide strengthening strips, which decreased the edge distance from 127 mm (5 in.) to 76 mm (3 in.). These connections could have been weakened by the cracking that occurred during the attachment of the composite strip, thereby causing premature detachment of the composite strip. Beam H1.5-4-Y-AL32 had

the highest load per fastener of the beams that failed by strip detachment, and since a large amount of spalling was seen, failure could have been caused by the presence of several poorly connected fasteners.

Experiment versus Analytical Model Comparison

The m - ϕ analytical model was used to calculate the ultimate moment for each of the beam tests. The analytical model predicted lower values for all tests. It is important to note that the standard Whitney stress block method predicts lower ultimate moments than the analytical model in all cases, except when the fasteners fail. Table 8 shows a comparison of the experimental ultimate moments to the analytical model ultimate moments.

Table 8
Experimental and Analytical Ultimate Moments

Test Name	Exp. Ultimate Moment (kN-m)	m - ϕ Model Ultimate Moment (kN-m)	% From Exp.	Actual Failure Mode[1]	m - ϕ Model Failure Mode[1]	m - ϕ Model Ultimate Concrete Failure (kN-m)	% from Exp.
Control 1	136.4	105.0	-23.0	CC	CC		
Control 2	136.4	105.0	-23.0	CC	CC		
S-4-Y-AL32	142.6	119.7	-16.0	CC	CC		
I-4-N-AL32	141.3	126.5	-10.4	CC	SD	128.6	-9.0
I-4-Y-AL32	150.4	126.5	-15.9	CC	SD	128.6	-14.5
I-4-Y-AL32-R	156.1	126.5	-18.9	CC	SD	128.6	-17.6
I-8-Y-AL32	152.8	145.9	-4.5	SD	CC		
H1.5-4-Y-AL32	146.2	121.4	-17.0	SD	SD	148.4	+1.5
H1.5-4-Y-AL42D	152.4	147.8	-3.0	CC	SD	148.4	-2.6
H1.5-4-Y-AL47D	163.9	147.8	-9.8	CC	SD	148.4	-9.5
H1.5-4-Y-AL47D-3	159.4	132.7	-16.8	CC	SD	148.4	-6.9
H1.5-4-Y-AL47D-3-R	158.3	132.7	-16.2	CC	SD	148.4	-6.3
H1.5-4-B	163.2	148.4	-9.1	SD	CC		
H1.5-4-Y-AL47D-5	136.0	114.5	-15.8	CC	SD	148.4	+9.1
H1.5-8-Y-AL32	148.7	144.6	-2.8	SD	SD	148.4	-0.2

[1] CC = Concrete Compression
SD = Strip Detachment

The model underpredicted the strength of the beams in all cases. In the cases of beams strengthened with a single intermediate strip, the model was low by 10.4 to 18.9 percent. For these beams, the model predicts strip detachment. Even if the fastener capacity was increased above 2,269 N (510 lb), the model predicted a failure strength by concrete compression lower by 9.0 to 17.6 percent. Beam I-8-Y-AL32 was predicted to fail by concrete crushing at an ultimate strength of 4.5 percent lower than the experimental strength. The experimental beam failed by strip detachment.

For the beams strengthened with the hybrid strip, the model was low by 2.8 to 17.0 percent. The closest prediction occurred for beam H1.5-8-Y-AL32, where the model predicted strip detachment at a strength only 2.8 percent lower than the experimental strength.

Beam Test Conclusions

The strengthening capacity of beams H1.5-4-Y-AL47D, H1.5-4-Y-AL47D-3, and H1.5-4-Y-AL47D-3-R was similar to the strengthening capacity of the traditional bonded method; however, the proposed method provides an added benefit of increased ductility. Figure 25 shows the moment-center deflection behavior for these three beams and the control beams. Since microcracking begins in the concrete and bearing failure initiates in the composite strip, the system fails progressively in a pseudo-ductile manner.

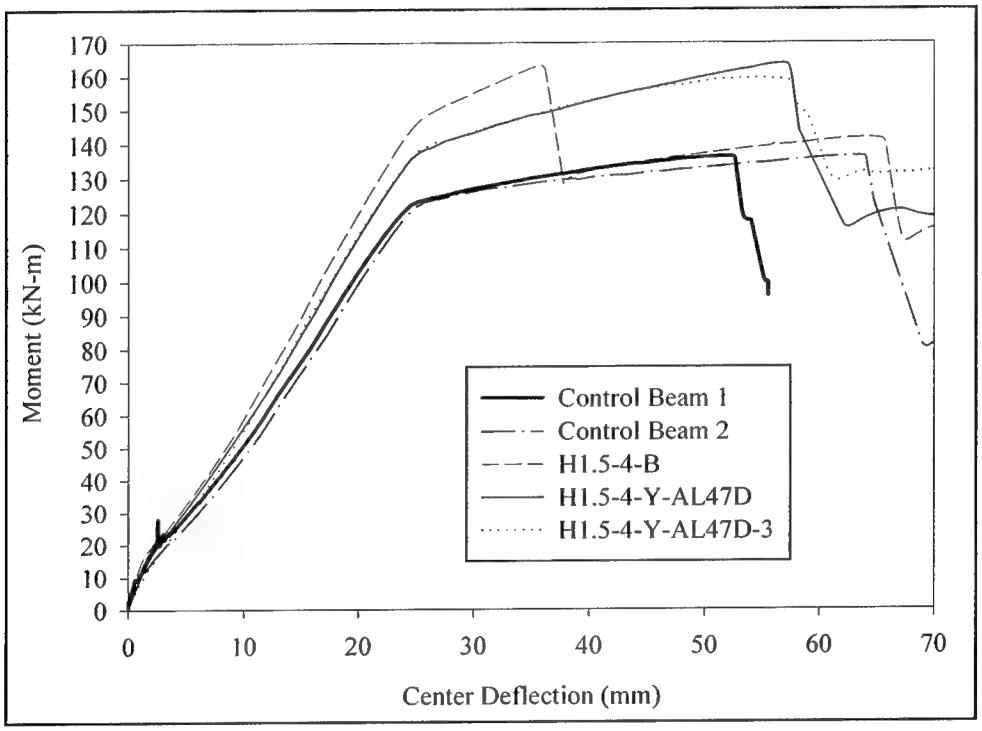

Figure 25. Moment versus center deflection for selected beams

It appears that attaching FRP strengthening strips to full-scale reinforced concrete beams with powder-actuated fasteners is as effective as the traditional method of bonding the strips to the beams. The fastened method takes much less time, which makes it a viable option for instances where speed of installation is a major factor.

8 Conclusions and Recommendations

A series of tests on large-scale reinforced concrete beams strengthened with powder-actuated fasteners and FRP strengthening strips has shown that with the correct fastener layout and strip properties, strengthening capacity equal to that of beams strengthened by bonding the strip to the beam can be achieved.

The large-scale tests showed increases in yield and ultimate strength up to 13.8 and 20.1 percent for beams strengthened with predrilled fasteners. All beams with predrilled fasteners failed in a pseudo-ductile manner, where the tensile steel yields, then the concrete crushes. Beams without predrilled fasteners showed increases in yield and ultimate strength up to 21.6 and 14.4 percent. These numbers are misleading because the higher the strengthening effect with fasteners without predrilling, the more likely the failure was the result of strip detachment.

The current analytical model under predicts the strength, because the load in the fasteners in the model reaches failure and the strip detaches before the concrete crushes in compression. One factor contributing to this discrepancy is that the strain distribution through the cross section may not be linear when the beam has passed the yield point (Bonacci and Maalej 2000). Another factor may be the slip in the fasteners causing the beam to have higher curvature, different moment force moment arms, and therefore, different strengths.

This study has demonstrated that the method is comparable to the current method of bonding composite strengthening strips to reinforced concrete beams in terms of strengthening, and that the method is potentially better than the bonded method in terms of ductility. In order to continue to develop the proposed method as a viable, real-world rapid strengthening method, the following are recommended:

a. Conduct a series of tests on concrete beams of real-life proportions, larger than the beams tested in the second year of this study.

b. Conduct a series of tests on concrete beams of the same proportions as those tested in the second-year study in order to examine the effect of shear span to moment span ratio.

c. Develop a design guide draft.

d. Develop an application guide draft.

e. Conduct additional coupon tests on composite strips fastened to concrete to determine the amount of slip between the concrete surface and the strip.

f. Continue work on the analytical model to incorporate slip between the concrete surface and the composite strip.

g. Further investigate different failure modes in concrete beams reinforced with composite strengthening strips.

h. Determine the feasibility of strengthening loaded and precracked beams.

i. Determine the feasibility of using the method to strengthen beams for shear or compression.

j. Determine the influence of cyclic and dynamic loads on beams strengthened with this method.

k. Determine the long-term load-carrying capacity of beams strengthened by this method.

l. Determine the effect of environmental factors on the behavior of beams strengthened with this method.

References

American Concrete Institute Committee 318. (1999). "Building code requirements for structural concrete (318-99) and commentary (318R-99)," Farmington Hills, MI, 391.

American Concrete Institute Committee 440F. (2000a). "Guide for the design and construction of externally bonded FRP systems for strengthening concrete structures," (May 24, 2000, revision, accepted and pending publication), Detroit, MI.

American Concrete Institute Committee 440H. (2000b). "Guide for the design and construction of concrete reinforced with FRP bars," (October 1, 2000, revision, accepted and pending publication), Detroit, MI.

American Society Testing and Materials. (1999). "Standard test method for tensile properties of polymer matrix composite materials," Designation D 3039, West Conshohocken, PA.

Arduini, M., and Nanni, A. (1997). "Behavior of precracked RC beams strengthened with carbon FRP sheets," *ASCE Journal of Composites for Construction* 1(2), 63-70.

Bank, L. C., and Lamanna, A. J. "Final Report: Rapid repair of concrete structures using composite materials and power actuated fastening systems" (unpublished), provided to the ERDC under Contract No. DACA39-99-K-0001.

Bonacci, J. F., and Maalej, M. (2000). "Externally bonded fiber-reinforced polymer for rehabilitation of corrosion damaged concrete beams," *ACI Structures Journal* 97(5), 703-711.

Buyukozturk, O., and Hearing, B. (1998). "Failure behavior of precracked concrete beams retrofitted with FRP," *ASCE Journal of Composites for Construction* 2(3), 138-144.

Comite Euro-International du Beton (CEB). (1994). *Fastenings to concrete and masonry structures.* Thomas Telford Services Ltd., London, England.

Emmons, P. H., Vaysburg, A. M., and Thomas, J. (1998a). "Strengthening of concrete structures, part I, current practice," *Concrete International* 20(3), 53-58.

_____. (1998b). "Strengthening of concrete structures, part II, advanced composites," *Concrete International* 20(4), 56-60.

Hognestad, E. (1951). "A study of combined bending and axial load in reinforced concrete members," Bulletin No. 399, Engineering Experiment Station, University of Illinois, Urbana.

Hussain, M., Sharif, A., Basunbul, I. A., Baluch, M. H., and Al-Sulaimani, G. J. (1995). "Flexural behavior of precracked concrete beams strengthened externally by steel plates," *ACI Structures Journal* 92(1), 14-22.

Lamanna, A. J., Bank, L. C., and Scott, D. W. (2001a). "Flexural strengthening of RC beams using fasteners and FRP strips," *ACI Structures Journal* 98(3), 368-376.

_____. (2001b). "Rapid flexural strengthening of RC beams using powder actuated fasteners and FRP strips." *FRPRCS-5 Conference on Non-Metallic Reinforcement for Concrete Structures.* Cambridge, England, July 16-18. 1, 389-397.

Mason, N. (2000). "Strength and stiffness of fiber reinforced plastic and concrete fastener connections," CEE 699 Independent Study Report, Department of Civil and Environmental Engineering, University of Wisconsin – Madison.

Ray, J. C., Scott, D. W., Lamanna, A. J., and Bank, L. C. (2000). "Flexural behavior of reinforced concrete members strengthened using mechanically fastened fiber reinforced polymer plates." *22nd Army Science Conference.* Baltimore, Maryland, December 11-13.

Soroushian, P., and Choi, K. (1991). "Analytical evaluation of straight bar anchorage design in exterior joints," *ACI Structures Journal*, 161-168, March-April 1991.

Spadea, G., Bencardino, F., and Swamy, R. N. (1998). "Structural behavior of composite RC beams with externally bonded CFRP," *ASCE Journal of Composites for Construction* 2(3), 132-137.

Swamy, R. N., Jones, R., and Bloxham, J. W. (1987). "Structural behavior of reinforced concrete beams strengthened with epoxy-bonded steel plates," *The Structural Engineer* 65A, 59-68.

Wang, C., and Salmon, C. G. (1998). *Reinforced Concrete Design.* 6th ed., Harper Collins Publishers, Inc., New York, 1028.

Appendix A
FRP Strengthening Strip Test Data

Standard Strip
Tensile Test

Test:
S 20 Series
Operator Name:
NTH
Test Date:
06/13/00

FRP Plate Manufacturer:
Strongwell
Width (in.)[1]
1 in. Nominal
Thickness (in.)
0.125

FRP Plate Type:
[Standard]

Stress vs. Displacement

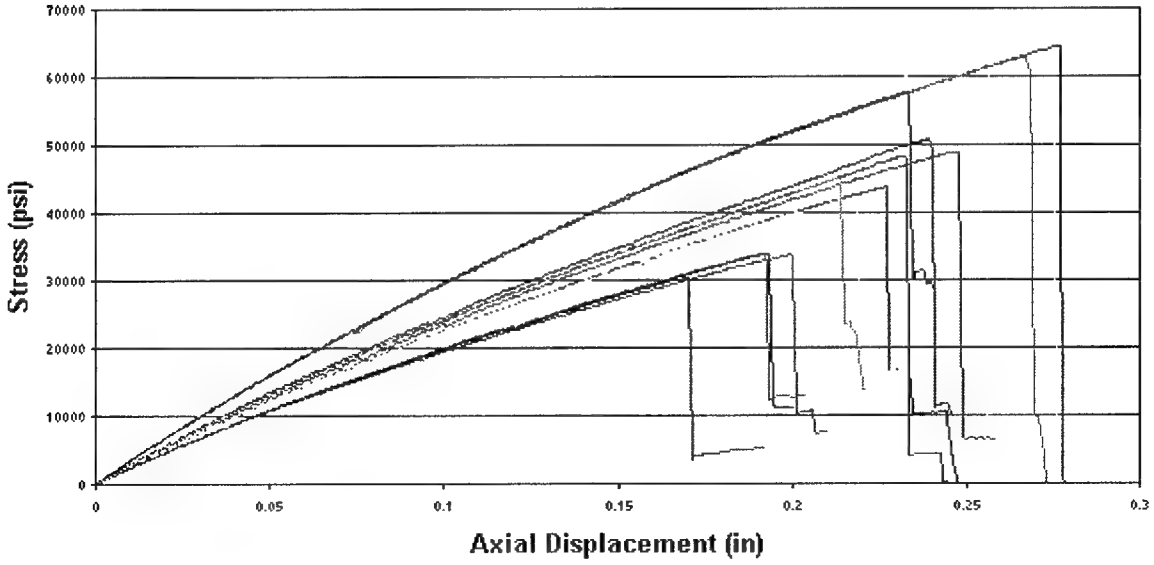

[1] To convert U.S. Customary units of measurement to SI units, refer to the conversion factors table presented on page viii.

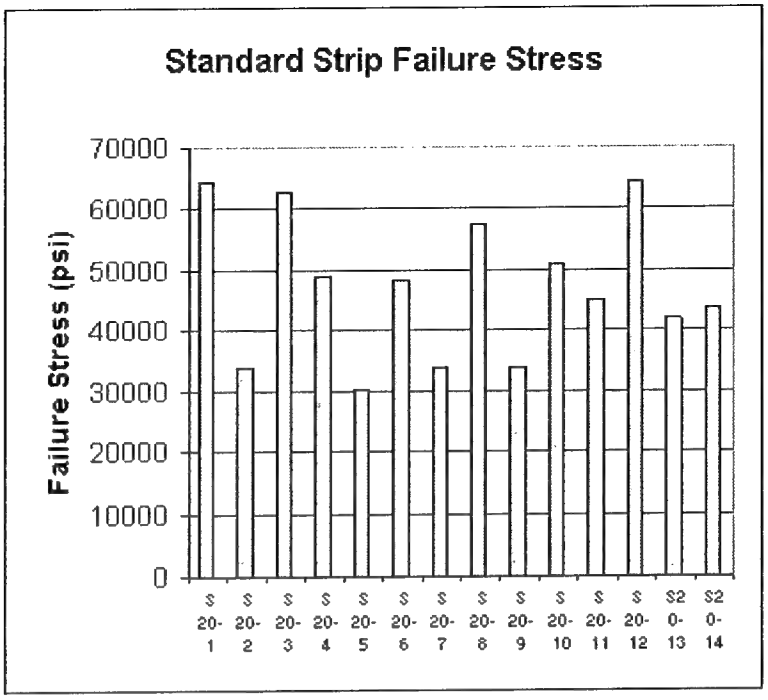

Test #	Failure Stress (psi)	Modulus of Elasticity (psi)
S 20-1	64,513	n/a
S 20-2	33,700	n/a
S 20-3	62,761	2,767,302
S 20-4	48,921	n/a
S 20-5	30,376	1,794,881
S 20-6	48,277	2,159,841
S 20-7	33,965	1,883,796
S 20-8	57,608	2,980,793
S 20-9	33,802	1,682,335
S 20-10	50,807	2,378,863
S 20-11	45,066	2,158,020
S 20-12	64,329	2,562,087
S20-13	42,059	1,999,443
S20-14	43,744	1,894,889
Average	47,138	2,205,659
Std. Dev.	11,844	419,880
COV	25	19

Intermediate Strip
Tensile Test

Test:
I 56 Series
Operator Name:
NTH
Test Date:
06/14/00

FRP Plate Manufacturer:
Strongwell
Width (in.)
1 in. Nominal
Thickness (in.)
0.125

FRP Plate Type:
[Intermediate]

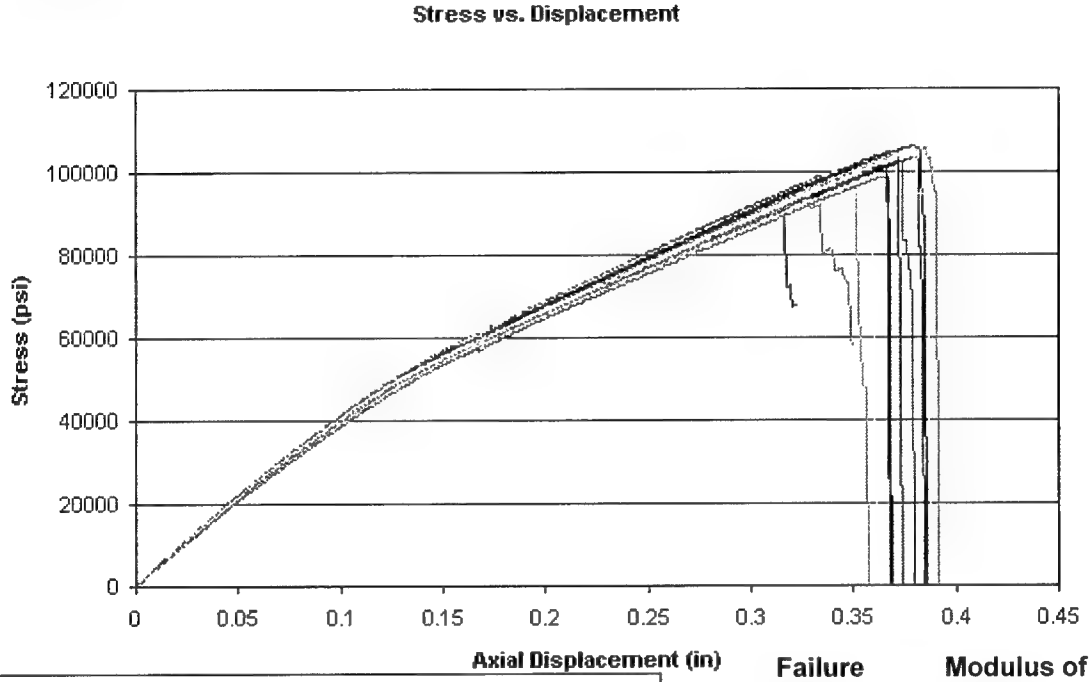

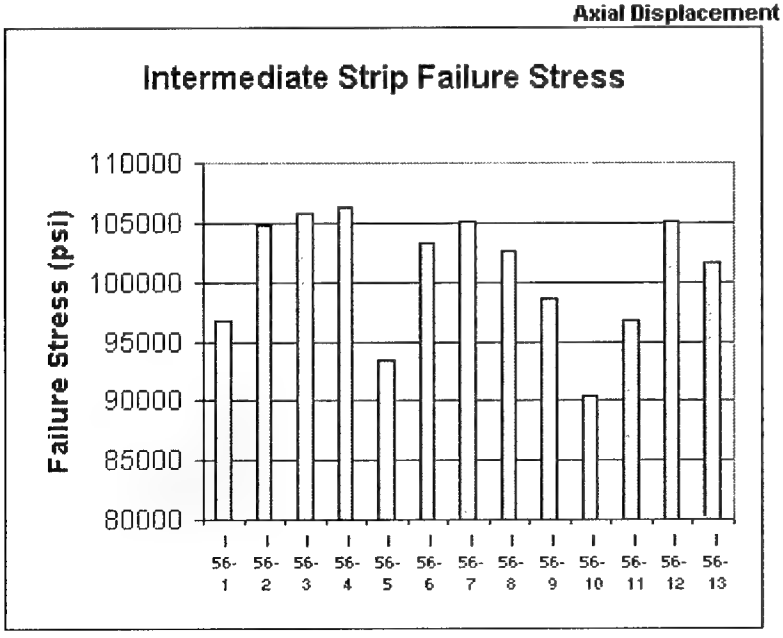

Failure Stress (psi)	Modulus of Elasticity (psi)
96,765	n/a
104,774	n/a
105,755	3,960,419
106,272	3,676,848
93,424	3,755,993
103,372	3,791,549
105,076	4,065,208
102,645	3,730,407
98,660	3,608,891
90,417	3,726,776
96,730	3,856,068
105,085	3,814,543
101,670	3,990,085
100,819	3,816,072
5,143	140,220
5.1	3.7

Hybrid 1.0 Strip
Tensile Test

Test:
Hybrid 1.0 Series
Operator Name:
NTH
Test Date:
06/14/00

FRP Plate Manufacturer:
Strongwell
Width (in.)
1 in. Nominal
Thickness (in.)
0.125

FRP Plate Type:
[Hybrid 1.0]

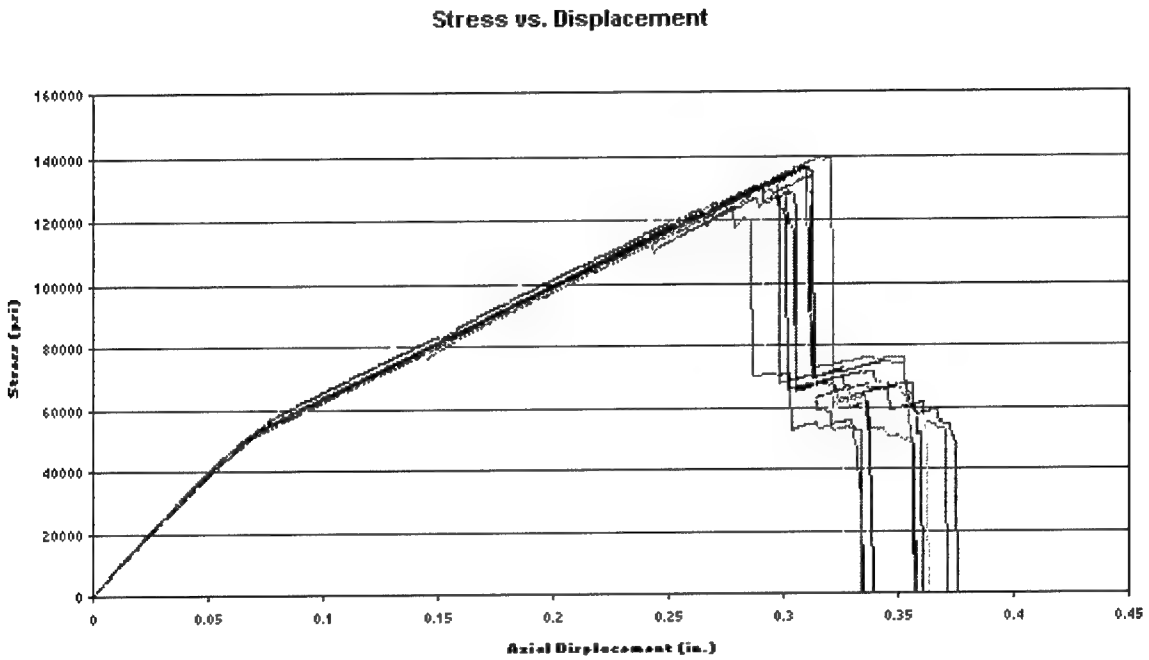

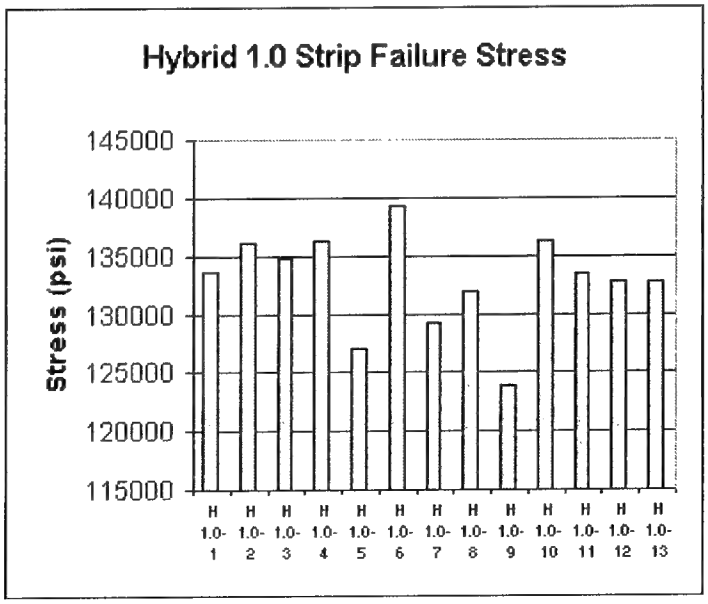

Test #	Failure Stress (psi)	Modulus of Elasticity (psi)
H 1.0-1	133,528	n/a
H 1.0-2	136,073	n/a
H 1.0-3	134,840	8,142,803
H 1.0-4	136,325	7,824,849
H 1.0-5	127,001	8,144,074
H 1.0-6	139,229	8,273,743
H 1.0-7	129,296	7,978,581
H 1.0-8	131,950	8,576,081
H 1.0-9	123,873	8,408,696
H 1.0-10	136,355	8,053,451
H 1.0-11	133,379	8,227,142
H 1.0-12	132,790	8,238,452
H 1.0-13	132,833	8,924,758
Average	132,882	8,253,875
Std. Dev.	4,167	300,604
COV	3.1	3.6

Hybrid 1.5 Strip
Tensile Test

Test:
Hybrid 1.5 Series
Operator Name:
NTH
Test Date:
06/14/00

FRP Plate Manufacturer:
Strongwell
Width (in.)
1 in. Nominal
Thickness (in.)
0.125

FRP Plate Type:
[Hybrid 1.5]

Stress vs. Displacement

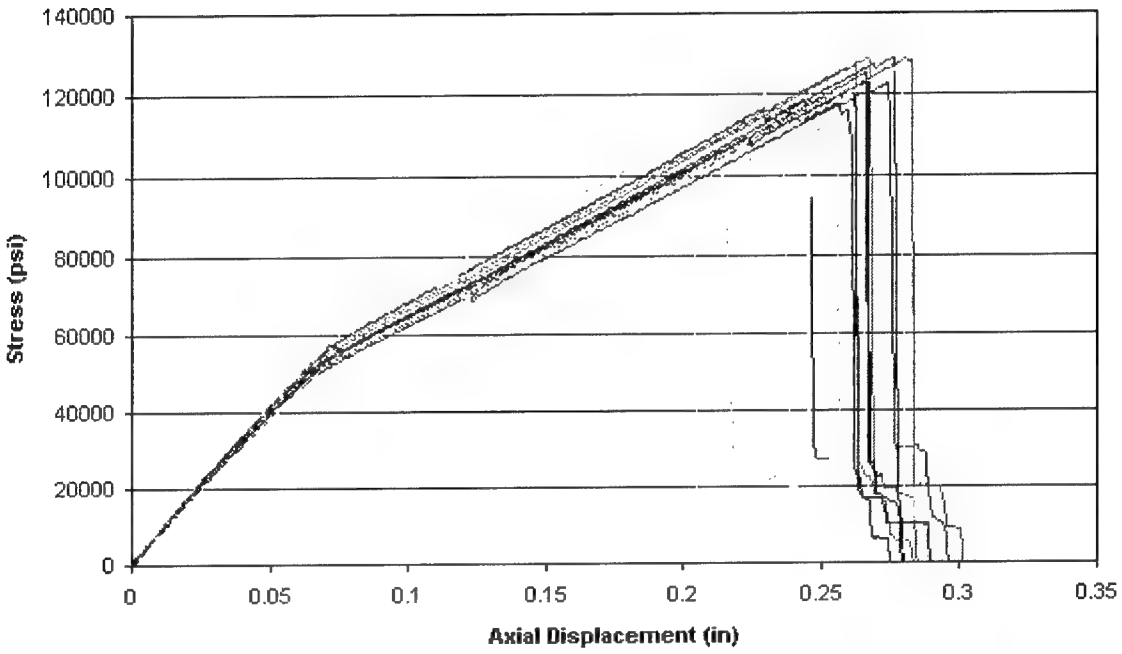

Test #	Failure Stress (psi)	Modulus of Elasticity (psi)		Test #	Modulus of Elasticity (psi)
H 1.5-1	128,826	n/a		H 1.5-11	n/a
H 1.5-2	122,680	n/a		H 1.5-12	n/a
H 1.5-3	126,164	8,253,129		H 1.5-13	8,279,870
H 1.5-4	127,928	8,216,159		H 1.5-14	9,080,774
H 1.5-5	120,813	8,417,242		H 1.5-15	7,165,571
H 1.5-6	128,834	9,313,291		H 1.5-16	7,747,446
H 1.5-7	128,863	8,794,495		H 1.5-17	7,518,711
H 1.5-8	122,413	8,290,681		H 1.5-18	7,430,356
H 1.5-9	124,952	9,037,802		H 1.5-19	7,585,055
H 1.5-10	117,391	8,595,431		H 1.5-20	8,927,321
		Average	120,114	8,290,833	
		Std. Dev.	9,216	653,108	
		COV	7.7	7.9	

Appendix B
FRP/Concrete Connection Test Data

Standard A

1-in.-wide S, 27-mm DNI w/ 18-mm Washer

Test:	**Max Aggregate Size:**	**FRP Plate Manufacturer:**	**FRP Plate Type:**
S A Series	38.1 mm	Strongwell	[S 20]
Operator Name:	**Age (Days):**	**Width (mm)**	**Fastener Type:**
NTH	28+	25.4 mm Nominal	X-DNI 27 P8
Test Date:	**Power Level**	**Thickness (mm)**	**Diameter (mm):**
06/12/00	Y2	3.18	3.68

Force vs. Displacement

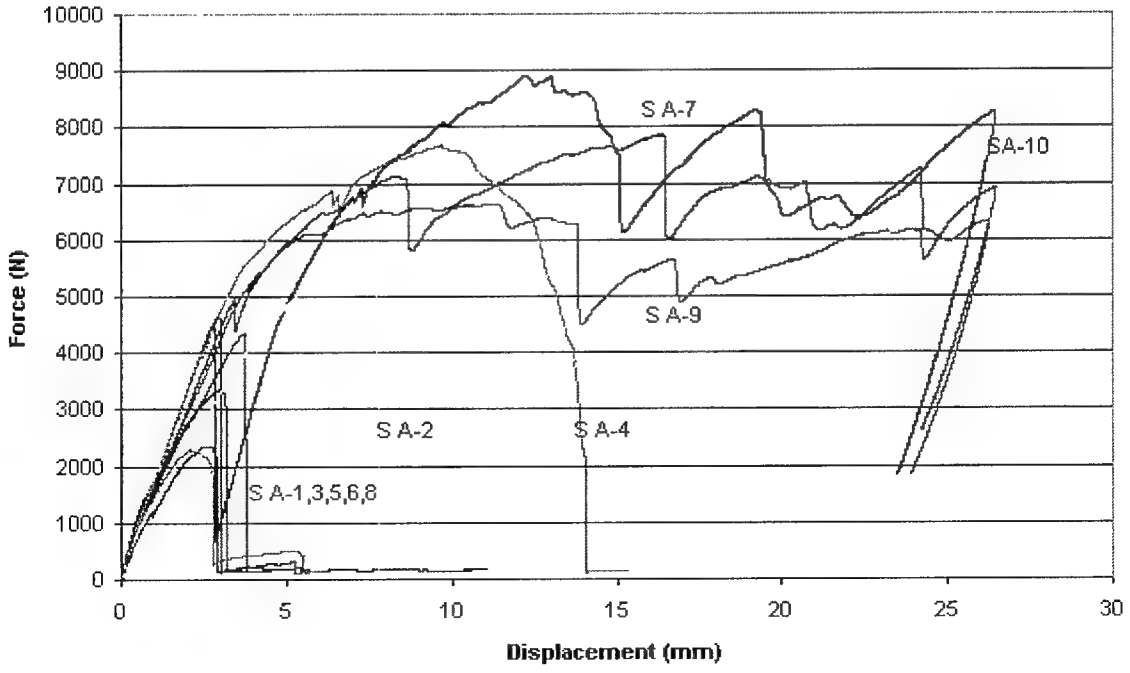

Failure Type	Concrete	Composite
Number of Failures	7	3
Average	4,357	7,806
Std. Dev.	1,931	1,137
COV	44.3	14.6

One sample failed by J-ing when the fastener was driven into the concrete

Test #	Failure Mechanism	Maximum Load (N)	Disp. @ Max Load (mm)
S A-1	Concrete	2,295	2.11
S A-2	Concrete	5,768	7.44
S A-3	Concrete	2,357	2.49
S A-4	Concrete	7,679	9.67
S A-5	Concrete	3,367	3.01
S A-6	Concrete	4,679	2.97
S A-7	Bearing	7,861	16.37
S A-8	Concrete	4,352	3.72
S A-9	Bearing	6,643	11.40
S A-10	Bearing	8,915	12.26
	Average	5,391	7.14
	Std. Dev.	2,356	5.05
	COV	43.7	70.6

Standard B

1-in.-wide S, 32-mm ZF w/ 18-mm Washer

Test:	**Max Aggregate Size:**	**FRP Plate Manufacturer:**	**FRP Plate Type:**
S B Series	38.1 mm	Strongwell	[S 20]
Operator Name:	**Age (Days):**	**Width (mm)**	**Fastener Type:**
NTH	28+	25.4 Nominal	X-ZF-32 P8
Test Date:	**Power Level**	**Thickness (mm)**	**Diameter (mm):**
06/21/00	Y2.5	3.18	3.51

Displacement vs. Force

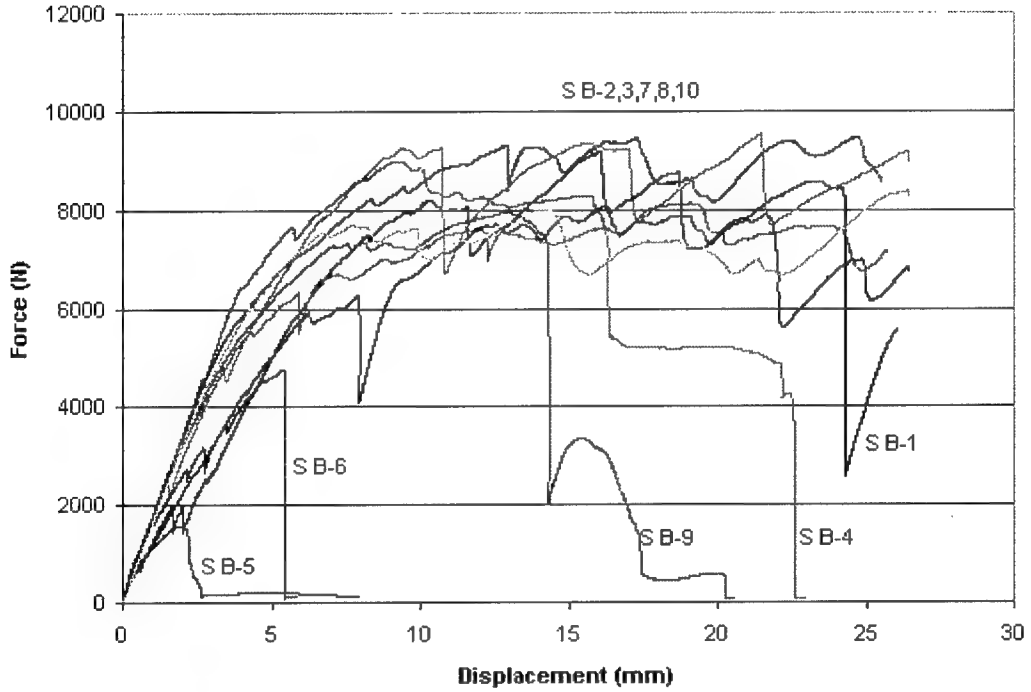

Failure Type	Concrete	Composite	Fastener
Number of Failures	3	6	1
Average	4,760	8,937	7,641
Std. Dev.	3,193	588	0
COV	67.1	6.6	0.0

One sample failed by J-ing when the fastener was driven into the concrete

Test #	**Failure Mechanism**	**Maximum Load (N)**	**Disp. @ Max Load (mm)**
S B-1	Bearing	9,166	16.02
S B-2	Bearing	8,988	9.30
S B-3	Bearing	9,467	24.76
S B-4	Fastener	7,641	11.98
S B-5	Concrete	1,567	1.89
S B-6	Concrete	4,758	5.40
S B-7	Bearing	9,533	21.51
S B-8	Bearing	8,080	16.29
S B-9	Concrete	7,954	12.87
S B-10	Bearing	8,386	26.44
	Average	7,554	14.64
	Std. Dev.	2,517	8.03
	COV	33.3	54.8

Intermediate A

1-in.-wide I (Translucent), 32-mm ZF w/ 18-mm Washer

Test:	Max Aggregate size:	FRP Plate Manufacturer	FRP Plate Type
I A Series	38.1 mm	Strongwell	[I 56]
Operator Name:	**Age (Days):**	**Width (mm)**	**Fastener Type:**
NTH	28+	25.4 mm Nominal	X-ZF-32 P8
Test Date:	**Power Level**	**Thickness (mm)**	**Diameter (mm):**
06/28/00	Y2.5	3.18	3.51

Force vs. Displacement

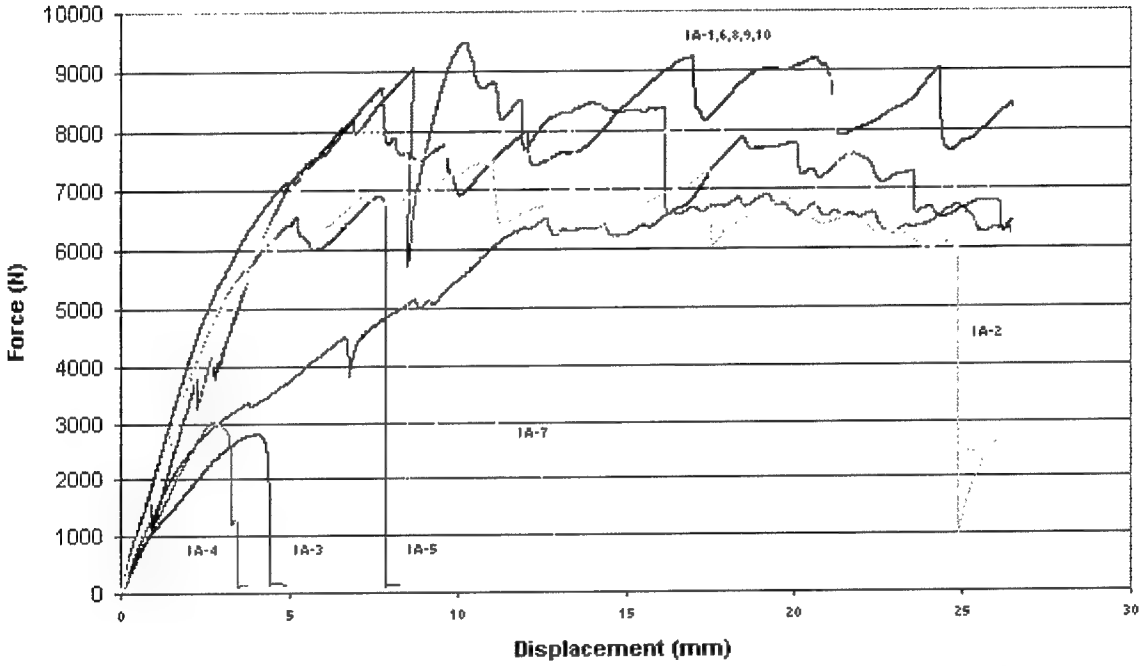

Failure Type	Concrete	Composite
Number of Failures	4	6
Average	5,357	8,428
Std. Dev.	2,914	1,012
COV	54.4	12.0

Test #	Failure Mechanism	Maximum Load (N)	Disp. @ Max Load (mm)
I A-1	Bearing	8,870	21.19
I A-2	Cleavage	7,504	11.11
I A-3	Concrete	2,803	4.08
I A-4	Concrete	3,021	2.78
I A-5	Concrete	6,925	7.70
I A-6	Bearing	9,487	10.29
I A-7	Concrete	8,680	8.32
I A-8	Bearing	8,533	12.73
I A-9	Bearing	6,924	19.16
I A-10	Bearing	9,249	17.01
	Average	7,200	11.44
	Std. Dev.	2,432	6.16
	COV	33.8	53.9

Hybrid 1.0 A

1-in.-wide H1.0, 32-mm ZF w/ 18-mm Washer

Test:	**Max Aggregate Size:**	**FRP Plate Manufacturer:**	**FRP Plate Type:**
H 1.0 A	38.1 mm	Strongwell	[H 1.0]
Operator Name:	**Age (Days):**	**Width (mm.)**	**Fastener Type:**
NTH	28+	25.4 mm Nominal	X-ZF-32 P8
Test Date:	**Power Level**	**Thickness (mm)**	**Diameter (mm):**
06/19/00	Y2.5	3.18	3.51

Force vs. Displacement

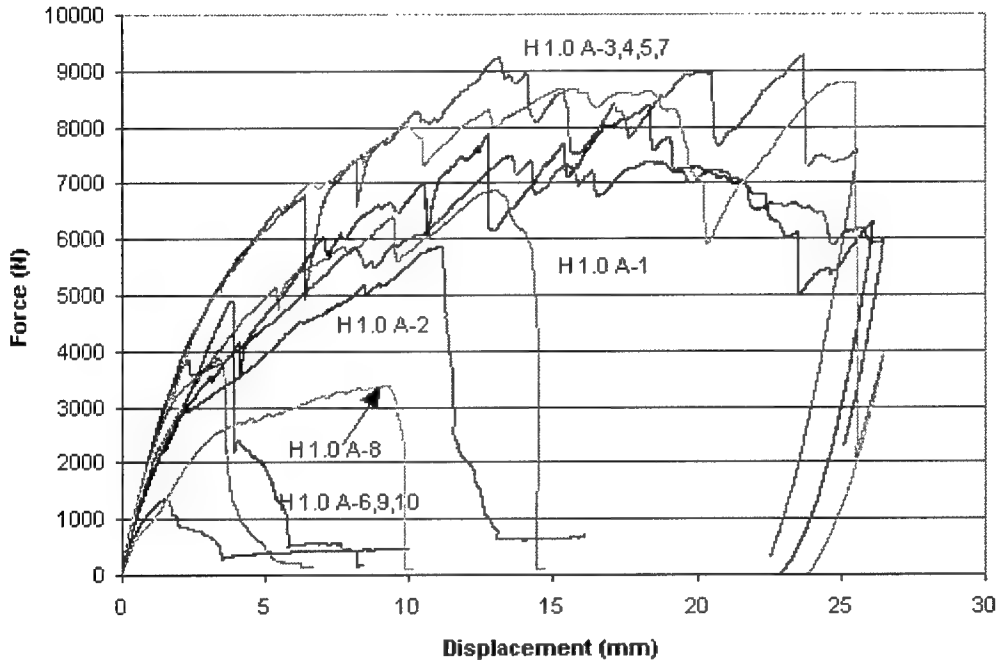

Failure Type	Concrete	Composite
Number of Failures	6	4
Average	4,378	8,486
Std. Dev.	1,953	758
COV	44.6	8.9

Three samples failed by J-ing when the fastener was driven into the concrete

Test #	**Failure Mechanism**	**Maximum Load (N)**	**Disp. @ Max Load (mm)**
H 1.0 A-1	Concrete	6,871	13.02
H 1.0 A-2	Concrete	5,874	11.03
H 1.0 A-3	Bearing	7,482	13.58
H 1.0 A-4	Bearing	8,399	18.28
H 1.0 A-5	Bearing	9,267	23.70
H 1.0 A-6	Concrete	1,357	1.48
H 1.0 A-7	Bearing	8,794	25.43
H 1.0 A-8	Concrete	3,388	9.19
H 1.0 A-9	Concrete	3,883	3.36
H 1.0 A-10	Concrete	4,892	3.85
	Average	6,021	12.29
	Std. Dev.	2,610	8.300
	COV	43.3	67.5

Hybrid 1.5 A

1-in.-wide H1.5, 32-mm ZF w/ 18-mm Washer

Test:	**Max Aggregate Size:**	**FRP Plate Manufacturer:**	**FRP Plate Type:**
H 1.5 A Series	38.1 mm	Strongwell	[H 1.5]
Operator Name:	**Age (Days):**	**Width (mm)**	**Fastener Type:**
NTH	28+	25.4 mm Nominal	X-ZF-32 P8
Test Date:	**Power Level**	**Thickness (mm)**	**Diameter (mm):**
06/20/00	Y2.5	3.18	3.51

Force vs. Displacement

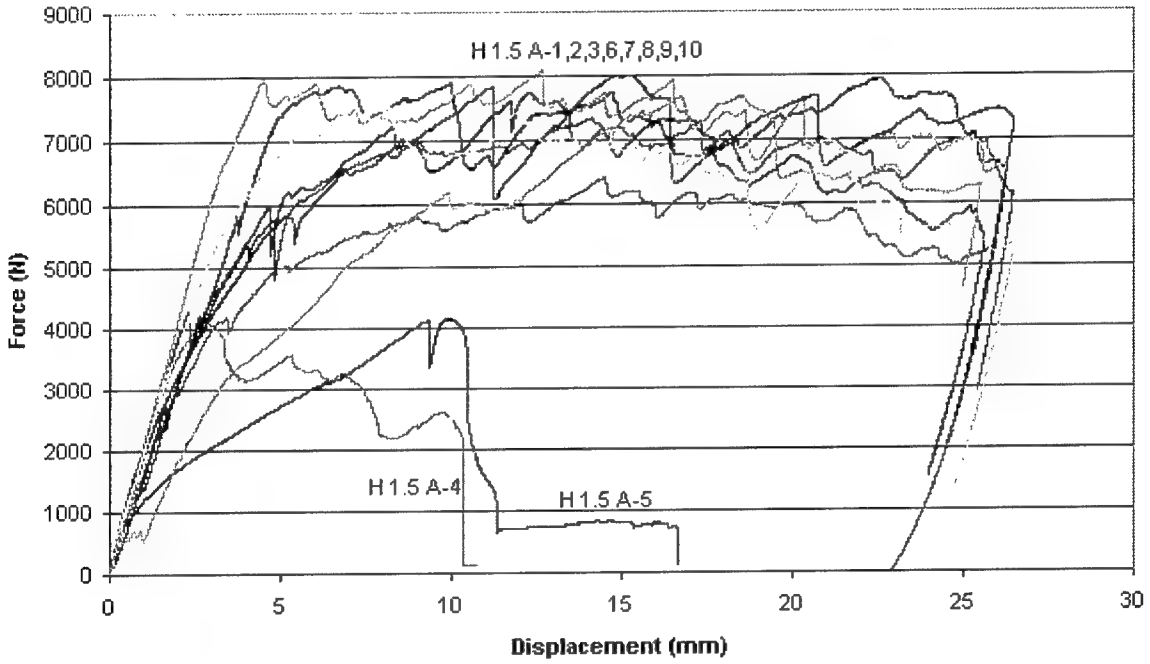

Failure Type	Concrete	Composite
Number of Failures	2	8
Average	4,128	7,613
Std. Dev.	33	551
COV	0.8	7.2

Six samples failed by J-ing when the fastener was driven into the concrete

Test #	**Failure Mechanism**	**Maximum Load (N)**	**Disp. @ Max Load (mm)**
H 1.5 A-1	Bearing	7,671	18.47
H 1.5 A-2	Bearing	7,604	7.22
H 1.5 A-3	Bearing	7,897	9.97
H 1.5 A-4	Concrete	4,105	2.90
H 1.5 A-5	Concrete	4,151	9.92
H 1.5 A-6	Bearing	8,007	14.92
H 1.5 A-7	Bearing	6,414	14.53
H 1.5 A-8	Bearing	8,091	12.71
H 1.5 A-9	Bearing	7,279	17.30
H 1.5 A-10	Bearing	7,944	22.57
	Average	6,916	13.05
	Std. Dev.	1,548	5.776
	COV	22.4	44.3

Hybrid 1.5 B

1-in.-wide H1.5, Predrilled 47-mm AL w/ 18-mm Washer

Test:	**Max Aggregate Size:**	**FRP Plate Manufacturer:**	**FRP Plate Type:**
H 1.5 B Series	38.1 mm	Strongwell	[H 1.5]
Operator Name:	**Age (Days):**	**Width (mm)**	**Fastener Type:**
NTH	28+	25.4 mm Nominal	X-AL-H47 P8
Test Date:	**Power Level**	**Thickness (mm)**	**Diameter (mm):**
08/10/00	P2	3.18	4.5

Displacement vs. Force

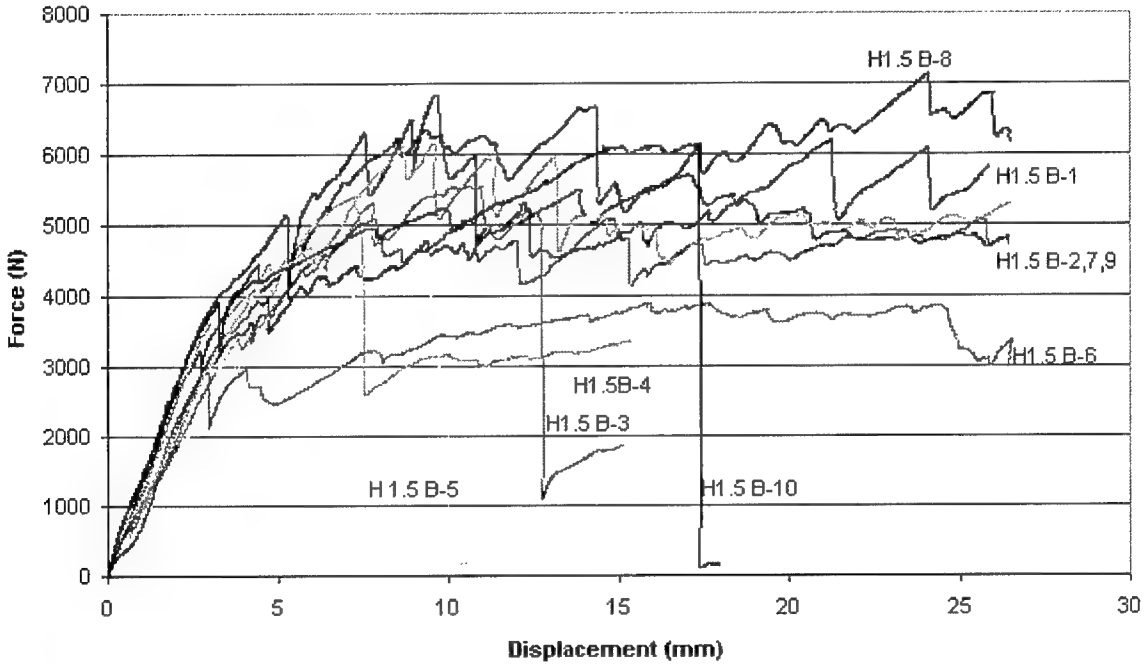

Failure Type	Concrete	Composite	Fastener
Number of Failures	4	5	1
Average	4,770	6,079	1,384
Std. Dev.	827	757	
COV	17.3	12.4	

All the concrete failures were cracks radiating from the connection to the edges of the block. These cracks were the results of a finished test. H1.5-21 was the only one to fail by forming a shear cone.
The fastener failure was the fastener shearing in half with the bottom remaining embedded in the block

Test #	**Failure Mechanism**	**Maximum Load (N)**	**Disp. @ Max Load (mm)**
H 1.5 B-1	Bearing	6,296	9.28
H 1.5 B-2	Bearing	5,704	17.04
H 1.5 B-3	Concrete	5,548	10.66
H 1.5 B-4	Concrete	5,401	7.23
H 1.5 B-5	Concrete	4,235	9.16
H 1.5 B-6	Concrete	3,897	15.91
H 1.5 B-7	Bearing	5,097	7.88
H 1.5 B-8	Bearing	7,144	24.10
H 1.5 B-9	Bearing	6,152	9.62
H 1.5 B-10	Fastener	6,154	17.37
	Average	5,563	12.83
	Std. Dev.	974	5.495
	COV	17.5	42.8

Hybrid 1.5 C

1-in.-wide H1.5, Predrilled 47-mm AL w/ 18-mm Washer (x2)

Test:	**Max Aggregate Size:**	**FRP Plate Manufacturer:**	**FRP Plate Type:**
H 1.5 C Series	38.1 mm	Strongwell	[H 1.5]
Operator Name:	**Age (Days):**	**Width (mm)**	**Fastener Type:**
NTH	28+	25.4 mm Nominal	X-AL-H47 P8
Test Date:	**Power Level**	**Thickness (mm)**	**Diameter (mm):**
08/20/00	P2	3.18	4.5

Displacement vs. Force

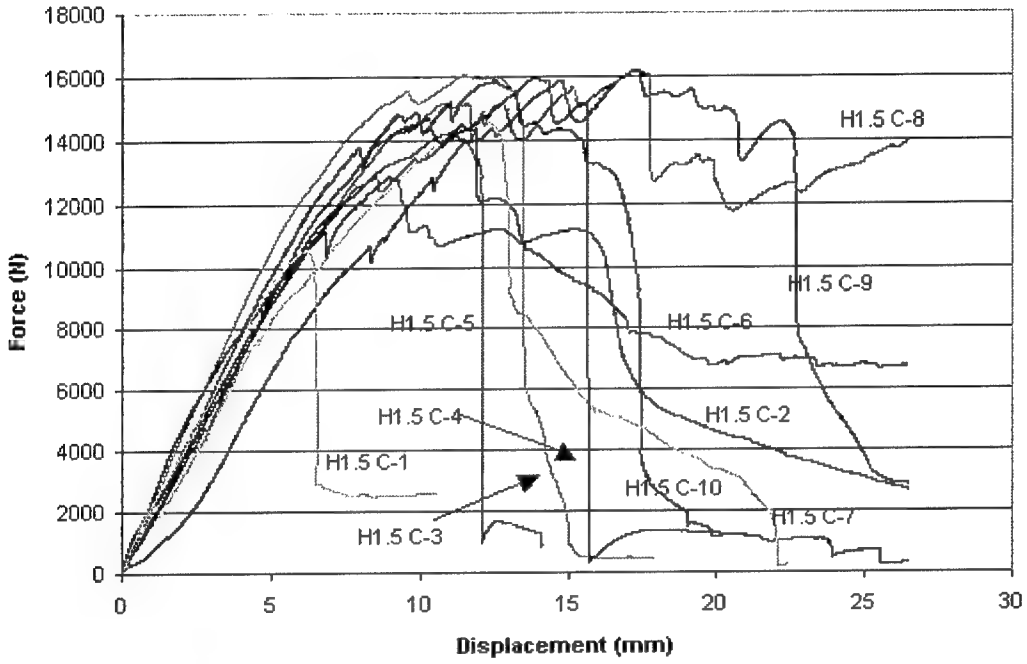

Failure Type	Concrete	Composite
Number of Failures	8	2
Average	14,539	15,417
Std. Dev.	1,986	1,036
COV	13.7	6.7

12"x 6"x 6" blocks	**Cage**	**No Cage**
Number of Failures	6	4
Average	15,086	14,158
Std. Dev.	1,314	2,530
COV	8.7	17.9

Test #	**Failure Mechanism**	**Maximum Load (N)**	**Disp. @ Max Load (mm)**
H 1.5 C-1	Concrete	10,535	6.20
H 1.5 C-2	Concrete	12,855	9.04
H 1.5 C-3	Concrete	16,030	11.53
H 1.5 C-4	Concrete	15,953	13.95
H 1.5 C-5	Concrete	14,303	11.23
H 1.5 C-6	Bearing	14,684	10.31
H 1.5 C-7	Concrete	14,599	12.29
H 1.5 C-8	Bearing	16,149	17.46
H 1.5 C-9	Concrete	16,199	17.21
H 1.5 C-10	Concrete	15,841	12.47
	Average	14,715	12.17
	Std. Dev.	1,823	3.45
	COV	12.4	28.3

Hybrid 1.5 D

4-in.-wide H1.5, Predrilled 47-mm AL w/ 18-mm Washer (x2)

Test:	**Max Aggregate size:**	**FRP Plate Manufacturer**	**FRP Plate Type**
H 1.5 D Series	38.1 mm	Strongwell	[H 1.5]
Operator Name:	**Age (Days):**	**Width (mm)**	**Fastener Type:**
NTH	28+	101.6 mm Nominal	X-AL-H47 P8
Test Date:	**Power Level**	**Thickness (mm)**	**Diameter (mm):**
08/24/00	P2	3.18	4.5

Displacement vs. Force

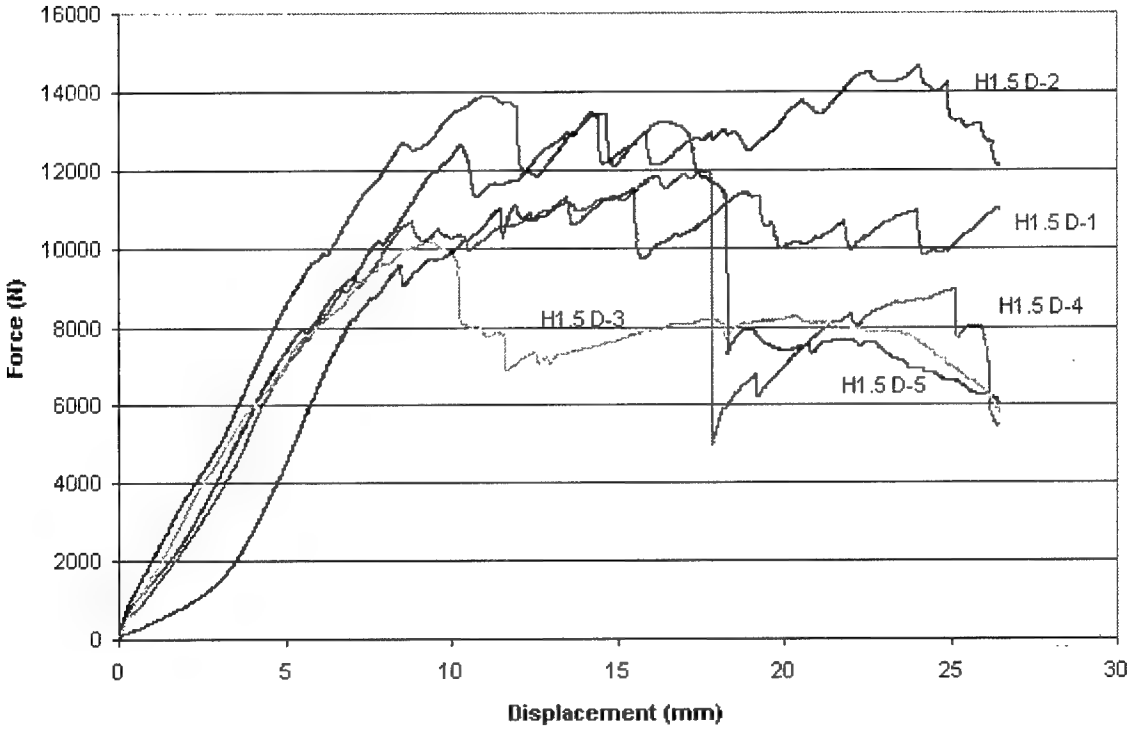

Failure Types	**Concrete**	**Composite**
Number of Failures	3	2
Average	12,012	13,098
Std. Dev.	1,878	2,194
COV	15.6	16.7

Test #	**Failure Mechanism**	**Maximum Load (N)**	**Disp. @ Max Load (mm)**
H1.5 D-1	Bearing	11,547	15.54
H 1.5 D-2	Bearing	14,649	24.04
H 1.5 D-3	Concrete	10,154	9.34
H 1.5 D-4	Concrete	11,972	17.67
H 1.5 D-5	Concrete	13,909	11.02

12"x 6"x 6" blocks	**Cage**	**No Cage**
Number of Failures	5	0
Average	12,446	
Std. Dev.	1,822	
COV	14.6	

Average	12,446	15.52
Std. Dev.	1,822	5.82
COV	14.6	37.5

Appendix C
Testing on Full-Scale Beams at U.S. Army Engineer Research and Development Center (ERDC)

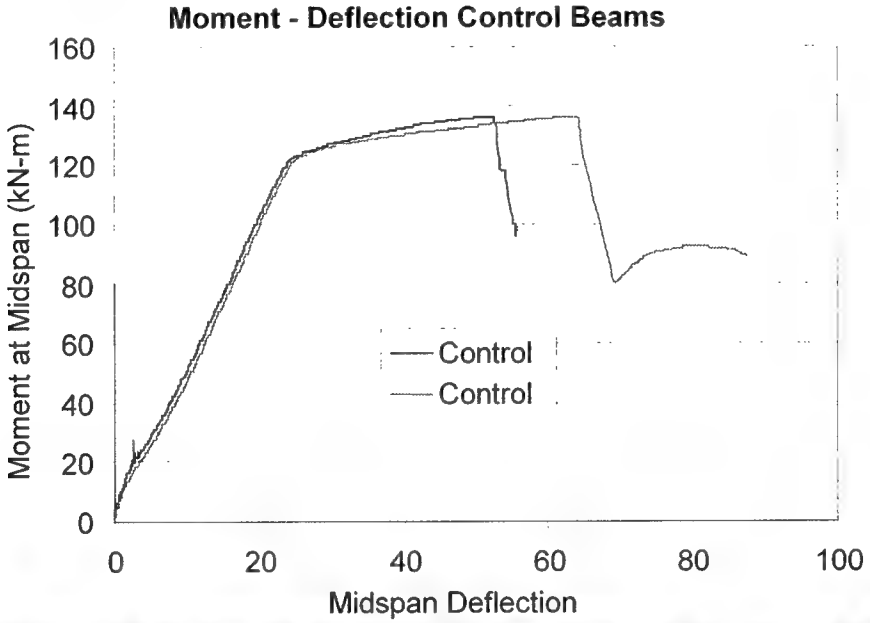

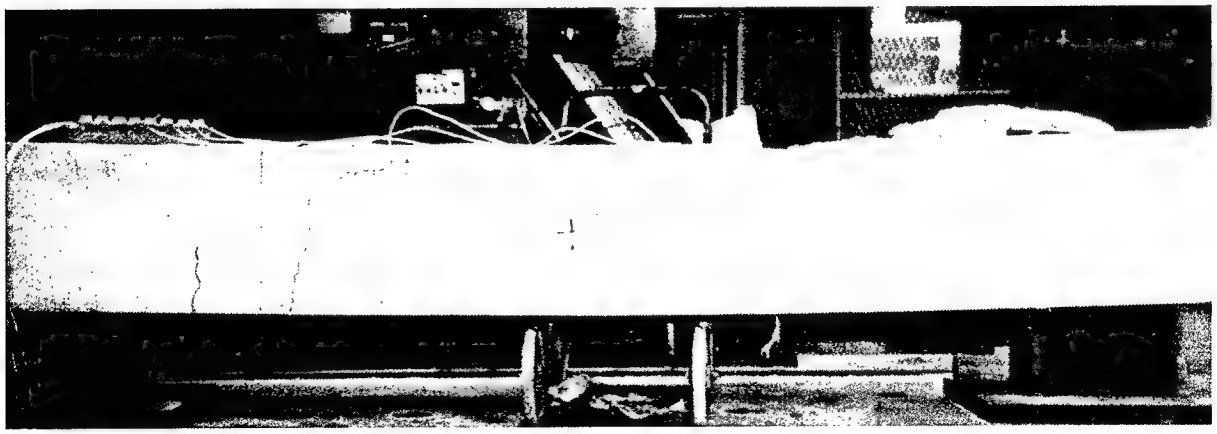

Control 1 crack pattern

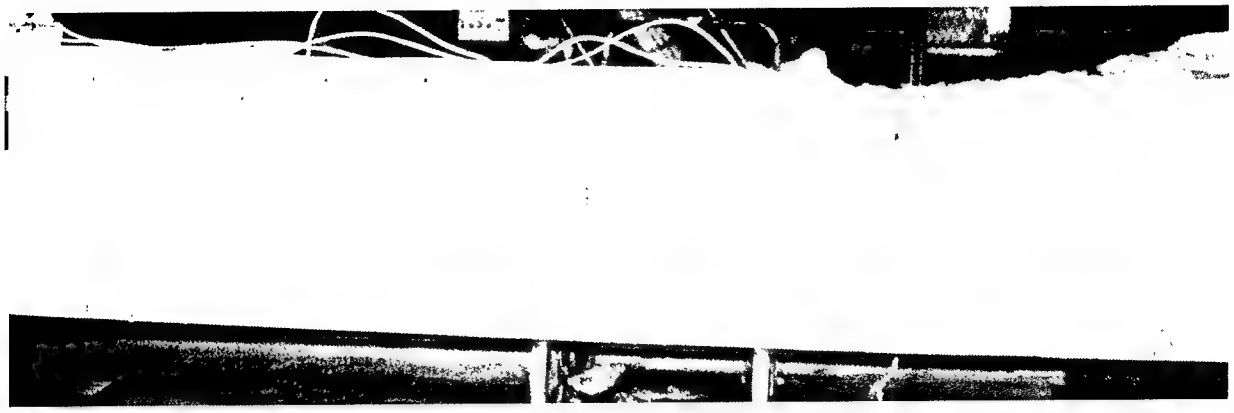

Control 1 crack pattern in the moment span

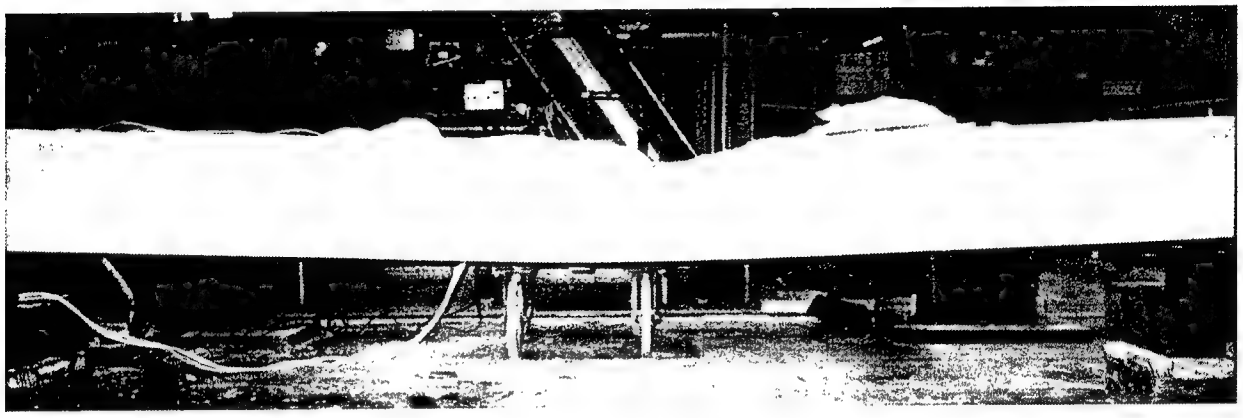

Control 2 crack pattern

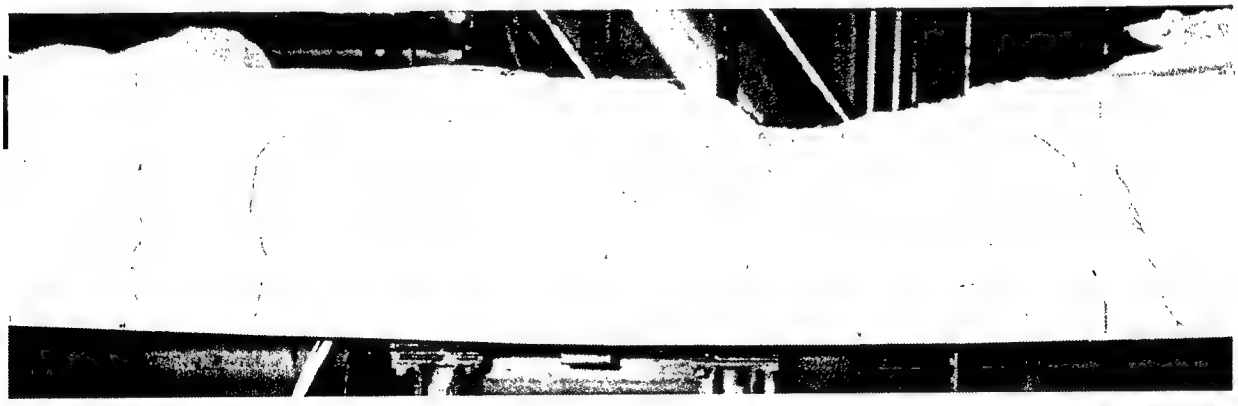

Control 2 crack pattern in the moment span

Moment - Deflection S-4-Y-AL32

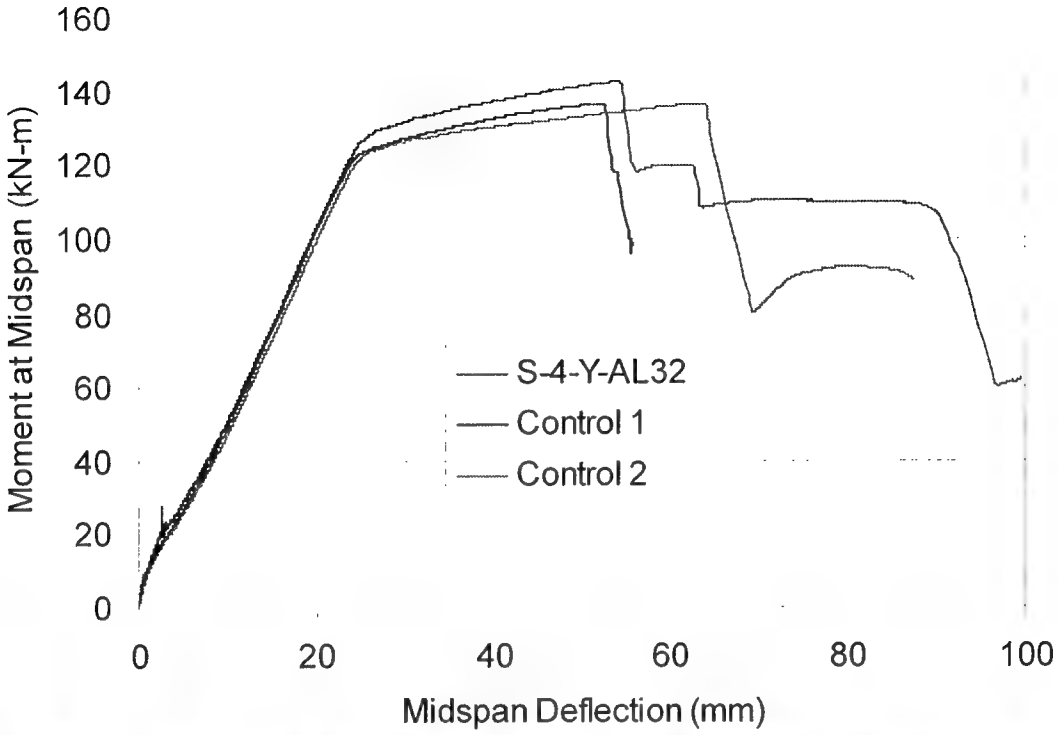

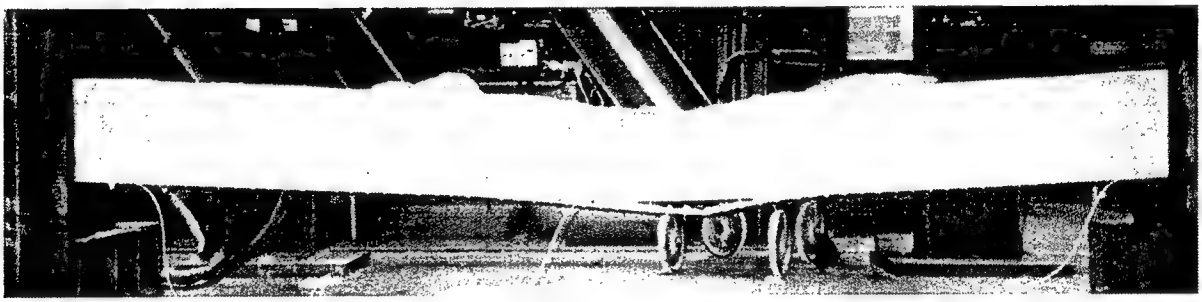

S-4-Y-AL32 crack pattern

S-4-Y-AL32 crack pattern in the moment span

Moment - Deflection I-4-N-AL32

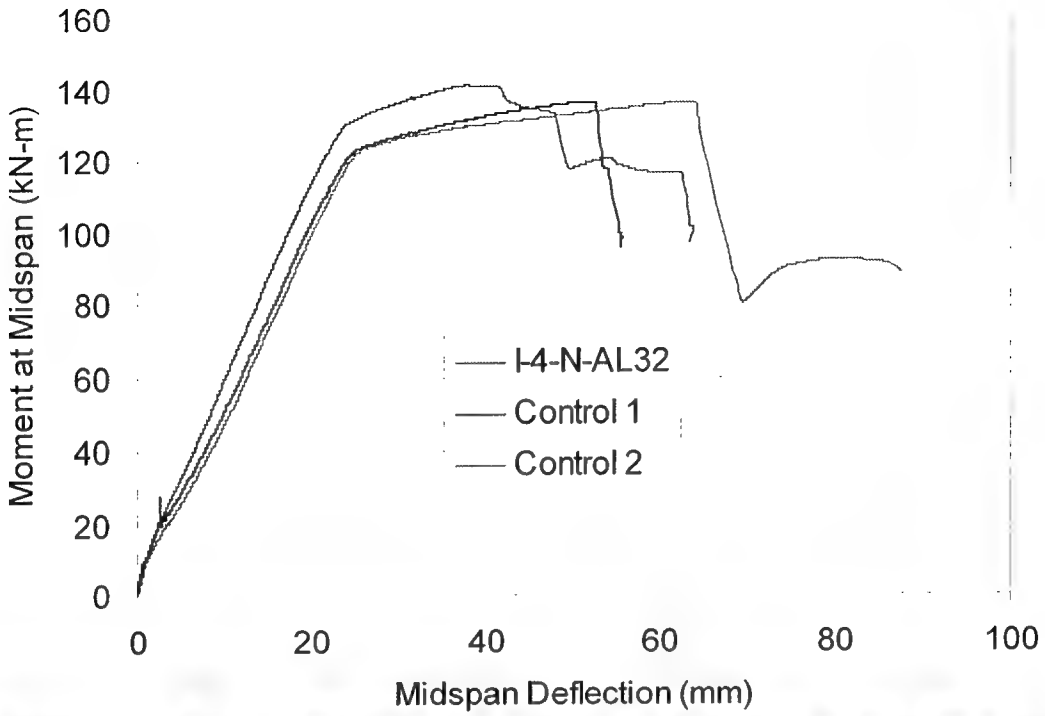

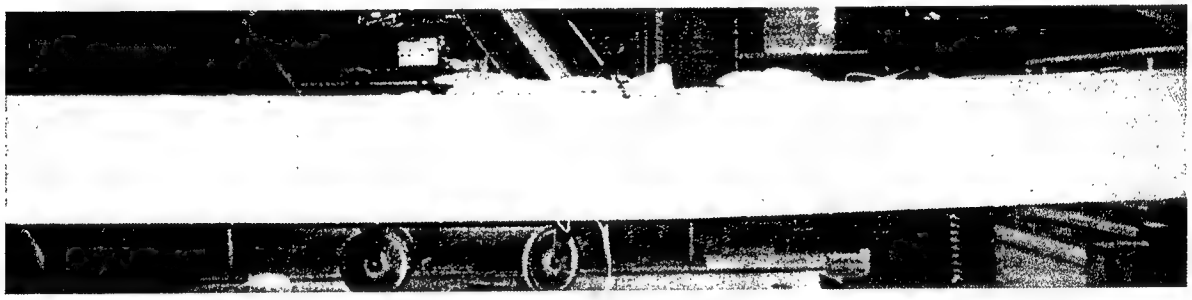

I-4-N-AL32 crack pattern

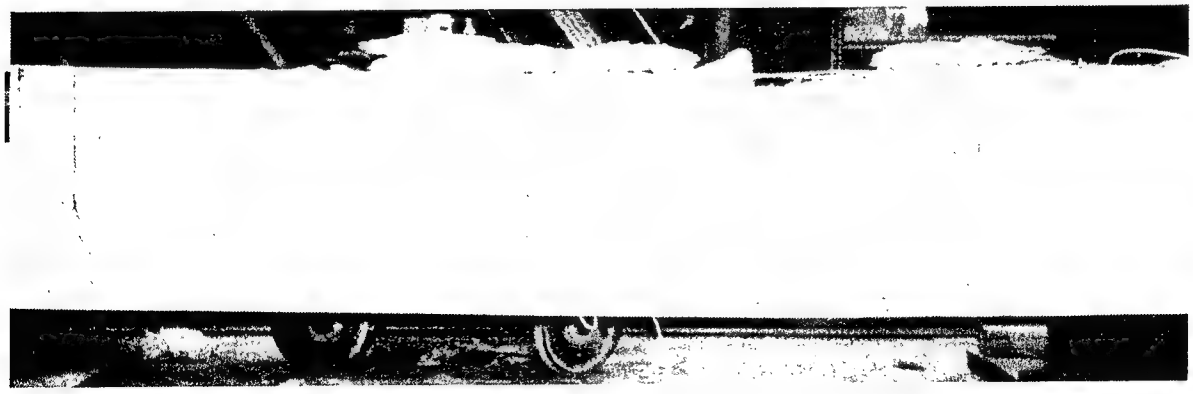

I-4-N-AL32 crack pattern in the moment span

Moment - Deflection I-4-Y-AL32

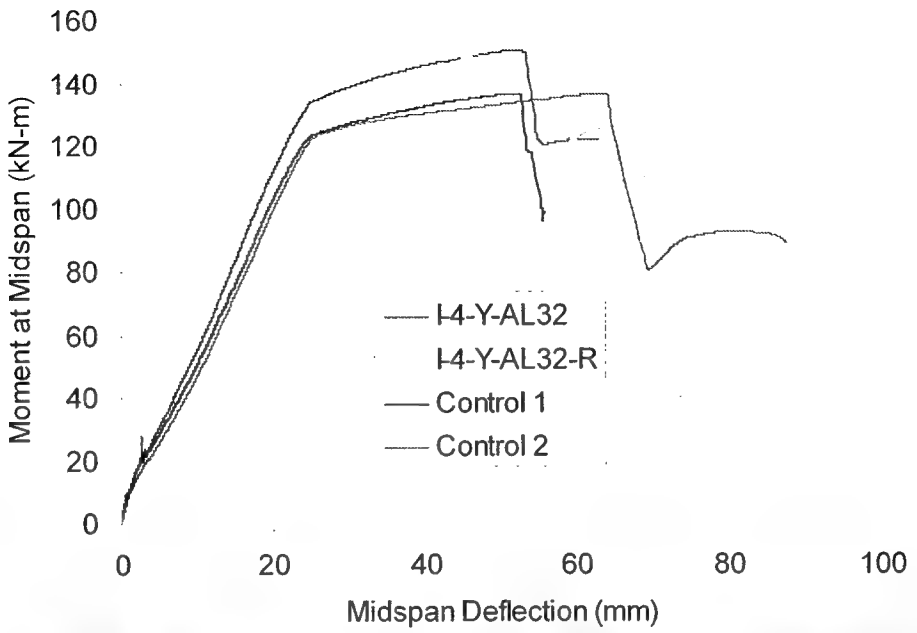

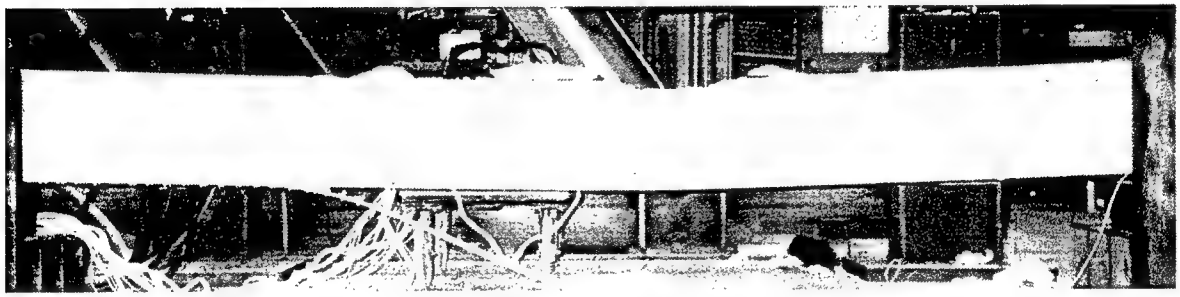

I-4-Y-AL32-R crack pattern

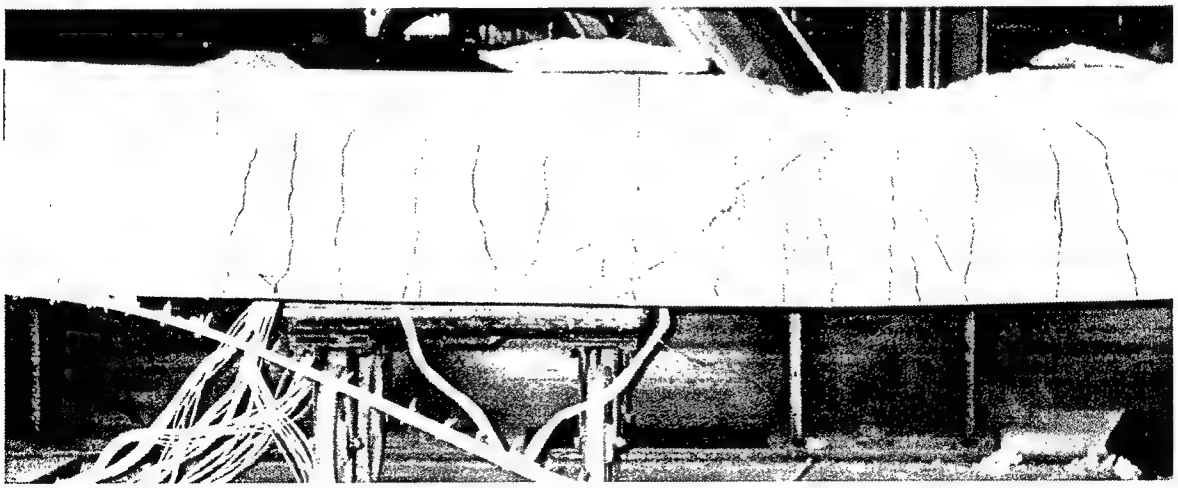

I-4-Y-AL32-R crack pattern in the moment span

Moment - Deflection I-8-Y-AL32

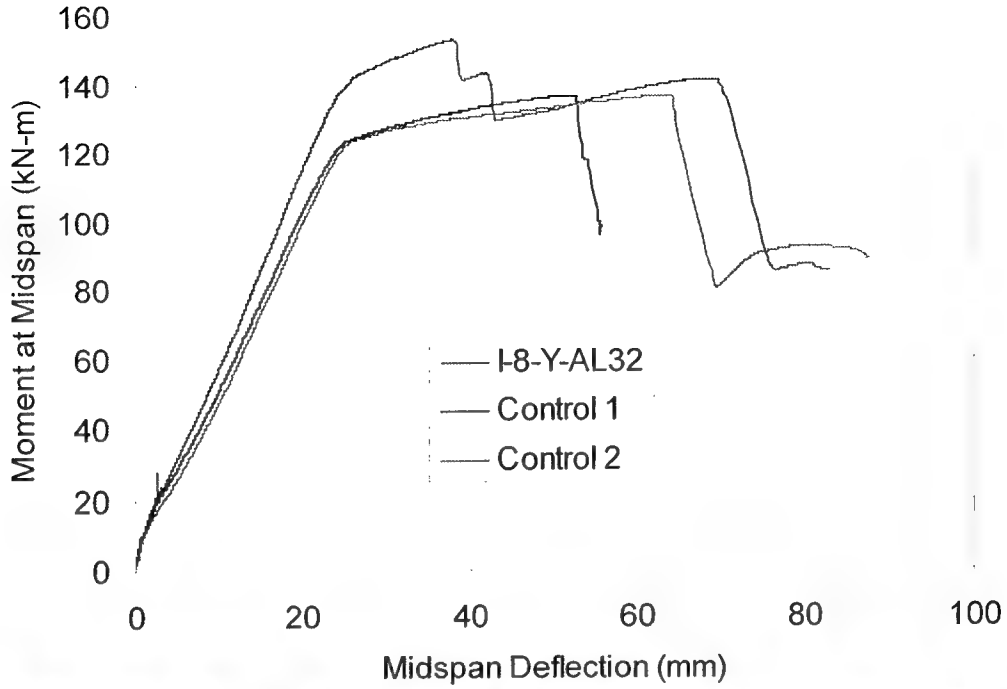

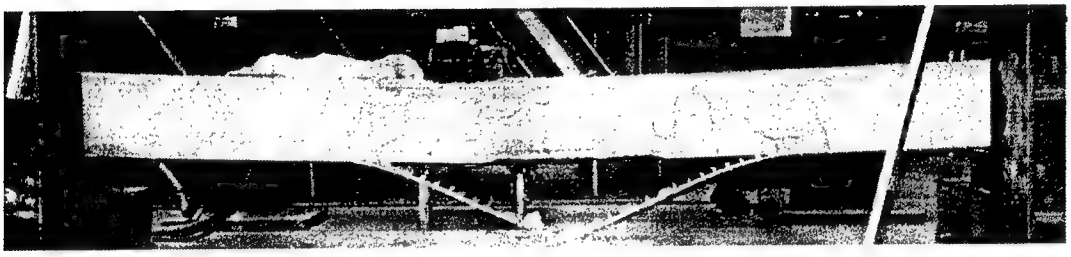

I-8-Y-AL32 crack pattern

I-8-Y-AL32 crack pattern in the moment span

Moment - Deflection H1.5-4-Y-AL32

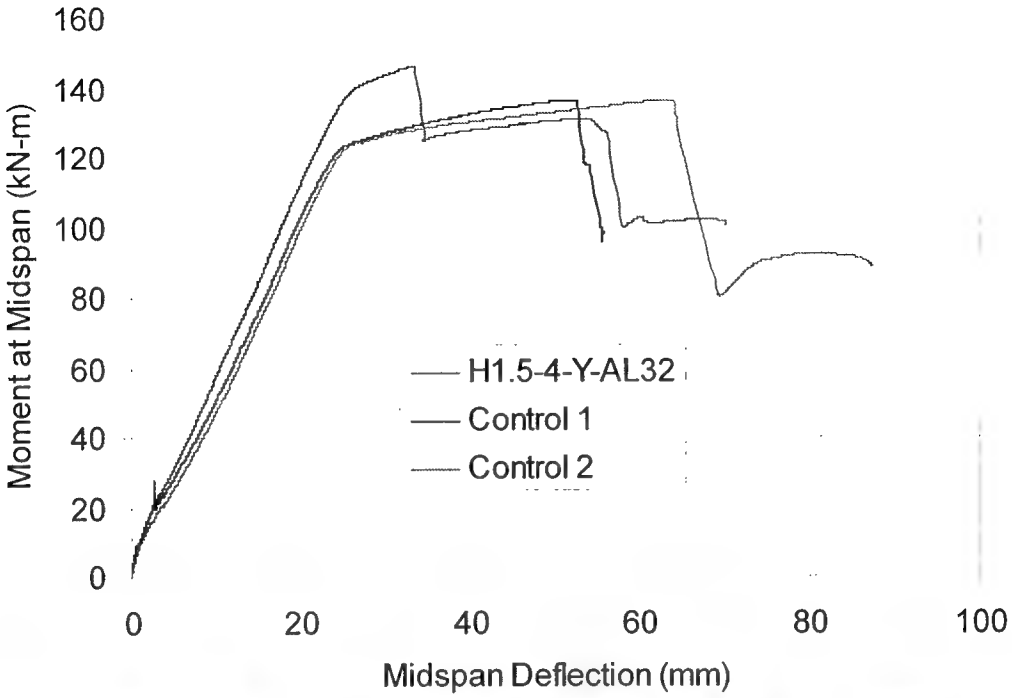

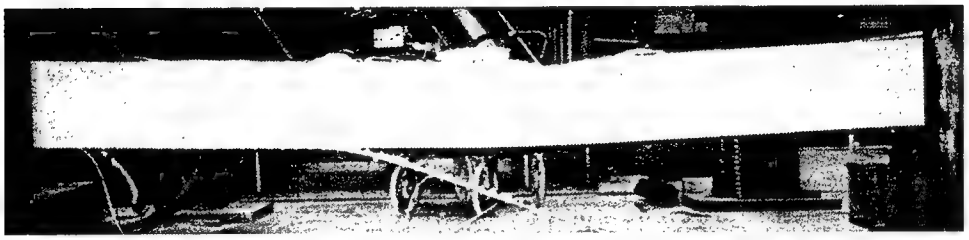

H1.5-4-Y-AL32 crack pattern

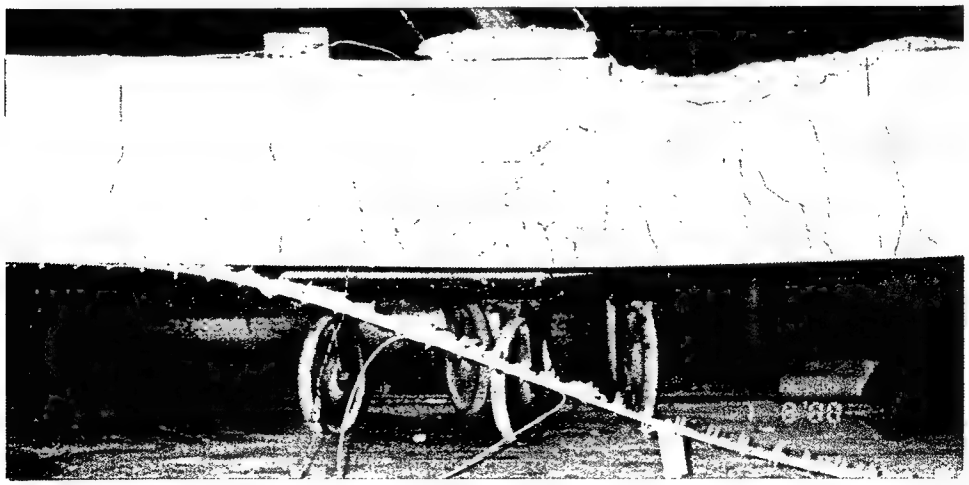

H1.5-4-Y-AL32 crack pattern in the moment span

Moment - Deflection H1.5-4-Y-AL42D

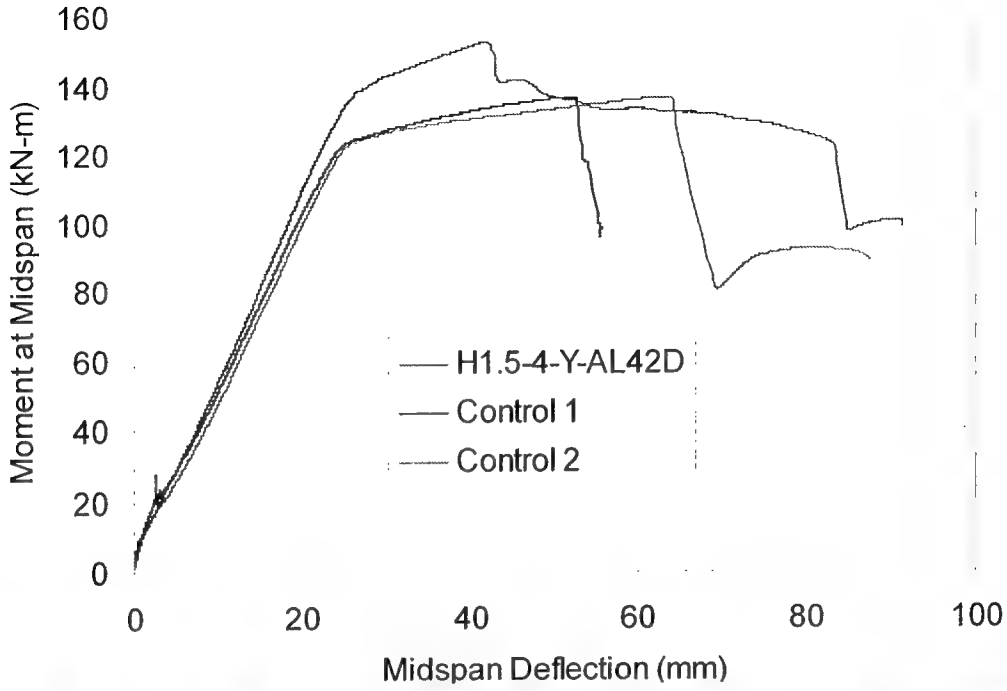

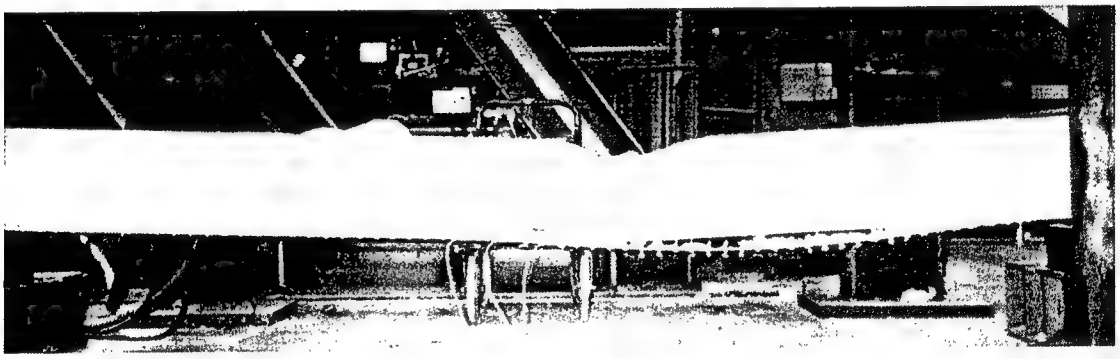

H1.5-4-Y-AL42D crack pattern

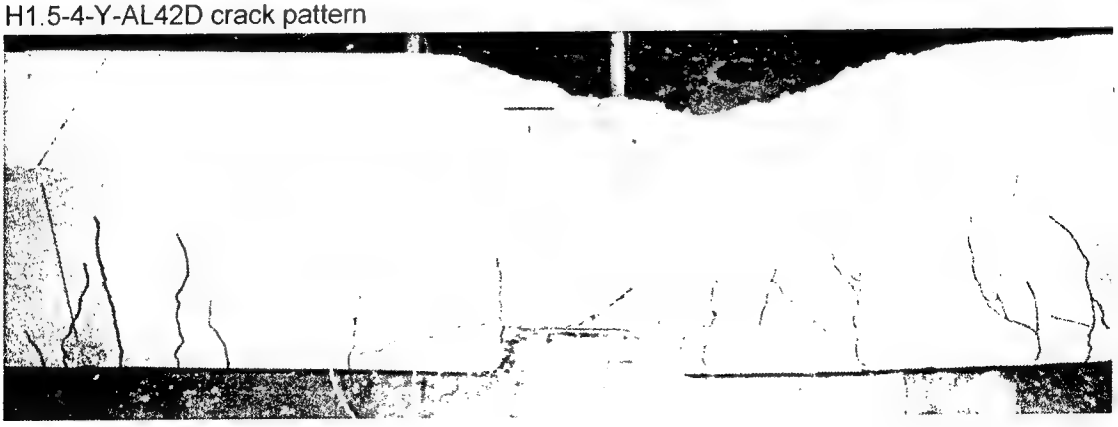

H1.5-4-Y-AL42D crack pattern in the moment span

Moment - Deflection H1.5-4-Y-AL47D

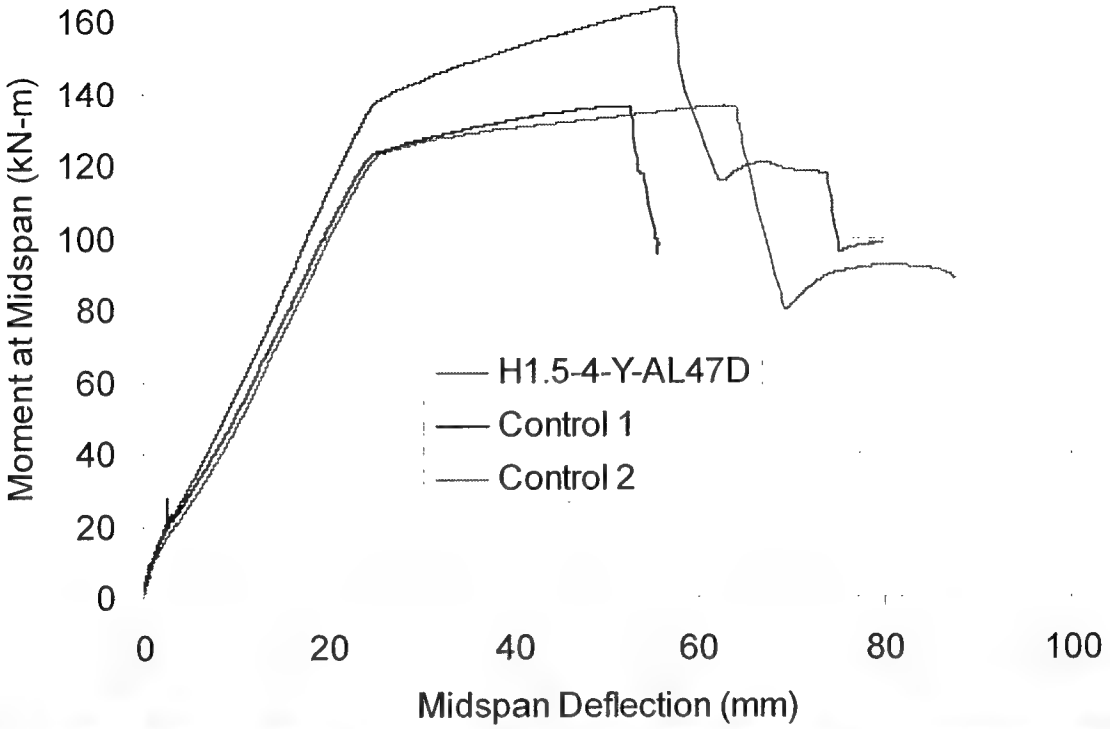

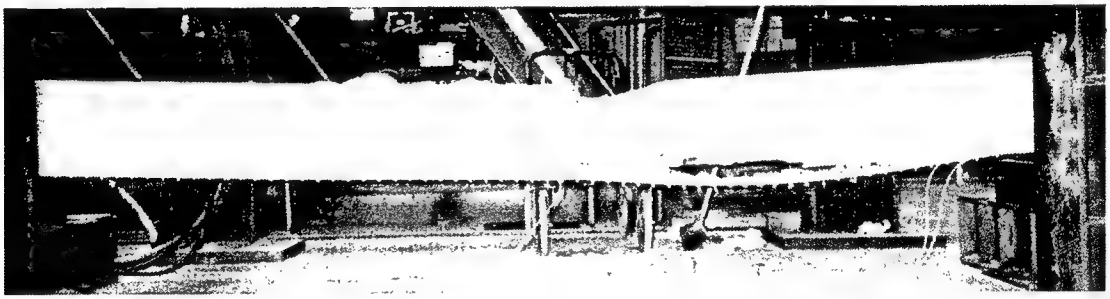

H1.5-4-Y-AL47D crack pattern

H1.5-4-Y-AL47D crack pattern in the moment span

Moment - Deflection H1.5-4-Y-AL47D-3

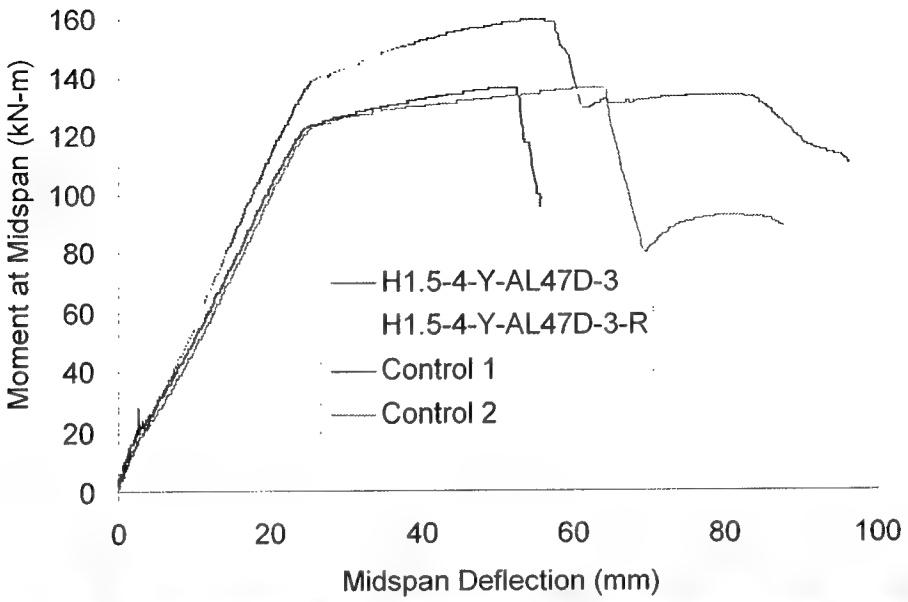

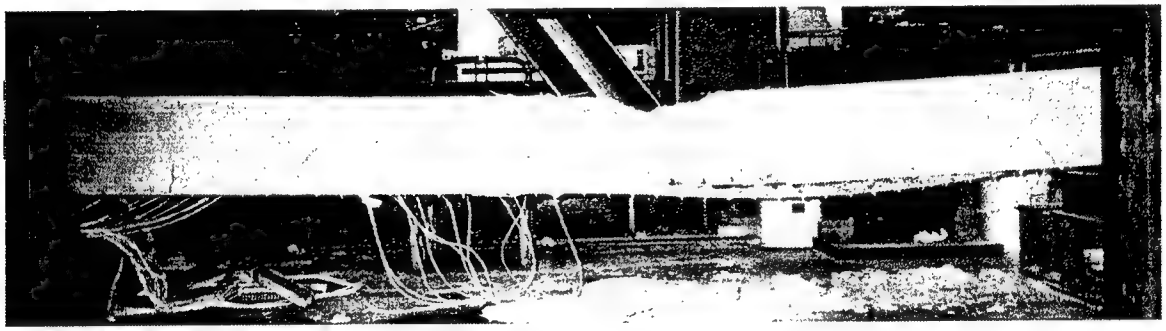

H1.5-4-Y-AL47D-3 crack pattern

H1.5-4-Y-AL47D-3 crack pattern in the moment span

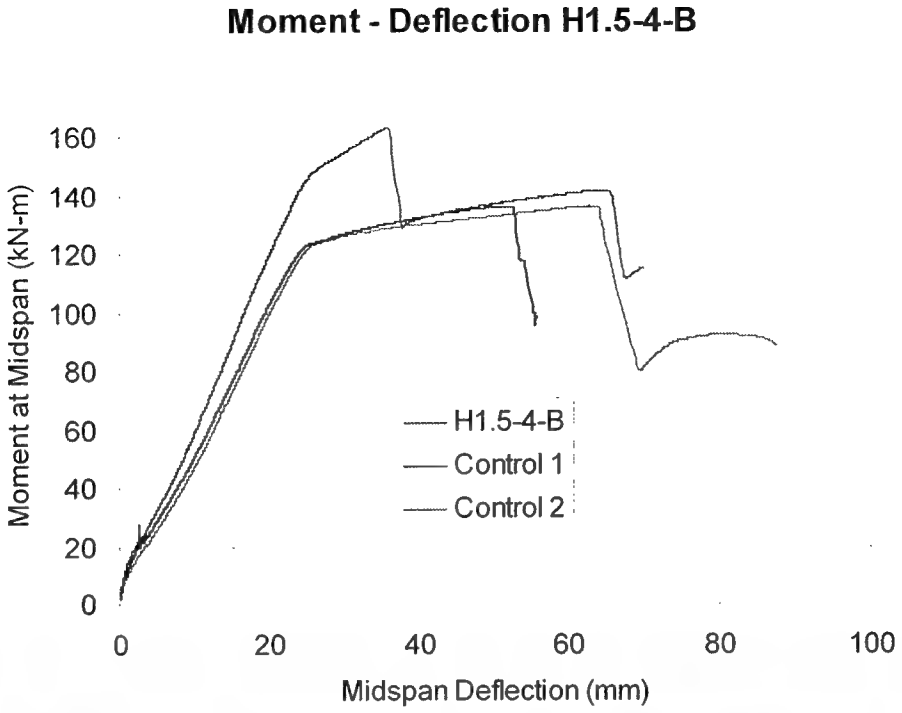

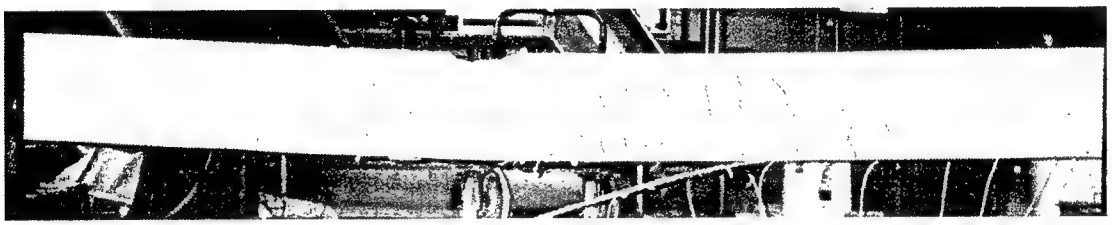

H1.5-4-B crack pattern

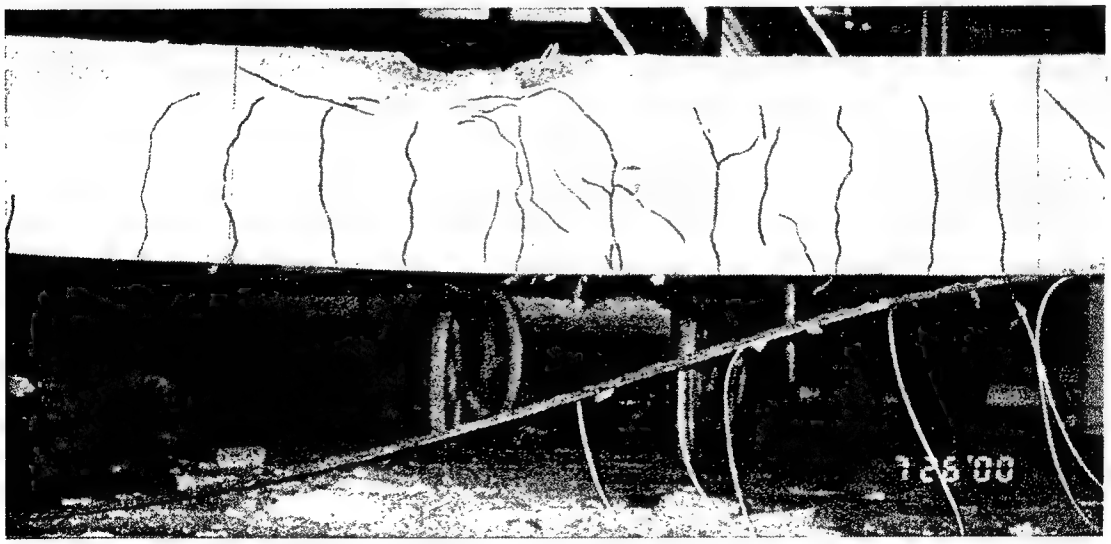

H1.5-4-Y-B crack pattern in the moment span

Moment - Deflection H1.0-4-Y-AL47D-5

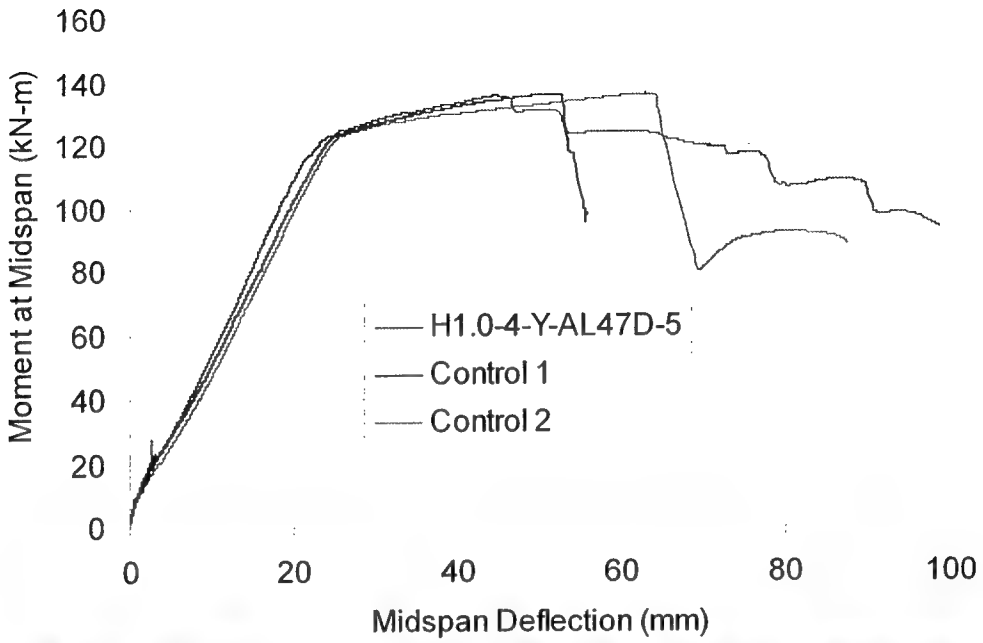

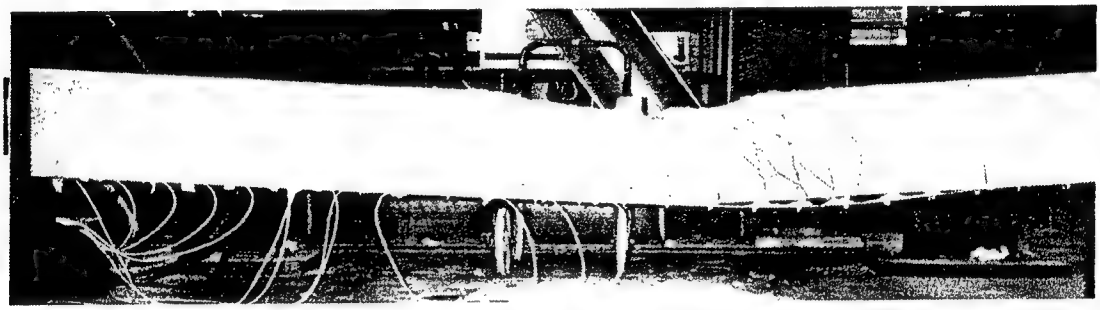

H1.0-4-Y-AL47D-5 crack pattern

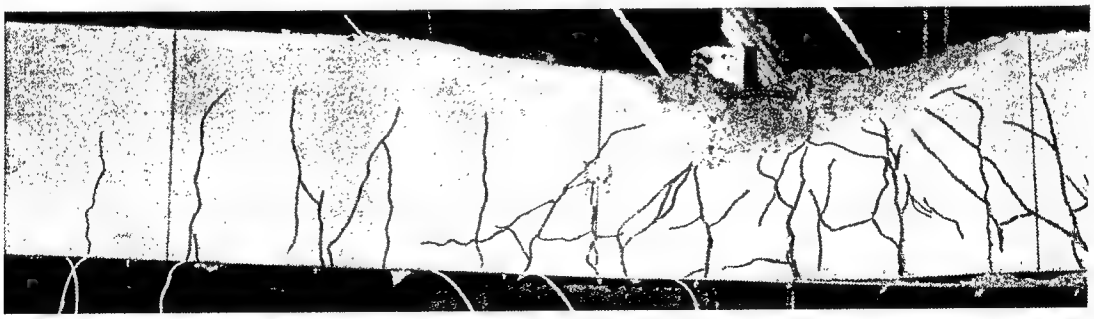

H1.0-4-Y-AL47D-5 crack pattern in the moment span

Moment - Deflection H1.5-8-Y-AL32

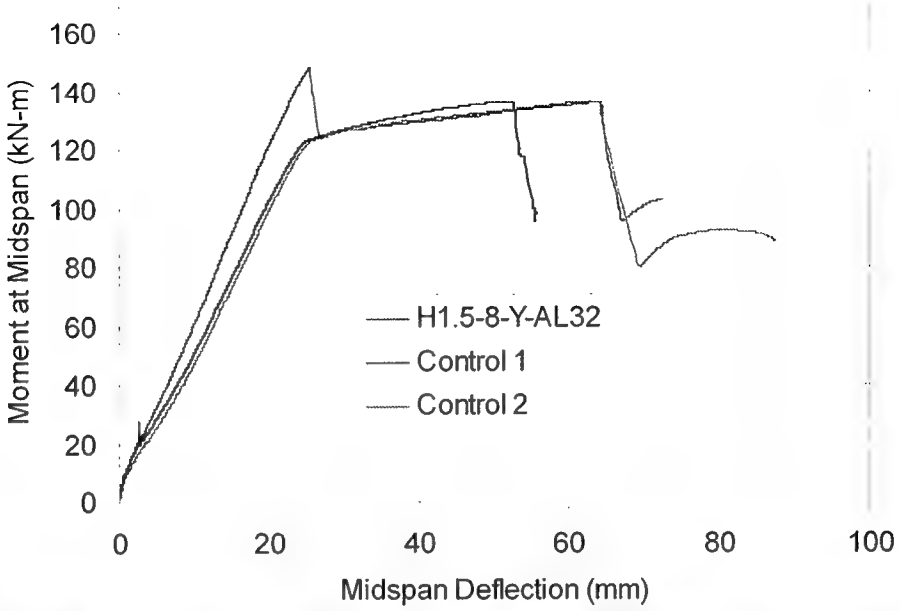

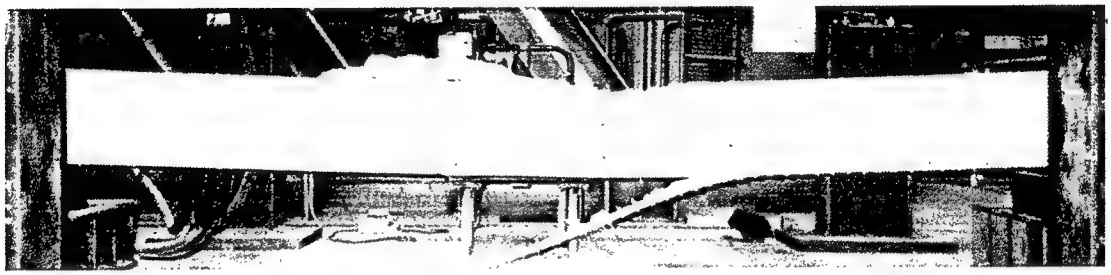

H1.5-8-Y-AL32 crack pattern

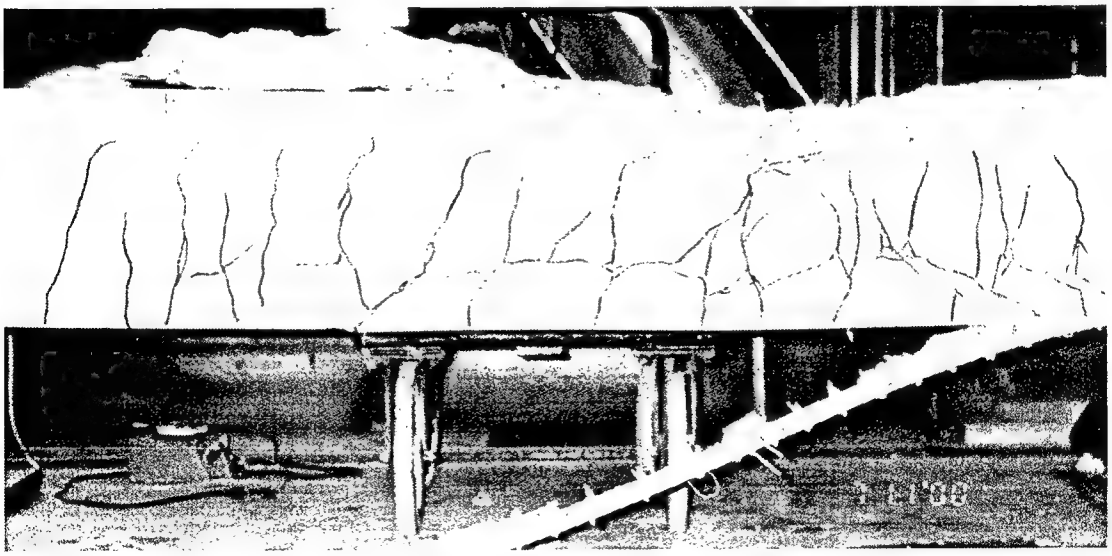

H1.5-8-Y-AL32 crack pattern in the moment span

Appendix D
Strain Distribution in the Strip

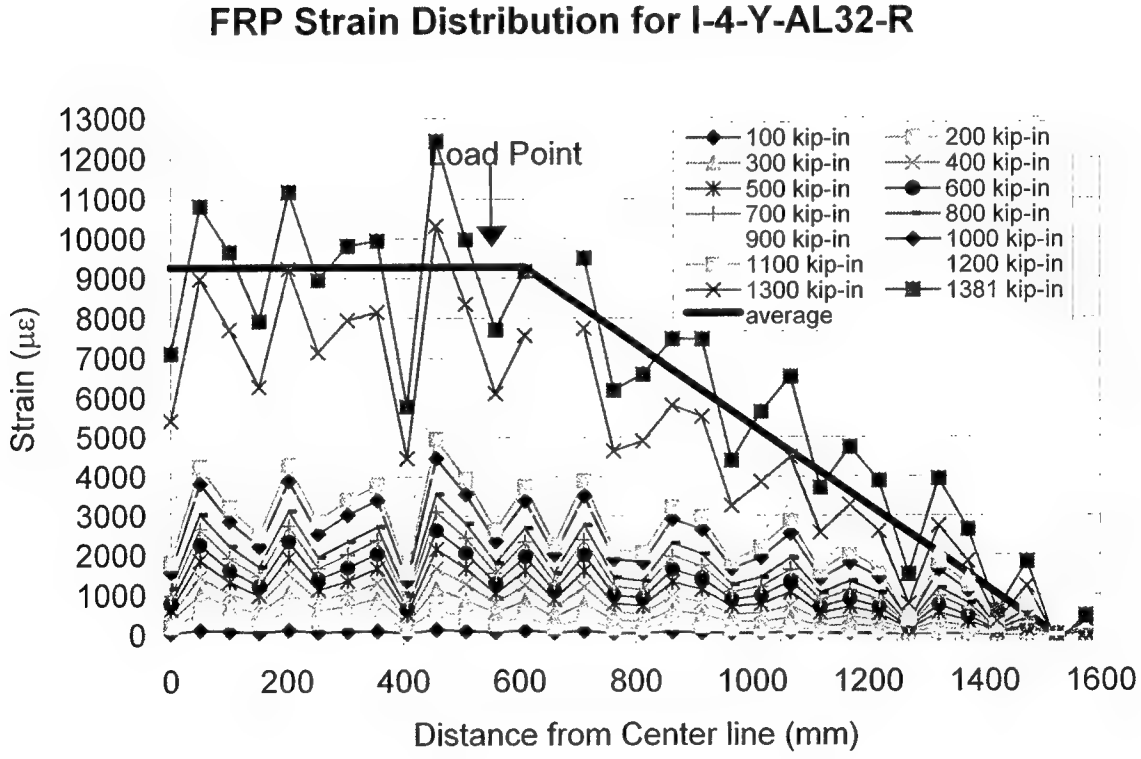

To convert U.S. Customary units of measurements to SI units, refer to the Conversion Factors Table presented on page viii.

FRP Strain Distribution for I-4-Y-AL32-R

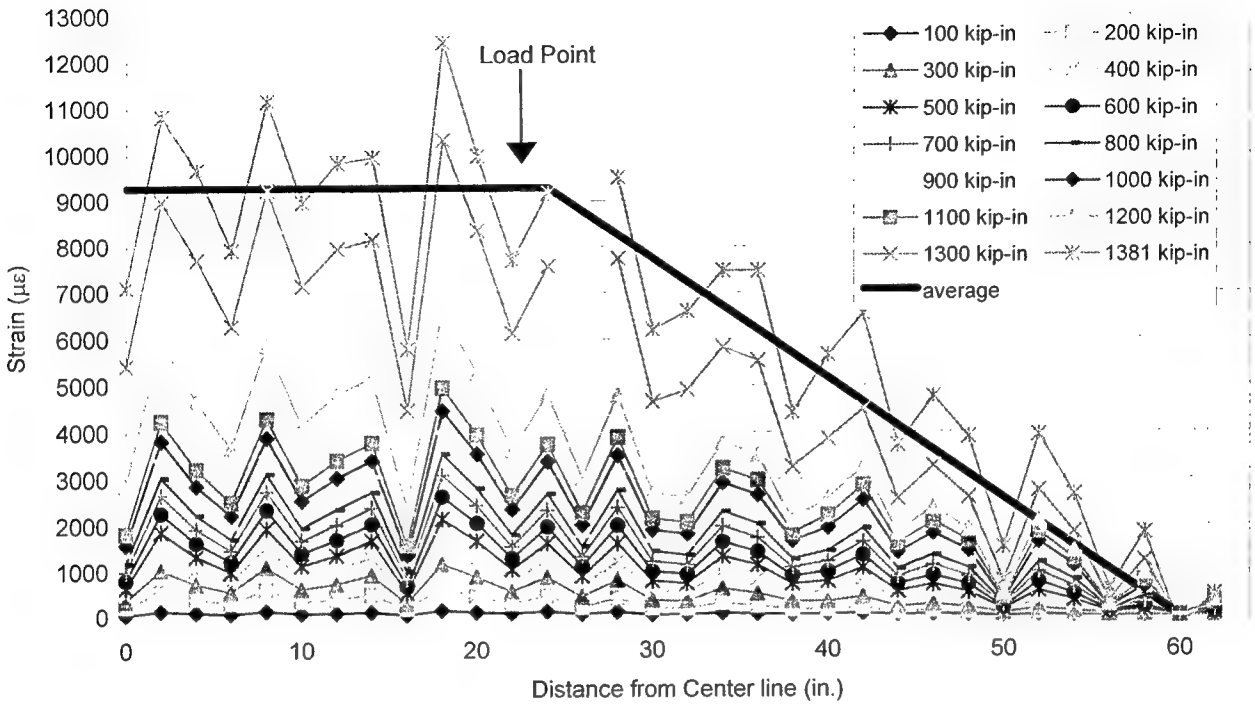

FRP Strain Distribution for H1.0-4-Y-AL47D-5

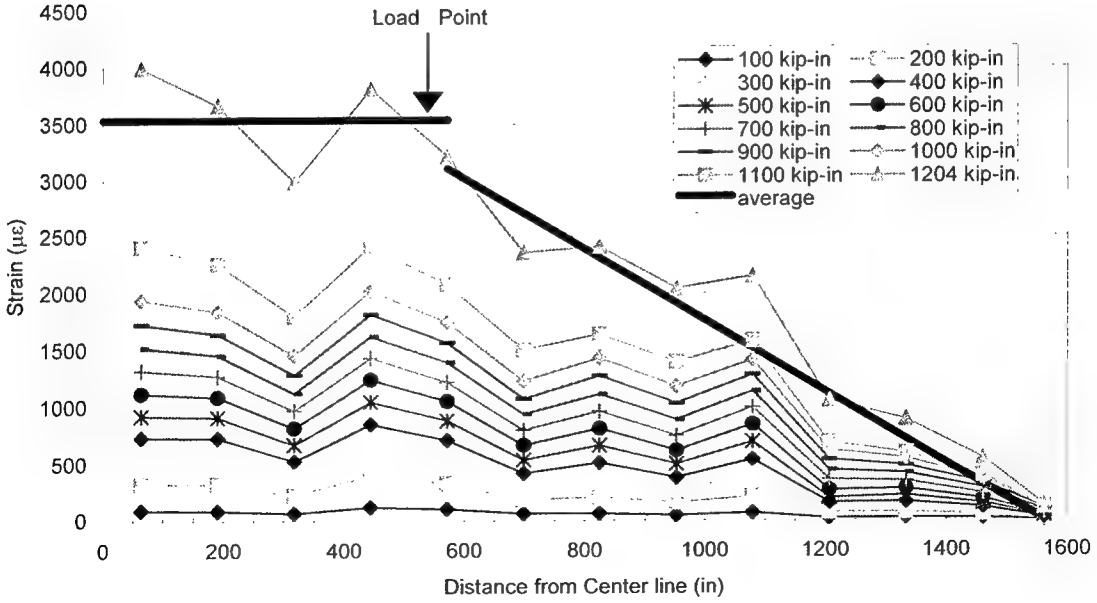

FRP Strain Distribution for H1.5-4-Y-AL47D-3-R

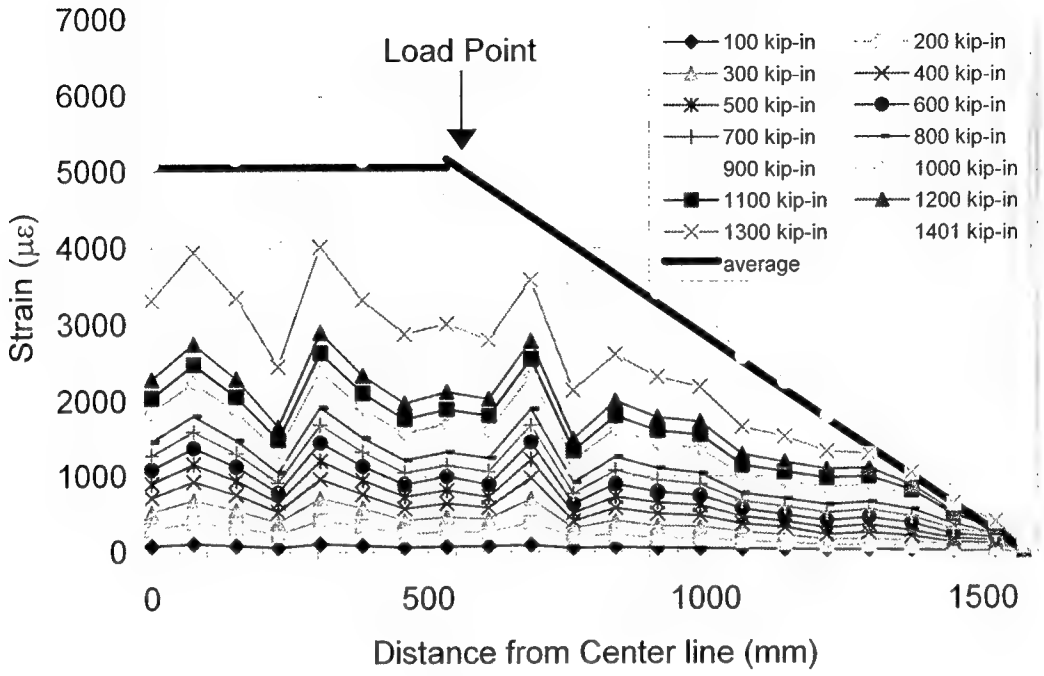

Appendix E
Strain Data

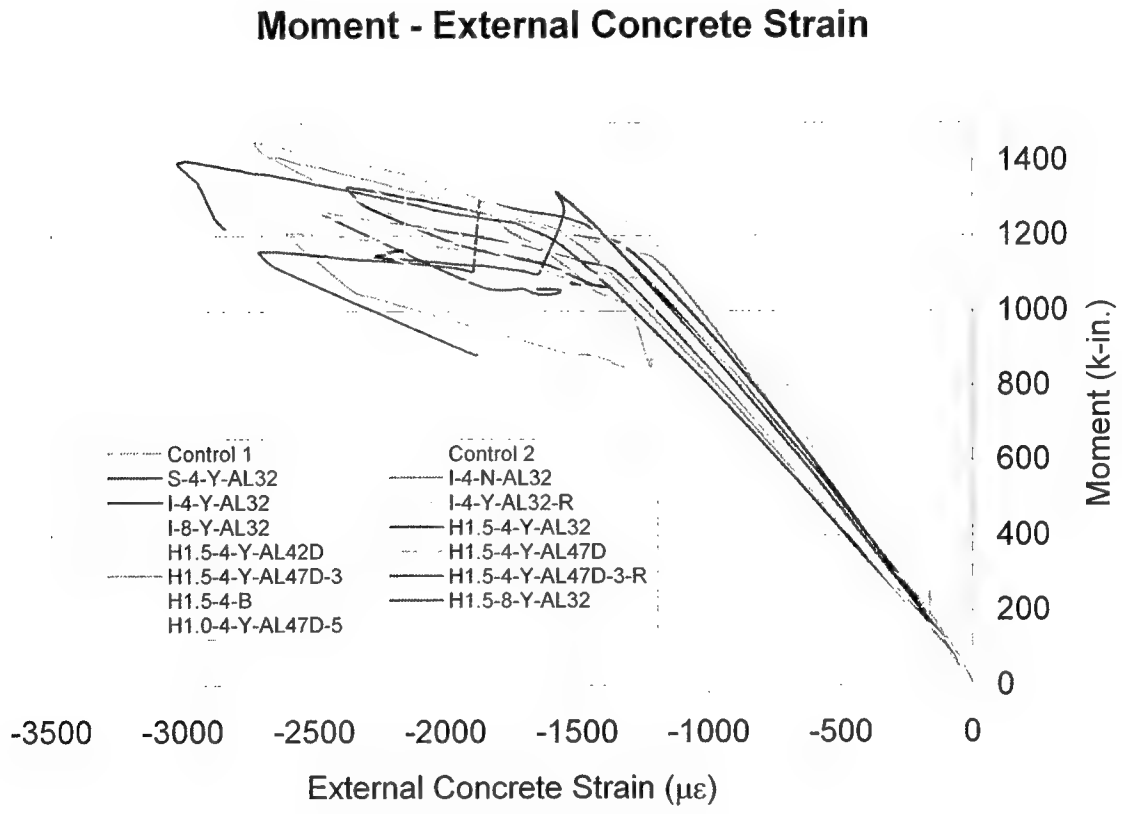

Moment - Compression Steel Strain

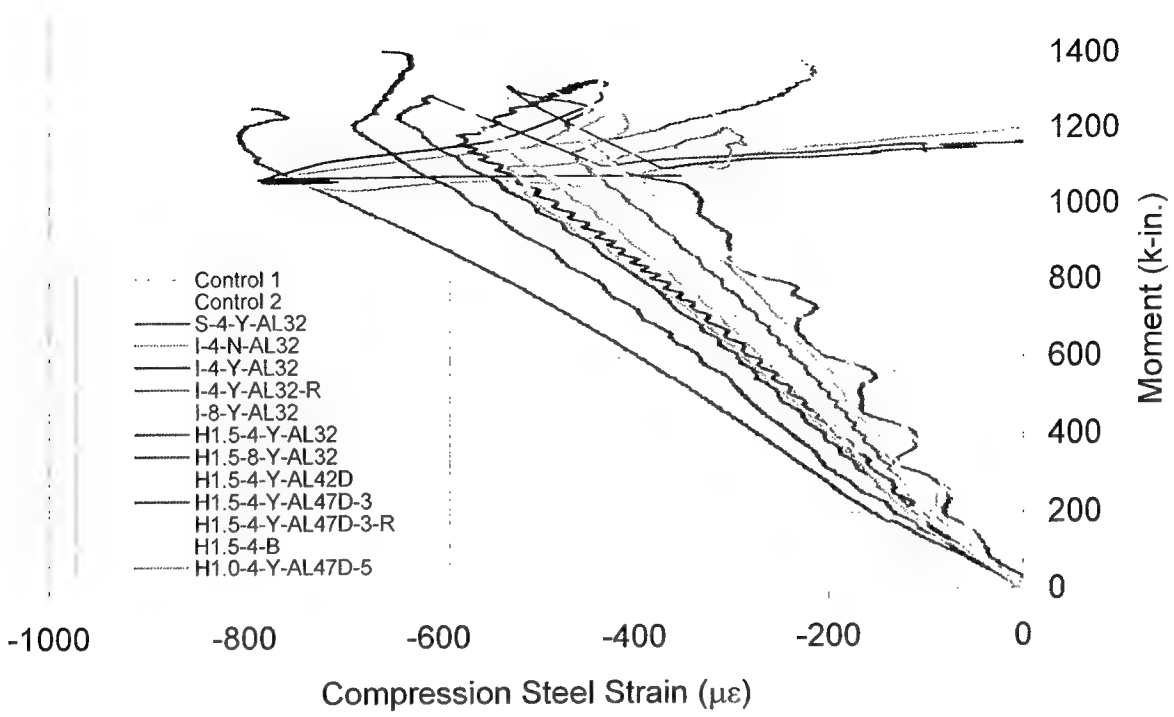

Moment - Tension Steel 1 Strain

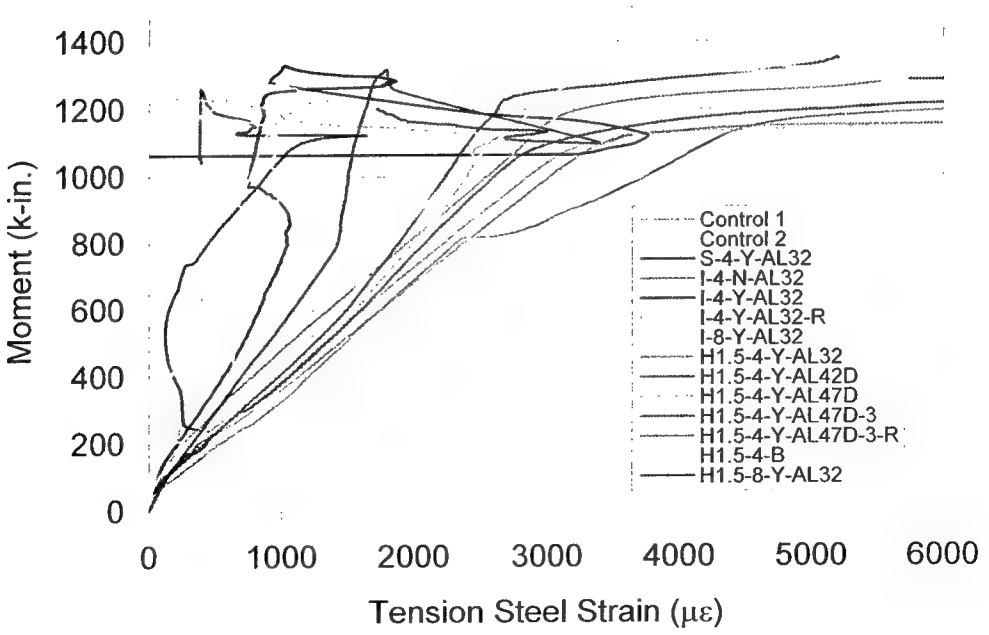

Moment - Tension Steel 2 Strain

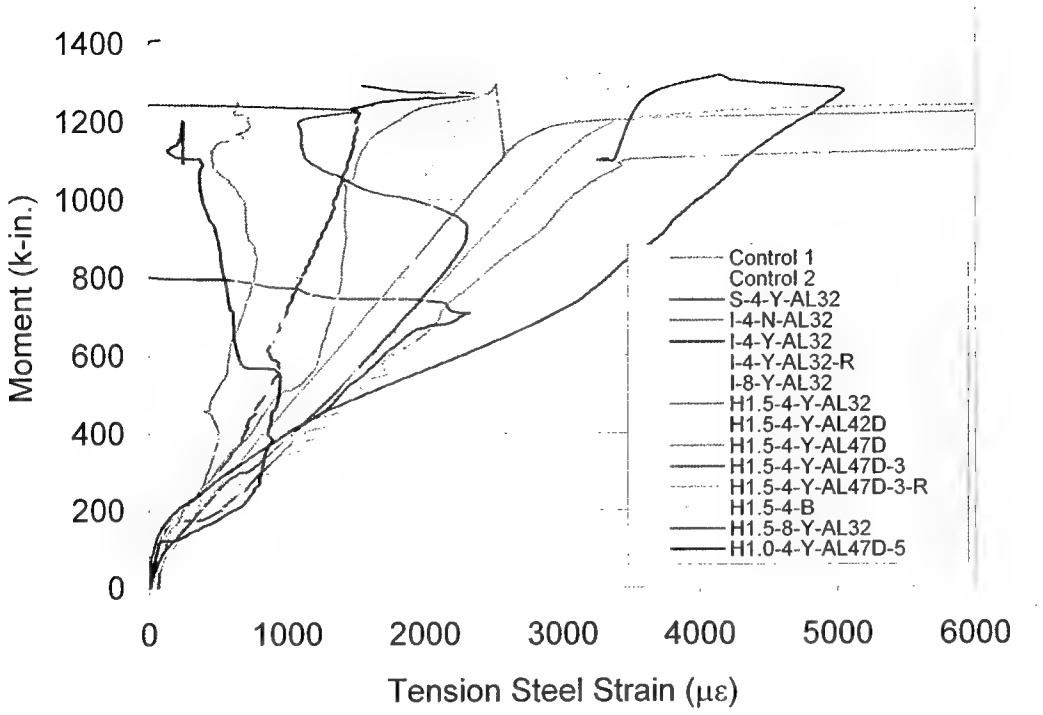

Moment - FRP Center Strain

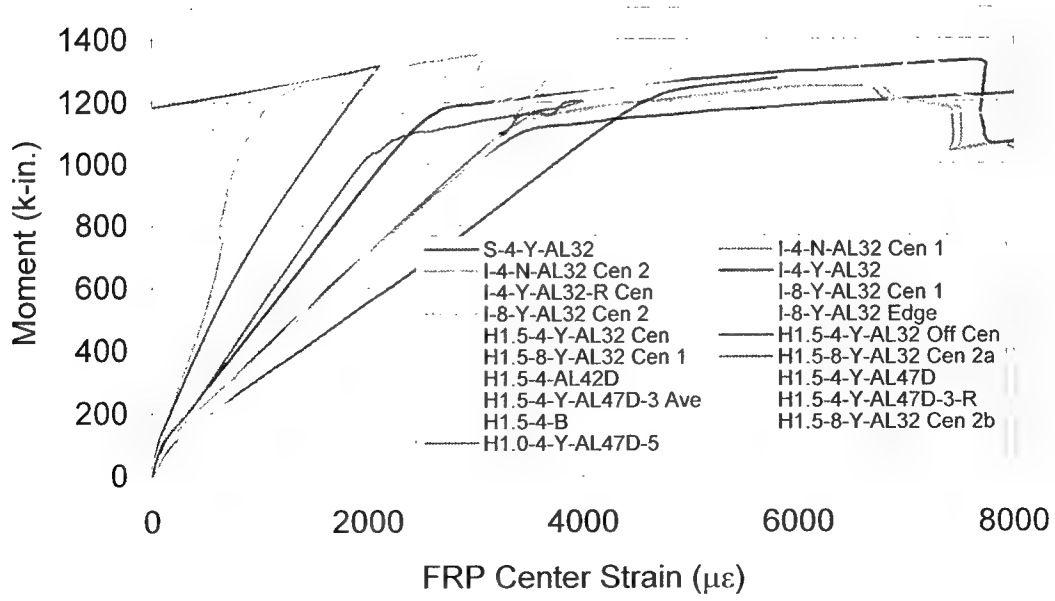

Moment - FRP End Strain

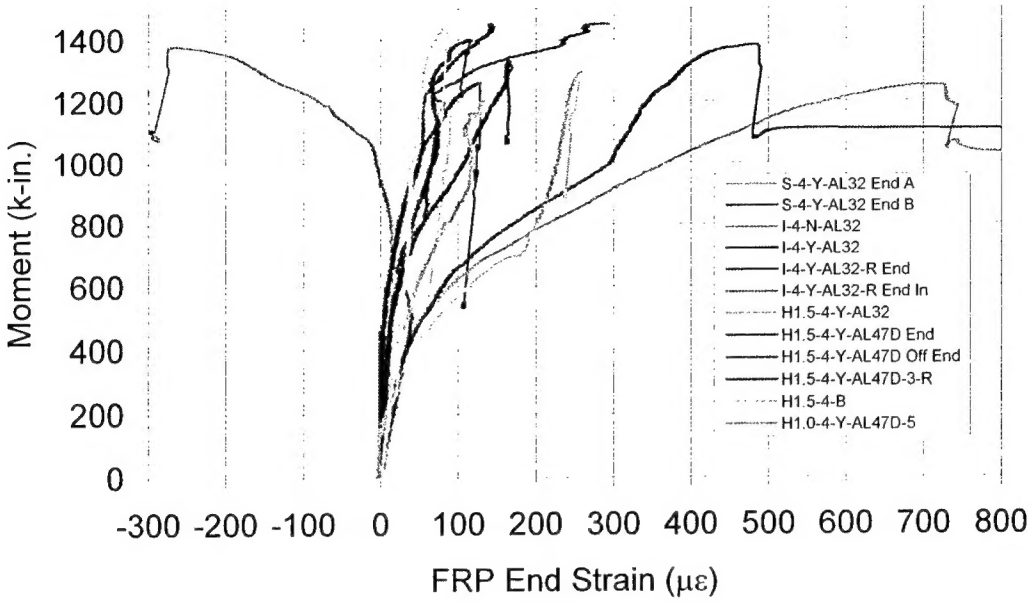

Appendix F
Notation

b	Width of the concrete beam
c	Depth of the neutral axis from the extreme fiber in compression
d	Depth of the tensile steel from the extreme fiber in compression
d_{cs}	Depth of the compression steel from the extreme fiber in compression
d_{frp}	Depth of the FRP strengthening strip from the extreme fiber in compression
f_c'	Compressive strength of the concrete
f_y	Yield stress of steel
A_{cs}	Area of compression steel
A_{frp}	Area of FRP strengthening strip
A_s	Area of tension steel
C_c	Compressive force in the concrete
C_s'	Force in the compression steel
E_{frp}	Elastic modulus of FRP strengthening strip
E_{pys}	Postyield modulus of steel
E_s	Elastic modulus of steel
M	Current moment on the cross section
T_{frp}	Tensile force in the FRP strengthening strip
T_s	Force in the tensile steel

α	Magnitude factor from Hognestad concrete model
β_1	Beta factor from 10.2.7.3 of ACI 318-99 (ACI 1999)
γ	Depth factor from Hognestad concrete model
ε_{frp}	Strain in the FRP strengthening strip
ε_c	Strain in the concrete at the extreme fiber in compression
ε_s	Strain in the layer of tensile steel
ε_s'	Strain in the layer of compression steel
σ_c	Stress in the concrete
σ_{frp}	Stress in the FRP strengthening strip
σ_s	Stress in the tensile steel
σ_s'	Stress in the compression steel
ϕ	Curvature in the cross section at a given strain distribution

REPORT DOCUMENTATION PAGE

Form Approved
OMB No. 0704-0188

1. REPORT DATE *(DD-MM-YYYY)*	2. REPORT TYPE	3. DATES COVERED *(From - To)*
March 2002	Final report	

4. TITLE AND SUBTITLE

Rapid Strengthening of Reinforced Concrete Beams with Mechanically Fastened, Fiber-Reinforced Polymeric Composite Materials

5a. CONTRACT NUMBER

5b. GRANT NUMBER

5c. PROGRAM ELEMENT NUMBER

6. AUTHOR(S)

Lawrence C. Bank, Anthony J. Lamanna, James C. Ray, Gerardo I. Velázquez

5d. PROJECT NUMBER

5e. TASK NUMBER

5f. WORK UNIT NUMBER

7. PERFORMING ORGANIZATION NAME(S) AND ADDRESS(ES)

Department of Civil and Environmental Engineering
University of Wisconsin-Madison
Madison, WI 53706;

U.S. Army Engineer Research and Development Center
Geotechnical and Structures Laboratory
3909 Halls Ferry Road
Vicksburg, MS 39180-6199

8. PERFORMING ORGANIZATION REPORT NUMBER

ERDC/GSL TR-02-4

9. SPONSORING / MONITORING AGENCY NAME(S) AND ADDRESS(ES)

U.S. Army Corps of Engineers
Washington, DC 20314-1000

10. SPONSOR/MONITOR'S ACRONYM(S)

11. SPONSOR/MONITOR'S REPORT NUMBER(S)

12. DISTRIBUTION / AVAILABILITY STATEMENT

Approved for public release; distribution is unlimited.

13. SUPPLEMENTARY NOTES

14. ABSTRACT

The U.S. military must often deploy to other countries where bridges may have insufficient strength for their heavy tactical vehicles. In recent years, fiber-reinforced polymeric (FRP) materials have emerged as a viable retrofit scheme for strengthening reinforced concrete bridges. However, because of stringent application requirements, long cure times, and climatic sensitivity, this technology has yet to prove feasible for military operations where time is often the most critical factor. Furthermore, Army operations are conducted under the broadest range of climatic conditions. For these reasons, the U.S. Army Engineer Research and Development Center has undertaken to develop a unique FRP application methodology utilizing powder-actuated mechanical fasteners (i.e., nails from a conventional carpenter's nail gun). This method shows great promise for military applications, since no substrate preparation or adhesive curing is required. Additionally, this method should work well in all but the most extreme environments. For this purpose, numerous laboratory tests have been conducted, and the results have been very promising. This report provides a detailed summary of the first 2 years of testing on this concept.

15. SUBJECT TERMS

Beam retrofit	Bridge retrofit	Fiber reinforced polymetric	FRP plates
Beam upgrade	Bridge upgrade	FRP	Mechanical fasteners

16. SECURITY CLASSIFICATION OF:			17. LIMITATION OF ABSTRACT	18. NUMBER OF PAGES	19a. NAME OF RESPONSIBLE PERSON
a. REPORT	b. ABSTRACT	c. THIS PAGE			19b. TELEPHONE NUMBER *(include area code)*
UNCLASSIFIED	UNCLASSIFIED	UNCLASSIFIED		93	